ENDOTHELIAL CELL RESPONSE TO BIOACTIVE PEPTIDES AND STIFFENED EXTRACELLULAR MATRICES: AN INVESTIGATION INTO ATHEROGENIC PATHWAYS

By:

Farrah A. Edun

A Thesis Submitted in Partial Fulfillment of the Requirements for the Degree of

Master of Science (MSc.)

In

The Faculty of Science

Applied Bioscience

University of Ontario Institute of Technology

August 2017

ABSTRACT

Endothelial dysfunction is the initiating step in atherosclerosis and leads to cardiovascular disease outcomes. This dysfunction can be mitigated by cardioprotective signaling molecules such as nitric oxide (NO) which can be upregulated in the presence of bioactive milk peptides. An investigation into the NO liberating capacity of select bioactive peptides was performed on cultures of Human Umbilical Vein Endothelial Cells (HUVECs) and two tripeptides (VPP and IPP) were found to liberate ~50% more NO. This finding drove a further investigation into whether endothelial cells grown on varying matrix stiffness would experience mechanical forces resulting in cellular responses more indicative of *in vivo* conditions.

Polyacrylamide (PAC) gels of varying stiffness (2.5, 3, 10 and 30kPa) were prepared, and cell growth characteristics and inflammatory responses were measured over a nine day period. Findings showed that stiffer gels (10 and 30kPa) supported the growth of significantly higher numbers of HUVECs with smaller cell areas; however, gel stiffness did not induce a pro-inflammatory response in this cell line. Therefore, these results support PAC gels as useful in simulating a biologically relevant environment for the purposes of endothelial dysfunction investigations.

ACKNOWLEDGMENTS

I would like to sincerely thank my supervisor, Dr. Holly Jones-Taggart, for the opportunity to work on this project. Her knowledge, expertise, and support are greatly appreciated through the research and writing process. I would also like to thank my advisory committee, Dr. Julia Green-Johnson and Dr. Janice L. Strap for their insights and willingness to help guide me towards success.

I would also like to extend my gratitude towards Donna Smeeton and Joanne Free for their assistance in training me in the proper use of the Panoptiq imaging microscope. Sincere gratitude is also extended to Dr. Hendrick de Haan, Christopher Drossis and Michael Greenberg for their guidance in navigating the Image J software. Deep gratitude is also extended to Ryan Howson, in his help in designing coverslip racks that were pertinent towards my methodology.' Heartfelt thanks are also extended to Michael Jeffrey and Dr. Sandra T. Clarke for your friendship and assistance in the completion of this project.

Finally, I would like to deeply thank my family and friends for their help, patience and support through this journey, especially my husband, Roger Sawh, my mother and father, Barbara and Siddiq Edun, and my dear friend Vishal Pua.

TABLE OF CONTENTS

LIST OF TABLES

LIST OF FIGURES

Supplementary Figure 1. HUVEC culture grown on collagen coated cover slips 3 days after initial seeding (passage=2,3). Fixed with 2% paraformaldehyde and stained with safranin. Images obtained using digital microscopy 10x (Panoptiq). Images were then loaded into Image J for cell count and area measurements. The image above was loaded into ImageScope (Leica Biosystems) and a sample of the image was captured at 5x magnification (total magnification 500x).

Supplementary Figure 2. HUVEC culture grown on collagen coated cover slips 6 days after initial seeding (passage=2,3). Fixed with 2% paraformaldehyde and stained with safranin. Images obtained using digital microscopy 10x (Panoptiq). Images were then loaded into Image J for cell count and area measurements. The image above was loaded into ImageScope (Leica Biosystems) and a sample of the image was captured at 5x magnification (total magnification 500x).

Supplementary Figure 3. HUVEC culture grown on collagen coated cover slips 9 days after initial seeding (passage=2,3). Fixed with 2% paraformaldehyde and stained with safranin. Images obtained using digital microscopy 10x (Panoptiq). Images were then loaded into Image J for cell count and area measurements. The image above was loaded into ImageScope (Leica Biosystems) and a sample of the image was captured at 5x magnification (total magnification 500x).

Supplementary Figure 4. HUVEC culture grown on 2.5kPa polyacrylamide gel overlaid on cover slips, 3 days after initial seeding (passage=2,3). Fixed with 2% paraformaldehyde and stained with safranin. Images obtained using digital microscopy 10x (Panoptiq). Images were then loaded into Image J for cell count and area measurements. The image above was loaded into ImageScope (Leica Biosystems) and a sample of the image was captured at 5x magnification (total magnification 500x).

Supplementary Figure 5. HUVEC culture grown on 2.5kPa polyacrylamide gel overlaid on cover slips, 6 days after initial seeding (passage=2,3). Fixed with 2% paraformaldehyde and stained with safranin. Images obtained using digital microscopy 10x (Panoptiq). Images were then loaded into Image J for cell count and area measurements. The image above was loaded into ImageScope (Leica Biosystems) and a sample of the image was captured at 5x magnification (total magnification 500x).

Supplementary Figure 6. HUVEC culture grown on 2.5kPa polyacrylamide gel overlaid on cover slips, 9 days after initial seeding (passage=2,3). Fixed with 2% paraformaldehyde and stained with safranin. Images obtained using digital microscopy 10x (Panoptiq). Images were then loaded into Image J for cell count and area measurements. The image above was loaded into ImageScope (Leica Biosystems) and a sample of the image was captured at 5x magnification (total magnification 500x).

Supplementary Figure 7. HUVEC culture grown on 3kPa polyacrylamide gel overlaid on cover slips, 3 days after initial seeding (passage=2,3). Fixed with 2% paraformaldehyde and stained with safranin. Images obtained using digital microscopy 10x (Panoptiq). Images were then loaded into Image J for cell count and area measurements. The image above was loaded into ImageScope (Leica Biosystems) and a sample of the image was captured at 5x magnification (total magnification 500x).

Supplementary Figure 8. HUVEC culture grown on 3kPa polyacrylamide gel overlaid on cover slips, 6 days after initial seeding (passage=2,3). Fixed with 2% paraformaldehyde and stained with safranin. Images obtained using digital microscopy 10x (Panoptiq). Images were then loaded into Image J for cell count and area measurements. The image above was loaded into ImageScope (Leica Biosystems) and a sample of the image was captured at 5x magnification (total magnification 500x).

Supplementary Figure 9. HUVEC culture grown on 3kPa polyacrylamide gel overlaid on cover slips, 9 days after initial seeding (passage=2,3). Fixed with 2% paraformaldehyde and stained with safranin. Images obtained using digital microscopy 10x (Panoptiq). Images were then loaded into Image J for cell count and area measurements. The image above was loaded into ImageScope (Leica Biosystems) and a sample of the image was captured at 5x magnification (total magnification 500x).

Supplementary Figure 10. HUVEC culture grown on 10kPa polyacrylamide gel overlaid on cover slips, 3 days after initial seeding (passage=2,3). Fixed with 2% paraformaldehyde and stained with safranin. Images obtained using digital microscopy 10x (Panoptiq). Images were then loaded into Image J for cell count and area measurements. The image above was loaded into ImageScope (Leica Biosystems) and a sample of the image was captured at 5x magnification (total magnification 500x).

Supplementary Figure 11. HUVEC culture grown on 10kPa polyacrylamide gel overlaid on cover slips, 6 days after initial seeding (passage=2,3). Fixed with 2% paraformaldehyde and stained with safranin. Images obtained using digital microscopy 10x (Panoptiq). Images were then loaded into Image J for cell count and area measurements. The image above was loaded into ImageScope (Leica Biosystems) and a sample of the image was captured at 5x magnification (total magnification 500x).

Supplementary Figure 12. HUVEC culture grown on 10kPa polyacrylamide gel overlaid on cover slips, 9 days after initial seeding (passage=2,3). Fixed with 2% paraformaldehyde and stained with safranin. Images obtained using digital microscopy 10x (Panoptiq). Images were then loaded into Image J for cell count and area measurements. The image above was loaded into ImageScope (Leica Biosystems) and a sample of the image was captured at 5x magnification (total magnification 500x).

Supplementary Figure 13. HUVEC culture grown on 30kPa polyacrylamide gel overlaid on cover slips, 3 days after initial seeding (passage=2,3). Fixed with 2% paraformaldehyde and stained with safranin. Images obtained using digital microscopy 10x (Panoptiq). Images were then loaded into Image J for cell count and area measurements. The image above was loaded into ImageScope (Leica Biosystems) and a sample of the image was captured at 5x magnification (total magnification 500x).

Supplementary Figure 14. HUVEC culture grown on 30kPa polyacrylamide gel overlaid on cover slips, 6 days after initial seeding (passage=2,3). Fixed with 2% paraformaldehyde and stained with safranin. Images obtained using digital microscopy 10x (Panoptiq). Images were then loaded into Image J for cell count and area measurements. The image above was loaded into ImageScope (Leica Biosystems) and a sample of the image was captured at 5x magnification (total magnification 500x).

Supplementary Figure 15. HUVEC culture grown on 30kPa polyacrylamide gel overlaid on cover slips, 9 days after initial seeding (passage=2,3). Fixed with 2% paraformaldehyde and stained with safranin. Images obtained using digital microscopy 10x (Panoptiq). Images were then loaded into Image J for cell count and area measurements. The image above was loaded into ImageScope (Leica Biosystems) and a sample of the image was captured at 5x magnification (total magnification 500x).

LIST OF APPENDICES

LIST OF ABBREVIATIONS

ACE - Angiotensin Converting Enzyme

AFM - Atomic Force Microscopy

AGE –Advanced Glycation End Products

Ang-I - Angiotensin I

Ang-II - Angiotensin II

BAEC - Bovine Aortic Endothelial Cell

CDK – Cyclin-Dependent Kinase

CVD - Cardiovascular Disease

DMEM - Dulbecco's Modified Eagle Medium

ECGS - Endothelial Cells Growth Supplement

ECM - Extracellular Matrix

EGF - Endothelial Growth Factor

ELISA - Enzyme-Linked Immunosorbent Assay

eNOS - Endothelial Nitric Oxide Synthase

ET-1 - Endothelin- 1

FCS - Fetal Calf Serum

G-LISA - Small G-protein Activation Assay

HAEC - Human Aortic Endothelial Cells

HRP - Horseradish Peroxidase

HUVEC - Human Umbilical Vein Endothelial Cell

ICAM-1 - Intercellular Adhesion Molecule- 1

IGF-1 - Insulin Growth Factor- 1

IL-1 – Interleukin-1

IL-4 – Interleukin- 4

IL-6 - Interleukin- 6

kPa - Kilo Pascal

LAB - Lactic Acid Bacteria

LFA-1 - Lymphocyte Function-Associated Antigen- 1

LPL - Lipoprotein Lipase

LPS - Lipopolysaccharide

mBMEC - Mouse Brain Microvascular Endothelial Cells

MCP-1 - Monocyte Chemoattractant Protein- 1

M-CSF - Monocyte Colony Stimulating Factor

MI – Myocardial Infarction

NO - Nitric Oxide

NOX2 - NAPDH oxidase

oxLDL - Oxidized Low-Density Lipoprotein

PAC - Polyacrylamide

PBS – Phosphate buffered saline

RAAS - Renin-Angiotensin-Aldosterone System

ROCK - RhoA kinase

sICAM-1 - Soluble Intercellular Adhesion Molecule- 1

SNP - Short Nucleotide Polymorphism

TdT - Terminal Deoxynucleotidyl Transferase

TEER - Transendothelial Electrical Resistance

TMB - 3,3',5,5'-tetramethylbenzidine

TNF-α - Tumor Necrosis Factor Alpha

TUNEL - TdT dUTP Nick-End Labeling

VCAM-1 - Vascular Cell Adhesion Molecule- 1

1. INTRODUCTION

1.1. Cardiovascular Disease

Cardiovascular Disease (CVD) is a term that refers to all diseases of the circulatory system, although the leading manifestations are heart disease and stroke (Public Health Agency of Canada, 2016). The two most prominent causes of CVD share the same underlying characteristic, whereby they are all initiated by some form of vascular blockage. This blockage is most commonly due to atherosclerosis, a gradual process that causes plaque to build up inside the arteries, causing the narrowing, obstructing, and occluding of the vasculature (National Heart, Lung and Blood Institute, 2016). Globally, the mortality rate of CVD is 17.7 million people, accounting for 31% of deaths (WHO, 2017). Statistics Canada estimated that approximately 50,000 Canadians died due to diseases of the heart in 2013, accounting for 20% of all deaths in Canada. Additionally, 1 in 12 Canadian adults lives with diagnosed CVD. The economic burden as a result of CVD is estimated to be $21.2 billion annually (Tarride *et al.,* 2009).

Although there are many risk factors that can contribute to CVD, these risks can generally be separated into two categories. The first category consists of modifiable risk behaviours, such as habits and/or addictions (i.e. smoking and sedentary lifestyle). The second category consists of underlying conditions that are able to promote the development of atherosclerosis, such as hypertension and

inflammation. Atherosclerosis can be exacerbated by inflammation and triggered by hypertension. Hypertension, as defined by the Public Health Agency of Canada, is an increase in systolic and diastolic blood pressure. Increased blood pressure disrupts the pattern of blood flow within the vasculature and initiates damage (Cybulsky and Marsden, 2014). The lining of the vasculature, known as the endothelium, is composed of specialized endothelial cells. These cells are subjected to low-velocity blood flow in normotensive individuals due to the fact that laminar blood flow allows the blood to move at its highest velocity at the centre of the vessel, and thus the outer endothelial layers experience minimal amounts of shear stress (Stonebridge and Brophy, 1991). In hypertensive individuals, blood moves and travels at differing magnitudes and velocities; this is referred to as turbulent flow and it causes an increase in endothelial cell stress and turnover (Cybulsky and Marsden, 2014). As the rate of cell renewal becomes lower than the rate of apoptosis and the number of cells decreases within the endothelial layer, there is a loss of cell connections along the endothelial lining and the normal function of the endothelial barrier deteriorates (Tricot *et al.*, 2000). Once the endothelial barrier becomes dysfunctional, inflammatory responses to the infiltration of the barrier further promote the pathological progression of atherosclerosis. Acute and chronic CVD from the development of blockages in the vasculature is a progressive, insidious disease that begins with the loss of the normal function of the endothelium.

1.2. *Inflammation and Atherosclerosis*

A common underlying factor of CVD is a vascular blockage that stops the flow of blood to various organs; the underlying cause of this vascular narrowing and blockage is due to a process termed atherosclerosis. Atherosclerosis progresses slowly and eventually manifests as a fatty streak that either occludes the arterial lumen or it ruptures, releasing stored material from the fatty streak into the artery causing a thromboembolism (Libby, 2006). A thromboembolism can rupture and release an embolism that will travel in the vasculature until an occlusion occurs, cutting off blood delivery of oxygen and nutrients to all downstream tissues. This will can cause myocardial infarctions (MI or heart attack) or stroke if the embolism reaches the brain.

Atherosclerosis, once believed to be caused solely by unmanaged cholesterol levels, has now been classified as an inflammatory disease, where the body's natural reaction to infection and cell damage turn against the body's endothelial cells (Libby, 2006). This inflammatory response is initiated by a change in the structure of the endothelium lining the arteries. Under normal conditions, monocytes are not able to attach to endothelial cells; however, a damaged or dysfunctional endothelium allows and perpetuates an immune response (Figure 1, Libby *et al.*, 2011). The change in morphology of the endothelial lining could be brought on by the factors of high oxLDL, impaired insulin and glucose metabolism, dysregulated blood flow and stiffening of the arteries as described

above. Each can stimulate the endothelial cells to release cytokines that activate an immune response. Inflammatory cytokines, such as intercellular adhesion molecule 1 (ICAM-1) and vascular cell adhesion molecule 1 (VCAM-1) as well as monocyte recruitment cytokines, such as macrophage colony stimulating factor (M-CSF) have been reported to be released by endothelial cells under stress (Libby *et al.,* 2011). M-CSF signals for the increased presence of monocytes while ICAM-1 and VCAM-1, as adhesion molecules, promote binding of these monocytes to the endothelial layer (Libby *et al.,* 2011). Once bound, these monocytes are able to migrate beneath the endothelial layer to the smooth muscle layer. This migration is mediated by a chemoattractant gradient of MCP-1 released by the endothelium (Libby *et al.,* 2011).

Once under the endothelial layer, the monocytes differentiate into macrophages; these macrophages express scavenger receptors which allow them to attract and ingest LDLs. The phagocytosis of LDLs increases the volume of the monocyte cytoplasm, eventually leading to differentiation into foam cells (Libby, 2002). These foam cells then express E-cadherin, a signaling molecule that attracts other foam cells for further aggregation, eventually leading to the formation of the atheromatous core – the center of the atherosclerotic plaque characterized by the collection of cellular debris and oxLDL (Bobryshev, 2006). The foam cells and endothelial cells are then able to secrete signaling factors for smooth muscle cells

to replicate and migrate to the apical surface of the endothelial layer forming the fibrous cap that eventually covers the atherosclerotic area (Figure 2, Libby, 2011).

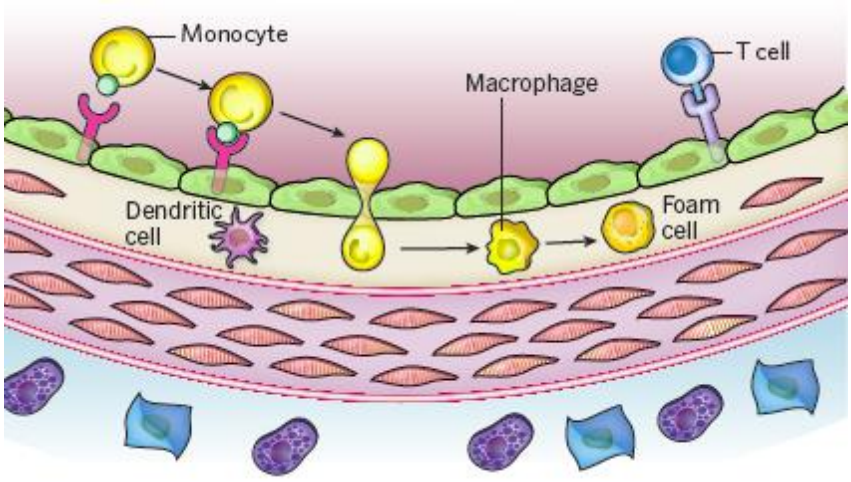

Figure 1. Endothelial expression of adhesion molecules directing the migration of monocytes towards innermost muscle layer, leading to the differentiation into macrophages, and eventually foam cells from the uptake of oxLDLs. T-cell mediated immunity can also be observed here, where the endothelial layer expresses MHC molecules signaling the infiltration of foreign bodies.

Adaptation by permission from Macmillan Publishers Ltd: [Nature] (Libby, P., Ridker, P., Hansson, G. 2011. Progress and challenges in translating the biology of atherosclerosis. *Nature. 473.)* Copyright 2011. (2011)

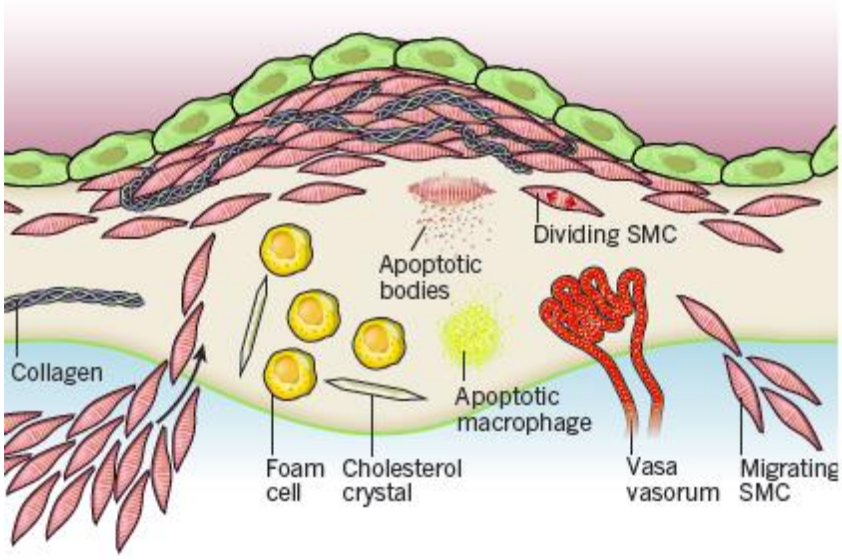

Figure 2. Foam cell aggregation forming the atheromatous core. Smooth muscle cells are also migrating to the luminal surface forming the fibrous cap of the fatty streak.

Adaptation by permission from Macmillan Publishers Ltd: [Nature] (Libby, P., Ridker, P., Hansson, G. 2011. Progress and challenges in translating the biology of atherosclerosis. *Nature. 473.)* Copyright 2011. (2011)

This atherosclerotic plaque is able to progress outwards, weakening the outer vessel wall; however, it may begin to grow inwards towards the lumen of the blood vessel, effectively narrowing the artery and decreasing the flow of blood. Eventually, this will lead to total occlusion of the artery or it may reach the elastic limits of the fibrous cap causing it to rupture and release the atheromatous core. The thromboembolism then travels downstream until a total blockage occurs, thereby causing an ischemic event (Libby, 2002).

1.2. Promotion of a Dysfunctional Endothelium

A healthy endothelium creates a barrier between the lumen of the blood vessel and the smooth muscle cells. It is a semipermeable membrane that mediates the diffusion of extracellular material into the smooth muscle layer of the vasculature. The endothelial lining is maintained by sufficient cell to cell communication allowing the cells to form junctional complexes with neighbouring endothelial cells (Bazzoni and Dejana, 2004). Through this efficient communication network and cell-cell contact, the endothelial lining is able to maintain barrier function as well as a homeostatic balance with the smooth muscle layer that regulates vasoconstriction and vasodilation. A key player in the homeostatic regulation of vasomotor activity is the signaling molecule nitric oxide (NO), which is a potent vasodilator produced and released by healthy endothelial cells in intricate responses to blood pressure changes (Ignarro *et al*., 1987). NO then diffuses into

the smooth muscle layer, signaling smooth muscle cell relaxation allowing for vasodilation.

Endothelial dysfunction is characterized by an increased permeability to blood components such as leukocytes, oxidized low-density lipids (oxLDL), and aggregated platelets (Davignon and Ganz, 2004), as well as a loss of NO generating capacity (Föstermann and Sessa, 2012). The loss of cell-cell connections, such as gap junctional complexes, causes the endothelial layer to lose barrier function and become susceptible to infiltration by these blood components. This progressively causes the endothelial cells within the layer to begin distress signaling to the immune system, resulting in further accumulation of leukocytes and platelets locally (Jongstra-Bilen *et al.,* 2006). Additionally, monocytes are able to easily migrate under the endothelial layer due to these gaps between endothelial cells, driving inflammatory response, and endothelial dysfunction, further (Rubin and Damjanov, 1989).

The process of endothelial dysfunction is complex and driven by factors outside of the endothelial cell to cause an imbalance of the homeostatic mechanisms required to maintain a functioning barrier. The factors contributing to the decline in barrier function include dysregulated blood flow - both hypertension (Hsieh *et al.,* 2014) and turbulent flow (Cybulsky and Marsden, 2014), age and/or pressure related arterial stiffening (Baeyens and Shwartz, 2015),

oxLDL infiltration, insulin and glucose dysregulation (Rask-Marsden and King, 2007) and plaque formation (Libby, 2006).

1.2.1. Dysregulated Blood Flow and Arterial Stiffening

Disturbances in blood flow dynamics can be characterized in one of two ways; an increase in overall blood pressure – typically referred to as hypertension or as turbulent flow – which is typically found at arterial branch points and occurs due to the divergence of blood flow. This dysregulated blood flow, if sustained, will eventually cause the pathology of arterial stiffening. Arterial stiffening is considered to be an inevitable consequence of age, however much evidence has been brought forward to implicate unmanaged hypertension as an early cause of arterial stiffening. This is mostly due to the constant cyclical shear stress endured by the arteries over time that causes changes in the extracellular matrix (ECM) such as increased collagen deposits as well as changes in the smooth muscle layer that alter its ability to stretch (Cecelja and Chowienczyk, 2012).

1.2.1.1. Hypertension

Blood vessels respond to differing hemodynamic forces. In areas where high pressure is present, the blood vessels need to adapt to maintain homeostasis by reacting to changes in shear stress and hydrostatic pressure. Shear stress is the tangential friction force acting on the vessel wall, whereas hydrostatic pressure is both the perpendicular force acting on the vascular wall and cyclic strain on the

stretch within the vessel wall (Hsieh *et al.*, 2014). In hypertensive individuals, arteries constantly undergo structural changes to adapt to the increased pressure. These structural changes are hypertrophic and typically involve an overall change in the smooth muscle layer and lumen ratios. Hypertrophic remodeling is a response to this change in pressure involving thickening of the muscle layer resulting in a reduction in lumen diameter (Intengan and Schiffrin, 2000). The decrease in the diameter of the lumen causes an increase in pressures on the endothelial layer. This increased pressure from the pulsating blood is transferred from the endothelium to the elastin and collagen fibers of the muscle layer of the arteries. This causes changes to the ECM – an increase in collagen production, the breakdown of elastin – and infiltration of smooth muscle cells leading to overall stiffening of the artery (Díez, 2007). If the increased pressure is sustained and the hypertrophic remodeling is not reversed, arterial stiffening will result, causing loss of the elastic recoil abilities of the vasculature (Cecelja and Chowienczyk, 2012) and a rigid ECM for the endothelium. This rigidity of the surface on which the endothelial cells attach compromises their ability to maintain cell-cell junctional connections for the optimal barrier function of the endothelium. In areas of increased stiffness, the junctional complexes that normally allow for healthy cell to cell communication disappear as endothelial cells begin to be pulled along the stiffened muscular layer (Krishnan *et al.,* 2011). In an experiment using human umbilical vein endothelial cells (HUVECs) cultured on polyacrylamide gel substrates, Krishnan *et al*. (2011) found that monolayer cultures grown on softer,

more compliant substrates were better able to withstand force in the presence of a permeability stimuli (thrombin), and the monolayer was observed to react in unison. In contrast, monolayers on stiffer polyacrylamide substrates could not withstand the same force, and gaps were generated between neighbouring endothelial cells (Krishnan *et al*., 2011).

1.2.1.2. Turbulent Blood Flow

Turbulent flow is typically present at the inner curvature or bifurcations of the arteries, however, laminar blood flow is normally regained a short distance away from the arterial branch point. Endothelial cells at these branch points display different morphologies and gene expression patterns than their counterparts under laminar flow, and it is at these locations where atherosclerotic lesions are most likely to initiate (Cybulsky and Marsden, 2014). This is likely due to factors such as chronic low-grade inflammation, increased cell proliferation, or cytoskeletal reorganization that may contribute to a dysfunctional endothelium.

Under turbulent flow, endothelial cells express a chronic low-grade inflammatory response, more specifically up-regulation of interleukin- 1 (IL-1), interleukin-6 (IL-6), and monocyte chemoattractant protein-1 (MCP-1) (Jongstra-Bilen *et al.*, 2006). This chronic low-grade inflammation does not normally lead to atherosclerosis; however, Davies *et al.,* (1986) demonstrated that cell turnover was significantly higher in a cell-based model using bovine aortic endothelial cells (BAECs). BAECs were placed under turbulent flow *in vitro* and compared to

BAECs under high shear stress experiencing laminar flow. The authors found that endothelial cell turnover was increased in cells undergoing low shear stress with the turbulent flow when compared to endothelial cells experiencing high shear stress in laminar flow. Therefore, it was suggested that this chronic low-grade immune response, coupled with high cell turnover could combine with other CVD risk factors to promote a dysfunctional endothelium and allow for the development of atherosclerotic plaques.

1.2.2. Oxidized Low-Density Lipoprotein and eNOS Activity

In atherosclerosis the fatty streak contains both low-density lipoproteins (LDLs) as well as their oxidized counterparts (oxLDL); however, the level of LDL is lower when compared to oxLDL (Steinbrecher *et al.,* 1984). This observation lead researchers to hypothesize that LDLs undergo endothelial cell mediated modifications. It was found that this modification was through oxidation of lipids by reactive oxygen species, such as superoxide and hydrogen peroxide (Morel *et al.*, 1983). Beyond this, oxLDLs were assumed to only contribute to the formation of foam cells present in the necrotic plaque in late-stage atherosclerosis; however, recent studies have demonstrated that oxLDLs also affect endothelial homeostasis through disruption of the regulation of endothelial nitric oxide synthase (eNOS) activity (reviewed by Levitan and Shenty, 2011). eNOS is the endothelial isoform of the enzyme responsible for catalyzing the conversion of the amino acid L-arginine to L-citrulline, which liberates NO (Cockcroft, 2005). eNOS activity has

been demonstrated to be directly regulated by the integral membrane protein of the phospholipid bilayer caveolae (Blair *et al*., 1999). Caveolae – Latin for "little caves" – are specialized, cholesterol-rich, invaginations of the plasma membrane and are found in many cell types but are most prevalent in endothelial cells and adipocytes (Govers and Rabelink, 2001). Caveolin-1 is able to bind to eNOS via its scaffolding domain and the interaction maintains eNOS in an inactive state when cytosolic calcium levels are low (Govers and Rabelink, 2001). When cytosolic calcium levels become elevated, eNOS dissociates from caveolin to become phosphorylated – this process is promoted by the calcium-calmodulin complex (Blair *et al*., 1999). In experiments using cultured endothelial cells, it was shown that oxLDLs are able to impede the association of eNOS and caveolae by altering the composition of caveolae by depleting them of cholesterol (reviewed by Shaul, 2003). In this way, oxLDLs contribute to endothelial dysfunction through the inhibition of eNOs activity in endothelial cells.

1.2.3 Hyperinsulinemia and Insulin Resistance

A healthy endothelial layer is able to regulate the passage of insulin into tissues along with glucose in order to feed the cellular process of glycolysis occurring within the tissues (King *et al.,* 2016). However, the effect of hyperinsulinemia and insulin resistant states are positively correlated with arterial stiffness across all age groups (Zieman *et al*., 2005). This is due to insulin signaling both through the insulin receptor and other pathways to stimulate gene expression

profiles that drive cell proliferation and specialized cell functions. In insulin resistance, these pathways are no longer responsive to insulin, leading to loss of normal endothelial cell responses. However, hyperinsulinemia drives other pathways apart from the insulin receptor signaling that continue to have proliferative effects on the vasculature.

Insulin's role in endothelial cell function was demonstrated through multiple reports of its upregulation of NO production. Kuboki *et al.,* (2000) showed eNOS mRNA and expression in BAECs increased 2-fold after 12 hours using physiological concentrations of insulin. Further, Kuboki *et al.,* (2000) exposed vascular tissue isolated from Zucker lean and fatty insulin-resistant rats to 100nmol/L of insulin. Insulin was found to increase eNOS mRNA expression by 50% in the lean rat model but had no effect on the insulin-resistant rats. The activity of insulin is now known to be mediated through cellular phosphatidylinositol-4,5-bisphosphate 3-kinase (PI3K) signaling in healthy endothelium; Montagnani *et al.,* (2002) used a HUVEC model to directly link PI3 kinase signaling to eNOS expression. Since insulin resistant states are characterized by inhibition of PI3 kinase signaling (due to loss of insulin receptor signaling) both endothelial eNOs activity and NO production are impacted, contributing to endothelial dysfunction.

Insulin has stimulatory properties mediated through other pathways that directly affect endothelial function. High insulin levels lead to upregulation of

endothelin-1 (ET-1), a potent vasoconstrictor. Nagai *et al.,* (2003) demonstrated this by using human aortic endothelial cells (HAECs) treated with insulin and anti-insulin-like growth factor- 1 (IGF-1) receptor antibody to show that concentrations of insulin 100μU/mL or higher significantly stimulated ET-1 production and this was inhibited in the presence of anti-IGF-1 receptor antibody. This study was extended to examine the effect of insulin on growth rates of vascular smooth muscle cells; it was found that culture growth was increased with greater than 330μU/mL of insulin. This study demonstrated that high insulin levels could increase vasoconstriction of the blood vessel through upregulation of ET-1 as well as promote vessel stiffening through increased proliferation of vascular smooth muscle cells.

Both of these conditions of high blood insulin levels and insulin resistance therefore further exacerbate and promote a dysfunctional endothelium.

1.2.4. Hyperglycemia

Hyperglycemia is characterized by an excess of circulating glucose; this glucose could spontaneously and irreversibly react with lysine residues on proteins – such as collagen – forming advanced glycation end products (AGEs) (Verzijl *et al.,* 2000). The formation of AGEs then alters the binding properties of collagen, therefore increasing arterial stiffness (Zieman *et al.,* 2005). AGEs have also been shown to bind to their receptor, receptor for advanced glycation end products (RAGE), which is able to elicit downstream signaling cascades leading to

the reduction of NO and eNOS expression (Ren *et al.,* 2017). RAGE downstream signaling can also activate NF-κB to stimulate a pro-inflammatory cytokine response, therefore further promoting a dysfunctional endothelium (Ren *et al.,* 2017).

1.3.Immunological Biomarkers

Atherosclerosis is initiated through the dysfunction of the endothelial lining which in turn causes the release of cytokines and overexpression of adhesion molecules, as described. In relation to this project, the endothelial cell expression levels of IL-6, MCP-1 and soluble ICAM-1 (sICAM-1) were investigated in relation to external mechanical stress induced by culturing them on increasing matrix stiffness, mimicking vascular stiffening.

1.3.1. Interleukin-6 (IL-6)

IL-6 is a cytokine released by various cells, such as T-cells, B cells, endothelial cells and fibroblasts, and plays a crucial role in the recruitment of leukocytes to sites of inflammation. As demonstrated by Romano *et al.,* (1997), mice deficient in IL-6 production showed defective recruitment of leukocytes to subcutaneous regions injected with an irritant that should otherwise induce an immune reaction. This effect was reversed by the local administration of IL-6. Analysis of the promoter region of the IL-6 gene revealed the presence of an NF-κB transcription factor binding site that would promote gene expression through inflammatory signaling (Libermann and Baltimar, 1990). Activation of NF-κB

occurs in response to a number of known inflammatory stimuli, such as lipopolysaccharide (LPS) and tumor necrosis factor α (TNF- α). Kobayashi *et al.,* (2003) demonstrated that NF-κB activation led to the upregulation and secretion of IL-6 in a culture of HUVECs that were stretched by a silicone membrane on which they had been grown.

1.3.2. Monocyte Chemoattractant Protein -1 (MCP-1)

MCP-1 is a potent chemotactic factor aiding in monocyte migration beneath the endothelial layer (Deshamne *et al.,* 2009). MCP-1 exposure has also been associated with a reduction of gap junctional complexes within the endothelium, promoting a dysfunctional state. Stamatovic *et al.,* (2003) investigated the transendothelial electrical resistance (TEER) as a measure of tight junction integrity through electrical resistance. A decrease in electrical resistance indicates a shortened electrical pathway and thus loss of gap junction complexes. In this model, mouse brain microvascular endothelial cells (mBMEC) were cultured in the presence or absence of MCP-1 protein. Resistance was observed to decline in a time-dependent manner when mBMECs were incubated with 100nM of MCP-1 for 60 minutes (declined from 118 $\Omega \bullet cm^2$ to 19 $\Omega \bullet cm^2$). Resistance was also found to decrease in a dose-dependent manner where the lowest concentration of MCP-1 to decrease endothelial resistance was 20nM, thus suggesting that even low levels of MCP-1 can reduce the gap junctional integrity of an endothelium.

1.3.3. Soluble Intercellular Adhesion Molecule-1 (sICAM-1)

Soluble ICAM-1 belongs to immunoglobulin superfamily but differs from its parent molecule ICAM-1 in that it represents the cleaved, circulating derivation.sICAM-1 has been demonstrated to promote angiogenesis through stimulating HUVEC cell migration and tube formation *in vitro* (Gho *et al.,* 1999).It has also been reported that sICAM-1 can induce tumor growth *in vitro* in human prostate adenocarcinoma (PC3), human fibrosarcoma (HT1080), and immortalized human mammary epithelial cells (HMECs) (Gho *et al.,* 2001). The parent molecule ICAM-1 interacts with lymphocyte function-associated antigen (LFA-1) in order to allow for leukocyte transmigration to the intimal surface. In a study by Meyer *et al.,* (1995), it was found that sICAM-1 is able to inhibit the interaction of LFA and ICAM-1 at an IC_{50} level of 20-40uM, giving rise to its anti-inflammatory properties. However, sICAM-1 can also signal for additional lymphocytes to congregate towards the area of expression – displaying its pro-inflammatory properties (Chae, C. *et al.,* 2001). sICAM-1 was chosen as a biomarker since in studies plasma levels of sICAM-1 have been shown to be indicative of atherosclerotic events. In a study by Hwang *et al.,* (1997) blood samples were taken from individuals presenting risk factors for heart disease e.g. hypertension, smoking, obesity etc. sICAM-1 levels were seen to be elevated in this group when compared to levels in the control group. This elevation was observed 5 years prior to subjects' first myocardial infarction (MI). These findings were further supported by Ridker *et al.,* (1998)

where sICAM-1 levels were seen to be elevated 9 years earlier in apparently healthy individuals who eventually experienced an MI.

1.4. Nitric Oxide as a Cardioprotective Molecule

Vasomotor activity is mediated by extrinsic factors such as hormones and nervous signaling, but the most potent intrinsic vasodilatory activity is controlled through NO release by endothelial cells (Govers and Rabelink, 2001). In the past there have been conflicting viewpoints regarding NO effects on the vasculature during ischemic events. Earlier researchers concluded that NO is detrimental to the vasculature due to the production of reactive oxygen species such as superoxide, peroxynitrite and hydrogen peroxide (Mori *et al.,* 1998, Wang *et al.,* 1999, Flögel *et al.,* 1999). However, the general consensus is that the benefits of NO in modulating vasodilation outweigh any potential detrimental effects (Heusche *et al.,* 2000, Zhao *et al.,* 2000, Gourine *et al.,* 2001).

Liberation of NO is facilitated by the activity of endothelial nitric oxide synthase enzyme (eNOS) described earlier (Section 1.2.2). eNOs activity is stimulated by extracellular signals such as shear stress, acetylcholine, or leukocyte adhesion. These stimuli either increase eNOS sensitivity to Ca^{2+} or increase intracellular Ca^{2+}, thus allowing for calmodulin to bind to two eNOS monomers, forming a dimer (Föstermann and Sessa, 2012). Upon dimerization, eNOS is able to catalyze the oxidation of L-arginine to L-citrulline, liberating NO from the guanidinium group of arginine (Rychter *et al.* 2016). NO then moves to the

vascular smooth muscle cells where it binds with soluble guanylate cyclase, which converts guanosine triphosphate to guanosine-3,5'-monophosphate, which drives the phosphorylation of downstream proteins signaling overall relaxation of the vascular smooth muscle. (Rychter *et al.* 2016). Thus, NO is a potent vasodilatory molecule and this mechanism is central to the finite control of homeostatic conditions.

With the knowledge of NO protection against ischemic attacks it has been suggested that clinical administration of nitrites could be beneficial against ischemic attacks; however increased dosage of nitrites may lead to major health concerns such as the development of methemoglobinaemia and emphysema in at risk groups (Mesinga *et al.,* 2003). To overcome this, agents that increase eNOS activity (Papapetropoulous *et al.,* 2004, Okayasu *et al.,* 2008) or nitric oxide donors (Wang *et al.,* 2002) have been recommended.

1.5.Dairy Consumption and Cardiovascular Disease

Dairy consumption is recommended in the daily dietary guidelines of many developed countries as well in dietary interventions to aid in lowering cardiovascular disease (CVD) risk (Muñoz *et al.,* 1997). However, there has been conflicting evidence regarding the influence of dairy products and the protection from developing CVD. These differing views can be attributed to the varied composition of dairy products. Evidence supporting CVD prevention stems from the fact that dairy products are typically rich in vitamins, minerals, and protein

which can exert beneficial health effects and therefore decrease the risk of CVD (Soedamah-Muthu *et al.,* 2011). Conversely, dairy products also contain saturated fat, which can raise low-density lipoproteins and therefore lead to the increased likelihood of developing CVD (Soedamah-Muthu *et al.,* 2011).

In a meta-analysis of cohort studies examining the impact of dairy consumption and risk of CVD, it was found that daily consumption reduced the risk of CVD by 12% (Qin *et al.,* 2015). The studies included in this meta-analysis included studies that investigated whole milk as well as dairy milk products (such as yogurt, cheese, butter and kefir). The studies differed in regards to which dairy products were investigated. It was found that if the cohort studies investigated only whole milk products, there was no significant correlation between dairy products exhibiting cardioprotection. However, in studies that utilized fermented milk products, such as yogurt and kefir, it was observed that there was some degree of association in protecting against a CVD (Qin *et al.,* 2015). It should be noted that these milk products can be derived from enzymatic digestion, occurring in the gut, or by bacterial fermentation. Enzymatic digestion is driven by the presence of digestive enzymes within the gut, whereas bacterial fermentation is due to the proteinase enzymes produced by lactic acid bacteria (LAB); the result of proteolytic action is the focus of the current research.

1.5.1. Cardioprotection by Bioactive Peptides

During bacterial fermentation, lactic acid bacteria (LAB), such as *Lactobacillus helveticus*, are able to digest large milk proteins, such as α-, β- and k-caseins, into smaller biologically active peptides and it is these bioactive peptides that have come to the forefront of much research (Fitzgerald *et al.,* 2000, Aihara *et al.,* 2009, Hirota *et al.,* 2011, Marcone *et al.,* 2015). Some of these bioactive peptides have been highly characterized in regards to their ability to attenuate hypertension *in vivo* (Fitzgerald *et al.,* 2000; Aihara *et al.,* 2015,), others have been characterized based on their ability to regulate the immune system (Marcone *et al.,* 2015), and some have also been implicated in influencing vascular tone (Jauhiainen *et al.,* 2007).

1.5.1.1. Antihypertensive Properties of Bioactive Milk Peptides

Bioactive peptides have been shown to demonstrate antihypertensive properties by acting as an angiotensin converting enzyme (ACE) inhibitor (Fitzgerald *et al.,* 2000). ACE acts as a member of the renin-angiotensin-aldosterone system (RAAS) which restores homeostatic conditions in response to blood volume or pressure decreases as detected by specialized cells of the kidneys. More specifically, ACE acts to convert the renin activated angiotensin-I (Ang-1) to angiotensin-II (Ang-II); Ang- II then acts as a potent vasoconstrictor to counteract

blood pressure drops (Turner and Hooper, 2002). The use of ACE inhibitors has become common in clinical practices to diminish conversion of Ang –I to Ang –II to counteract vasoconstriction and thereby aid in lowering blood pressure as a way to manage hypertension. By blocking ACE, blood pressure is reduced, thus effectively protecting the endothelial layer from sustained elevated levels of shear stress. The ACE inhibitory nature of these bioactive milk peptides has been attributed to their amino acid side groups (Fitzgerald *et al.*, 2000); in this review, the authors compile a list of previously discovered bioactive peptides and demonstrate that bioactive peptides containing proline, lysine, or arginine as the C-terminal residue will preferentially bind to and inactivate ACE in order to exhibit their antihypertensive effects. The ACE inhibition potential of the peptides used in this study was previously investigated by Adams (2015) who found bioactive peptides with C-terminal prolines were able to exhibit greater ACE inhibition activity.

Further to the ACE inhibitory effects of these bioactive peptides, there have also been studies demonstrating their NO liberating abilities. In a study by Hirota *et al.,* (2011), two small peptides, valine-proline-proline (VPP) and isoleucine-proline-proline (IPP), were able to increase NO production by 50% over controls in a HUVEC culture over a 1 hour incubation time. This study also investigated the ability of VPP and IPP to induce vessel relaxation by treating thoracic aortae isolated from male Wistar rats with varying concentrations of VPP

and IPP *ex vivo*. It was found that VPP and IPP were able to induce relaxation of isolated aortic rings.

1.5.1.2. Immunomodulatory Effects of Bioactive Milk Peptides

Studies have demonstrated that peptides liberated by LAB fermentation can exhibit anti-microbial properties and therefore engage the innate immune system. In a study by Sütas *et al.,* (1996) it was seen that non-specific bioactive peptides were able to down-regulate interleukin- 4 (IL-4) production in peripheral blood mononuclear cells treated with anti-CD3 antibodies taken from hypersensitive, allergic individuals. More recently, treatment of TNF-α activated HUVECs with a casein hydrolysate was shown to downregulate the expression of adhesion molecules such as vascular adhesion molecule -1 (VCAM-1), intercellular adhesion molecule -1 (ICAM-1) and E-selectin (Marcone *et al.,* 2015). Suppression of adhesion molecule expression by peptides was found to be mediated by inhibition of NF-κB signaling, decreasing expression levels of these cytokines.

Bioactive peptides liberated through bacterial fermentation have also been implicated in stimulating the proliferation of human lymphocytes and increasing phagocytic activities of monocytes (Sütas *et al.,* 1996). Additional studies using high-fat diet (HFD) fed mice showed that administration of VPP reduced macrophage infiltration into the adipose tissue (Aihara *et al*., 2014). These results suggest that VPP can regulate the recruitment of pro-inflammatory cells;

however the molecular mechanisms behind these actions are yet to be clarified (Aihara *et al*., 2014).

1.5.1.3. Bioactive Peptide Effect on Arterial Stiffness

VPP and IPP have been shown to influence the arterial muscle tone in some short term interventions, however, this was found to be attributed to a decrease in hypertension or an increase in vasodilatory mediators. In one study by Jauhiainen *et al.,* (2007), hypertensive subjects not taking hypertensive medication received fermented milk containing VPP and IPP or a placebo. Ambulatory arterial stiffness indices were then obtained for each group and the stiffness index was found to improve by 12% in the treatment group and by 5% in the placebo group. This change in muscle tone is proposed to be multifactorial, where the muscle tone may be mediated by the overall lowering of systolic and diastolic blood pressure. This change could also be attributed to the increased Ca^{2+} present within the ferments, which aids in vasorelaxation since Ca^{2+} has been shown to be necessary for NO production and thereby overall dilation (Föstermann and Sessa, 2012).

1.6. Development of Physiologically Relevant Models to Study the Endothelium

In typical cell culture investigations, cultures are grown on glass or plastic surfaces. However, *in vivo*, most cells adhere to much softer substrates, such as other cells, a basement membrane or some other extracellular matrix (Yeung *et al.*, 2005). Cell functions can depend on the stiffness of the substrate, where stiffness represents the circumferential stretch that would be experienced by endothelial cells *in vivo.* The impact of stiffness on cellular functions is likely mediated through the cytoskeleton or plasma membrane, causing transcriptional changes and changes in chemical signaling regarding cell survival, proliferation, and movement (Lo *et al.*, 2000). Cell survival, proliferation, and migration are key to wound healing and also to other physiological processes that seek to regain and maintain tight junctional cell barriers. Notably, maintaining cell – cell junctions that promote an endothelial barrier is critical to slow the pathology of atherosclerosis.

Wang *et al.,* (2000) investigated the growth rates of murine embryo fibroblasts (NIH/3T3) on soft substrates made of polyacrylamide gels. Apoptosis was measured by terminal deoxynucleotidyl transferase (TdT) dUTP Nick-End Labeling (TUNEL) assay as an *in situ* cell death detection measure. They found that cultures grown on flexible substrates were able to propagate, but cells grown on the stiffer substrates showed decreased DNA synthesis and increased

apoptosis. This study initially demonstrated that polyacrylamide substrates would be a viable option for culturing cells, and may offer a more physiologically relevant level of resistance as a surface for *in vitro* investigations.

Yeh *et al.,* (2012) further investigated proliferation rates of endothelial cells. In this study, endothelial cells were grown on soft substrates as well as stiffened substrates as determined by the composition of the polyacrylamide. It was found that cells grown on stiffened gels proliferated at higher rates than cells cultured on softer gels. This difference was attributed to the activation of integrins/Src/Vav2/RhoA pathway which controls the reorganization of the cytoskeleton of the cell in relation to the actin network. While the culture on softer gels demonstrated inhibition of the Src/Vav2/RhoA pathway, stiffer gels supported more cell proliferation. This study demonstrated that crosstalk within the microenvironment of the vasculature could aid in actin redistribution permitting increased cell proliferation within cultures grown on stiffened gel matrices (Yeh *et al.,* 2012). In addition to these growth studies, cultures grown on substrate matrices have been investigated in relation to fluid shear stress. Kohn *et al.,* (2015) demonstrated that endothelial cells grown on softer gel matrices became more elongated when placed under shear stress.

The use of polyacrylamide gels was also employed by Huynh *et al.,* (2011) to investigate the crosstalk between the endothelium and the extracellular matrix as well as leukocyte transmigration. In this study, BAECs and HUVECs were grown

on polyacrylamide gels of increasing stiffness and cells were stained for cadherin (as a gap junction protein) and actin for cellular imaging. It was found that intercellular distance differed significantly depending on the matrix on which the culture was grown, with high stiffness demonstrating the largest separation width between cells as measured by gap junction separation distance. RhoA activation was also investigated through a GTPase activation assay (G-LISA). It was postulated that RhoA is activated due to the increased mechanical stress of the ECM which would then stimulate RhoA kinase (ROCK) to increase cellular contractility by varying actomyosin contraction and cell matrix adhesion, therefore leading to increased gap junction distances between cells. The cultures were found to exhibit increasing amounts of RhoA with increasing gel stiffness that could be inhibited with a ROCK agonist. The cells were then co-cultured with neutrophils to investigate paracellular transmigration and shown that cultures with high RhoA and ROCK activity had increased leukocyte transmigration compared to those cultures treated with a ROCK inhibitor (Huynh *et al.,* 2011).

The collective studies conducted by Wang *et al.,* (2000), Huynh *et al.,* (2011), Yeh *et al.,* (2012), and Kohn *et al.,* (2015), demonstrate that the use of softer extracellular matrices to mimic *in vivo* environments is a viable replacement to traditional culture dishes. Although these studies provide information concerning cellular morphology and proliferation, effects of changes in extracellular matrices on immune-related cell activity is relatively unknown.

As described above, a hardened extracellular matrix brought about by arterial stiffening would impact gap junctional properties and endothelial barrier function (Huynh *et al*., 2011, Krishnan *et al*., 2011), contributing to endothelial dysfunction and possibly inducing pro-inflammatory immune activity. Typically, studies involving endothelial cells, this later stage inflammatory response is generated by stimulation with TNF-α or lipopolysaccharide (Franchi *et al.,* 2008, Marcone *et al.,* 2015) as a way to study endothelial response to stress. However, it can be argued that the use of chemical stimulation induces an exaggerated state of inflammation that does not simulate relevant states of inflammatory distress in endothelial cells.

As previously suggested, the use of other matrices on which to grow endothelial cells can produce models of varying vascular stiffness and can be made through the use of polyacrylamide gels. These levels of stiffness can be related to the degree by which human vessels experience age-related intimal stiffening and used to study endothelial dysfunction (Huynh *et al*., 2011, Kohn *et al*., 2015). By varying concentrations of polyacrylamide and bis-acrylamide within a polyacrylamide gel, varying levels of stiffness can be generated. The concentration of acrylamide to bis-acrylamide correlates to a stiffness that can be measured in kilopascal (kPa) using an atomic force microscope (AFM). The varying ratios of acrylamide and bis-acrylamide have been extensively studied and have been demonstrated to follow Young's Modulus (Fischer *et al.,* 2012, Yeh *et al.,* 2012). Young's Modulus is the theoretical measure of stiffness in accordance with the

pressure change per square centimeter (O'Rourke *et al.,* 2002) and increasing matrix stiffness from 2.5 to 10 kPa is predicted to mimic the age-related stiffening of the ECM in humans. Such a model should, therefore, mimic a range of arterial states from healthy to slightly diseased and even severely diseased arteries to be used in studies of endothelial dysfunction (Kohn *et al.*, 2015). The stiffened matrix will simulate the stiffened ECM in the vasculature and endothelial cells grown on such a range of substrate stiffness might begin to show characteristics of distress that characterize a response to endothelial dysfunction, including cytokine release.

1.7. Objectives

1.7.1. Characterization of Nitric Oxide Liberation by Bioactive Peptides in an Endothelial Cell Culture Model

Previous studies have linked consumption of fermented dairy products to a decrease in the risk factors of cardiovascular disease (Soedamah-Muthu *et al.,* 2011; Sonestedt *et al.,* 2011). Additionally, two small bioactive peptides (VPP and IPP) have demonstrated the ability to liberate nitric oxide in a HUVEC culture (Hirota *et al.,* 2011). The first objective was to further characterize the bioactivity of twelve antihypertensive peptides by comparing the relative the nitric oxide liberating capabilities.

1.7.2. Characterization of Behavioural Response of HUVECs to Growth on Stiffened Extracellular Matrices

Evidence to further support and define endothelial cell culture models that use gel extracellular matrices as more physiologically relevant is needed (Wang *et al.,* 2000, Yeh *et al.,* 2012 and Kohn *et al.,* 2015). Therefore, the second objective of this study was to more fully characterize the morphological appearance, growth behavior and immune related activity of HUVEC cells grown on polyacrylamide matrices.

2. METHODOLOGY

2.1. Cell Culture

The HUVEC cell line was obtained from Thermofisher (MA, USA) and was maintained in MCDB-131 media supplemented in accordance with the findings of Terramani *et al.* (2000). Briefly, basal media was supplemented with 20% fetal calf serum (FCS), 1mg/mL epidermal growth factor (EGF), 50µg/mL hydrocortisone, 10000 units/mL penicillin, 10mg/mL streptomycin, 50µg/mL heparin (all Sigma-Aldrich, MO, USA), 50µg/mL Endothelial Cell Growth Supplement (ECGS) (Corning, NY, USA) and 10mM L-Glutamine (Lonza Group, Switzerland). HUVEC growth medium was changed every three days. Cells were grown on collagen coated 25cm^2 culture flasks at 37^{o}C, 5% CO_2 in a humidified incubator (Thermofisher, MA, USA). To collagen coat, each flask, rat tail type II collagen (EMD Millepore, MA, USA) was diluted to 10ug/cm^2 in 0.02M acetic acid and 1.5mL/25cm^2 of this solution was then added to each culture flask. The collagen was allowed to adhere to the culture flasks for a minimum of 1 hour under UV light in a biosafety cabinet. The flasks were then washed three times with PBS. As the final wash, 2mL/25cm^{2,} PBS was added to the culture flask and placed under UV light in a biosafety cabinet for a minimum of 1 hour to allow for sterilization (Adapted from Sitterley, 2008). Cells were passaged at approximately 80% confluency by first aspirating spent media and washing once with room temperature PBS before adding 3mL of trypsin-EDTA (Sigma- Aldrich, MO, USA)

into the flask. Trypsin was allowed to wash over the monolayer momentarily, 1.5mL was then removed, and the culture flasks were returned to the incubator for 2 minutes to detach cells. Trypsin was then neutralized by the addition of 5mL of HUVEC cell culture media to the flask. Cells were collected and centrifuged at 220 x *g* for 5 minutes. Follow centrifugation, the supernatant was removed and the pelleted cell culture was resuspended in 1mL of HUVEC culture media. A trypan blue exclusion assay was performed to ascertain cell count and cells were seeded at assay specific concentrations.

HUVEC cells are a primary cell line obtained from a pooled population of umbilical veins harvested 14 days or less from a newborn (ThermoFisher, MA, USA). The doubling of HUVEC cultures grown on collagen coated flasks is approximately 48 hours (Terramani *et al.* 2000), with a limited number of doublings once cells are defrosted and plated. All experiments were done on passage 2 – 4, which corresponds to the limit of population doublings as recommended by ThermoFisher.

2.2. Synthesized Peptides

A list of bioactive peptides that were previously characterized and published based on antihypertensive or immunomodulatory activity was obtained from Adams *et al.*, 2015 (Table 1). The highly characterized VPP and IPP were previously assessed for their ability to liberate NO from cell culture and nine other

peptides were chosen for comparison. Synthesized peptides were obtained from Bio Basic Inc. (Markham, ON.)

From these stock solutions, working concentration of 10µmol/L were prepared and used to assess NO liberating abilities on cultured HUVECs.

Table 1. Synthesized peptide sequence, molecular weight and reference source of β-casein derived peptides from fermentation by *Lactobacillus helvicus*

ID#	Peptide Sequence	MW (g/mol)	Reference
P1	VPP	311.38	Nakamura *et al.*, 1995
P2	IPP	325.41	
P3	HQPHQPLPPT	1151.30	Tellez *et al.*, 2010
P4	WMHQPHQPLPPT	1468.71	
P5	LYEQPVLGPVR	1270.51	
P6	LDQWLCEK	1034.20	
P7	YP	278.31	Yamamoto *et al.*, 1999
P8	PGPIPN	593.69	Bourtrou *et al.*, 2013
P9	FFVAP	579.70	Yamamoto *et al.*, 1997
P10	KVLPVP	651.85	Maeno *et al.*, 1996
P11	KVLPVPQ	779.99	

2.3. Nitric Oxide Liberation Assay

Nitric Oxide liberation was assessed by employing a Griess colourimetric reaction that measures total nitric oxide; all reagents were prepared as per manufacturer's directions (Enzo Life Sciences, NY, USA). The Griess colourimetric reaction is based on the formation of an azo-dye that can be spectrophotometrically quantitated; this azo dye is formed by the coupling of N-(1-naphthyl) ethylenediamine and diazonium salt (Green *et al.*, 1982). The diazonium salt is generated by sulfanilic acid reacting with nitrite in solution, which is a direct indication of the amount of nitrite, or NO, within the sample.

For each experiment, 96-well collagen coated culture plates (Corning, NY, USA) were seeded with 3500cells/cm^2 and allowed to culture and attach for 20 hours; this was chosen based on initial investigations where NO liberation at 20 hours was found to be highest compared to 18 hours and 24 hours (data not shown). Once the set incubation time had elapsed, the cells were treated for 1 hour with 10µmol/L of the peptides in HUVEC medium. Treatment length of 1 hour was chosen based on the research of Hirota *et al.,* (2011), which showed no significant difference between treating HUVECs for 1 hour versus 2 hours with VPP and IPP. Control wells were treated with fresh HUVEC medium. Upon completion of the Griess reaction, the plates were read at 540nm wavelength using a Synergy HTTR microplate reader (Bio-Tek Instrumentation, VT, USA).

Later investigations took into account the level of arginine in the HUVEC medium. Arginine free DMEM medium was used to minimize the level of arginine that could act as a substrate to verify that NO being liberated by the HUVECs was due to the bioactive peptides. However, the cells were unable to survive for the 1 hour incubation period. Therefore, this methodology was abandoned and studies resorted to the previously outlined protocol.

2.4. Stiffness Controlled Extracellular Matrix

Extracellular matrices were manufactured in-house according to the protocol outlined by Fischer *et al.,* (2012); a general schematic could be seen in Figure 3. Matrix stiffness of 2.5kPa, 3kPa, 10kPa, and 30kPa were chosen. As outlined by Galie *et al.,* (2015), 2.5kPa would be below the pressure experienced by the normal vasculature; thus acting as a control. Gels exhibiting a stiffness of 3kPa would mimic the healthy vasculature, while 10kPa and 30kPa would allow for the simulation of the progressively diseased vasculature.

Coverslips were dried by flaming off ethanol and placed into a Wash-N-Dry™ coverslip rack (Sigma-Aldrich, MO, USA). The coverslips were then soaked in a 0.5% (3-aminopropyl) trimethoxysilane (in ddH_2O) for 30 minutes under agitation. The slips were then washed in six changes of ddH_2O and allowed to dry at 50^oC. The coverslips were then cooled to room temperature to ensure that a thin, stable layer of silane was present on each glass coverslip (Gunda *et al.*, 2014). Once cooled the slips were treated with a 0.5% glutaraldehyde in 1xPBS for an additional 30

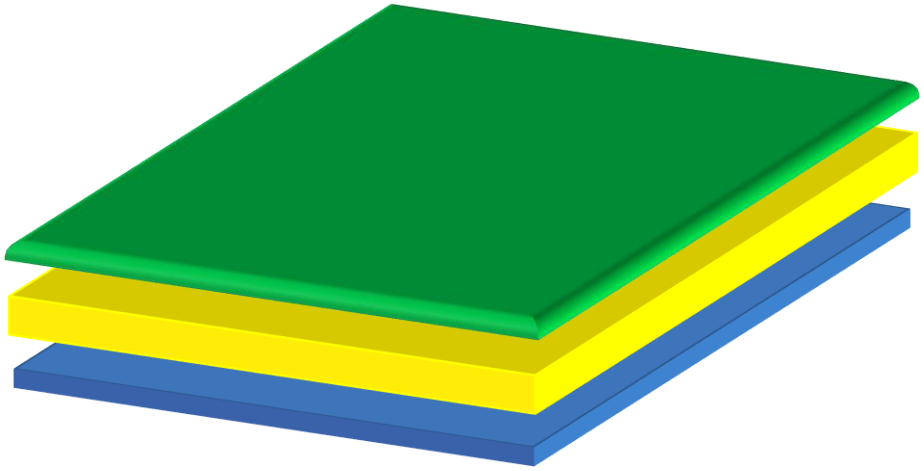

Legend	
	Activated coverslip
	Polyacrylamide gel
	Collagen

Figure 3. Schematic of polyacrylamide overlaid on top of an activated coverslip, further treated with collagen to allow for cell attachment and growth.

minutes under agitation. The coverslips were then washed in three changes of ddH_2O and allowed to air dry on a bench. By treating the layer of silane with glutaraldehyde, a Schiff base functional aldehyde intermediate is formed allowing for immobilization of biomolecules (MacMillan, 2009) – in this instance the polyacrylamide gel was bound to the coverslip due to this activation.

Polyacrylamide (PAC) gels were then made with differing volumes of acrylamide and bis-acrylamide (Sigma-Aldrich, MO, USA) to simulate differing stiffness (Table 2.). The gels were cast on Rain-X treated microscope slides – done in order to ensure a hydrophobic surface and therefore allow the gels to adhere to the coverslip; 12µL of the PAC gel activated with TEMED and APS was then added onto the surface of the slide and the cover slip was gently lowered onto the gel allowing for the gel to disperse onto the entire surface of the coverslip. The PAC gels were allowed to polymerize for 1 hour, the slides were placed in a petri dish and the surface of the slides was flooded with 50mM HEPES, pH 7.5. Using a scalpel the coverslips were gently dislodged from the surface of the slide; the coverslips were then washed in three changes of 50mM HEPES.

The coverslips were then placed on an inverted petri dish and covered with parafilm. In order to crosslink an extracellular matrix (ECM) suitable for cell culture, the PAC gels were treated with sulfo-SANPAH (Sigma-Aldrich, MO, USA) under UV light for 8 minutes, after which the coverslips were then washed twice in PBS. This treatment with sulfo-SANPAH was done twice to ensure that

the PAC gel was sufficiently covered. A 10µg/cm^2 solution of rat tail type II collagen (EMD Millipore, MA, USA) was then added to the bottom of a parafilm-covered petri dish and the coverslips were placed on top of the collagen (PAC side down). Treatment with sulfo-SANPAH allows for cross-linking through the amine reactive group which will adhere to the PAC gel and when placed under UV light, the photo-reactive non-specific nitrophenylazide group will be cleaved allowing for collagen to attach.

The coverslips were allowed to crosslink overnight, after which they were washed twice with PBS and sterilized under UV. All gels were used within one week of manufacture.

Table 2. Volume of acrylamide and bis-acrylamide used to produced 1000µL of stiffness controlled PAC gel (Galie *et al.,* 2015)

Stiffness (kPa)	**Volume of Acrylamide (µL)**	**Volume of bis-Acrylamide (µL)**
2.5	979	10
3	976	13
10	977	12
30	966	23

2.5. Cell Population Imaging

HUVECs cultured in 25cm^2 culture flasks to 80% confluence cells were lifted and seeded onto the stiffness controlled ECM at a cell concentration of 4000 cells/cm^2. Spent media was collected every three days over the course of a nine-day growth track. After collecting spent media the cells were fixed using a 2% paraformaldehyde solution, pH 7.0, for 10 minutes (Sigma-Aldrich, MO, USA), after which the coverslips were washed 3Xwith PBS. The fixed cells were then stained with safranin (Oxoid, Nepean, ON) for 1 minute and destained using ddH_2O. The coverslips were then placed PAC gel side down onto a microscope slide using ddH_2O as a mounting medium. The edges of the coverslips were then sealed using clear nail lacquer. The coverslips were then imaged using the Panoptiq microscope (ViewsIQ, Richmond, BC) which allows for an image of the total growth area to be rendered. The settings for the Panoptiq microscope were set to 10x magnification with high scanning capabilities to ensure that images were rendered at 1080p.

2.6. Cell Growth Metrics

Once total growth images were obtained, total cell number, total cell area on each slide and single cellular area measurements were collected using Image J software (NIH, MD, USA). Each image was cropped to an area of 13176µm x 13176µm and toned to gray using the software threshold function (set to ~98%). This allows for the image to be split into two classes of pixels, essentially splitting

the image into foreground and background. Cells, which would be in the foreground would be below 98% and therefore toned to black and objects in the background would be above 98%, and would then be toned to white, thus allowing for the elimination of background noise while simultaneously enhancing cell visibility. Area threshold was set to 10-1000μm^2 further allowing for the elimination of debris. Cell counts and area were collected and analyzed for each day and matrix stiffness.

2.7. Cytokine Quantification

Enzyme-linked immunosorbent assays (ELISAs) were carried out in order to quantify Human IL-6 (R&D Systems, Catalogue# DY206), MCP-1 (R&D Systems, Catalogue# DY279), and sICAM-1 (R&D Systems, Catalogue# DY720) from spent media collected through each growth track for each matrix stiffness. The capture antibodies were coated onto 96-well high-binding Microlon 600 ELISA plates (Greiner Bio-One, NC, USA) and allowed to incubate overnight at 4^{o}C. The plates were then washed according to R&D Systems specifications and the samples were loaded onto the plates and incubated at room temperature for 2 hours. Following incubation, the plates were washed and a detection antibody was added for an additional 2 hours, after which the plates were again washed and treated with horseradish peroxidase (HRP)-conjugated streptavidin for 20 minutes in the dark. The plates were washed once again and the substrate to HRP-conjugated streptavidin (3,3',5,5'-tetramethylbenzidine (TMB) (Sigma-Aldrich, MO, USA))

was then added to the plates for 20 minutes in the dark. The reaction was stopped with 2 N H_2SO_4 and the plates were gently shaken and read at a wavelength of 450nm using a Synergy HTTR microplate reader (Bio-Tek Instrumentation, VT, USA).

2.8. Statistical Analysis

Statistical analysis was done using SPSS (IBM, NY, USA) using a significance of $p<0.05$. For nitric oxide liberation and investigation of cell area, a non-parametric Mann-Whitney U test was performed. To further define the nitric oxide liberating abilities of these bioactive peptides η^2 was found for each peptide. This was done as described by Coolican (2009). A one-way ANOVA was used to analyze cell count, overall cell area and differences in cytokine production, once again a Mann-Whitney U test was done to disseminate differences in individual cell area between treatments. All data was graphed using Prism by GraphPad Software, Inc. (La Jolla, CA, USA).

3. RESULTS

3.1. Nitric Oxide Liberating Abilities of Bioactive Peptides.

The ability of eleven separate peptides (Table 1) to enhance liberation of the small signaling molecule NO from HUVEC cells in culture was investigated by incubating the cells with a 10μM solution of each peptide for one hour. Levels of NO were measured and recorded using an assay that colourimetrically indicates the level of nitrites within the spent media. A Mann-Whitney U-test for nonparametric data was used to compare the relative NO concentrations (%) in the spent media from each treatment after the incubation time had elapsed. NO liberated from HUVEC culture from each bioactive peptide treatment group did not differ significantly when compared to the untreated group (Figure 4.). NO liberated by the previously uncharacterized peptides WMHQPHQPLPPT, LYEQPVLGPVR, LDQWLCEK, YP, PGPIPN, FFVAP, KVLPVP, KVLPVPQ was then compared to the NO levels liberated by peptides 2 (VPP) and 3 (IPP), as these peptides have previously been reported to increase NO liberation by ~50% in a HUVEC culture (Hirota *et al*., 2011). Once again the relative NO concentrations did not differ significantly. By using the η^2 method to calculate the effect size for each peptide compared to the untreated group, it was found that, overall, up to 10.5% of the NO liberated by the HUVEC cultures could be attributed to the presence of each peptide.

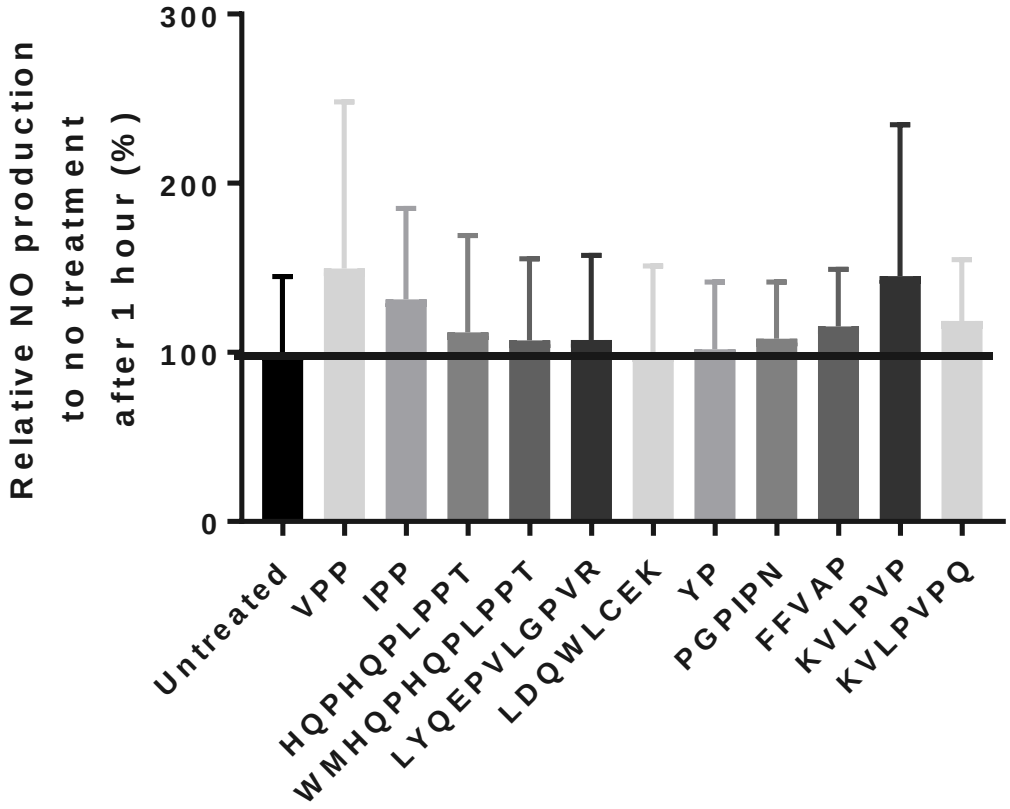

Figure 4. HUVEC were cultured with 10μM of each peptide in MCDB131 enriched media for 1 hour (n=6). Data shown are the relative nitric oxide amounts produced by each cell culture as a percentage of the untreated. Where the horizontal line at 100 represents the average nitric oxide produced while untreated. Statistical analysis was performed using Mann-Whitney U test ($p>0.05$).

3.2. Characterization of HUVECs Grown on Stiffened PAC Matrices – Growth Metrics

3.2.1. Cell Growth Metrics

To determine the effects of stiffened matrices on the growth behavior of endothelial cells in culture, HUVECs were grown on four different gels that simulated stiffness of 2.5kPa, 3kPa, 10kPa, and 30kPa. At 3, 6 and 9 days after the initial cell seeding the cultures were fixed, stained and visualized using digital microscopy. Sample images can be found in Appendix C.

3.2.2. Cell Count

Cell counts taken from each slide using the Image J software were analyzed for differences over time and differences between stiffness using a one-way ANOVA. Results showed a significant increase only for the day 6 treatment group where 30kPa cell count was significantly greater than other stiffnesses. (Figure 5). Although an overall increase in cell number was generally observed over all stiffness treatments, the rate at which each culture grew throughout the experiment was observed to be different due to variation in fold change (Table 3.); Further to this, it was observed that fold change increased in the softer, more compliant matrices of 2.5kPa and 3kPa by a factor of 0.345 and 1.062 respectively; however, on the stiffer matrices fold change was found to decrease at days 6-9

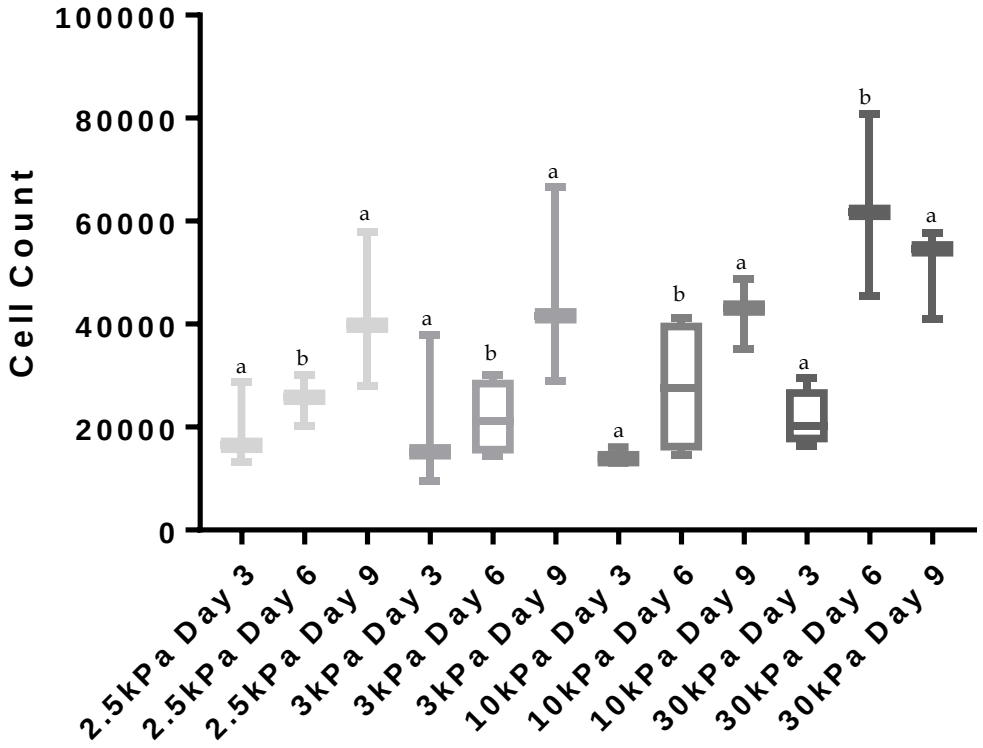

Figure 5. Comparison of cell count between stiffnesses across days; HUVEC cell count after 3, 6 and 9 days of incubation on varying PAC gel stiffness; with enriched MCBD 131 media at 37°C with 5% CO_2 (n=3-4). Cells imaged using Panoptiq digital imaging (ViewsIQ, Richmond, BC) and counted using Image J (NIH, MD, USA). 'a' denotes no statistical significance while 'b' represents statistically significant cell counts, as determined using a one-way ANOVA ($p<0.05$) and Tukey's multiple comparison tests. Cell counts found at day 6 at stiffness 30kPa was found to be statistically higher when compared to cell counts of other stiffness at the same time point.

Table 3. Fold change in HUVEC cell count between day 3-6 and day 6-9. Cells imaged using Panoptiq digital imaging (ViewsIQ, Richmond, BC) and counted using Image J (NIH, MD, USA). (n=3-4)

Stiffness Group	**Fold Change**	
(kPa)	Day 3-6	Day 6-9
2.5 (control)	1.305	1.650
3	1.040	2.102
10	1.939	1.524
30	2.908	0.816

compared to days 3 and 6 (Table 3). Specifically, for 10kPa and 30kPa, the fold increase was 1.939 and 2.908, respectively, for days 3-6 compared to 1.524 and 0.816, respectively, for days 6-9 (Table 3).

3.2.3. Cell Area

Cell areas were measured from specimens that fit the limits of threshold and particle size specifications in Image J. Normality tests were initially performed to investigate whether the area values were bimodal, perhaps indicating two distinct cellular area groups. It was found that the cell areas were positively skewed towards smaller values with the modes being 10.12μm^2 for days 3 and 6 and 2.24μm^2 for day 9 for all treatment groups.

A Mann-Whitney U test of nonparametric data was then performed to further define differences in cell areas between the extracellular matrices for each time point. Each treatment (3kPa, 10kPa, and 30kPa) was compared to the area of cells grown on 2.5kPa matrices. Using the rank means of each data set, cell areas differed significantly from each other at each time point ($p<<0.05$). Cell areas calculated from cells grown on softer gels were greater than those from cells grown on the stiffest gels; with the exception of 10kPa matrices (Table 4).

In order to understand how much total area was taken up on each slide by the cells at each stiffness (cell coverage), the average total area occupied by the HUVEC culture (n=3-4) was calculated (Figure 6). A one-way ANOVA was done.

Table 4. Mean cell area of fixed and stained HUVECs grown on various stiffened extracellular matrices. Cells imaged using Panoptiq digital imaging (ViewsIQ, Richmond, BC) and counted using Image J (NIH, MD, USA). Statistical Analysis was done using a Mann-Whitney-U test ($p<0.05$) (n=3-4)

Stiffness Group (kPa)	**Mean Cell Area (μm²)**		
	Day 3	Day 6	Day 9
2.5 (control)	103.966 ± 138.075	92.133 ± 107.813	108.067 ± 117.213
3	84.618 ± 119.775	105.266 ± 142.891	92.673 ± 109.992
10	120.643 ± 139.991	101.906 ± 127.531	117.753 ± 138.362
30	86.597 ± 105.684	56.844 ± 114.781	106.805 ± 128.611

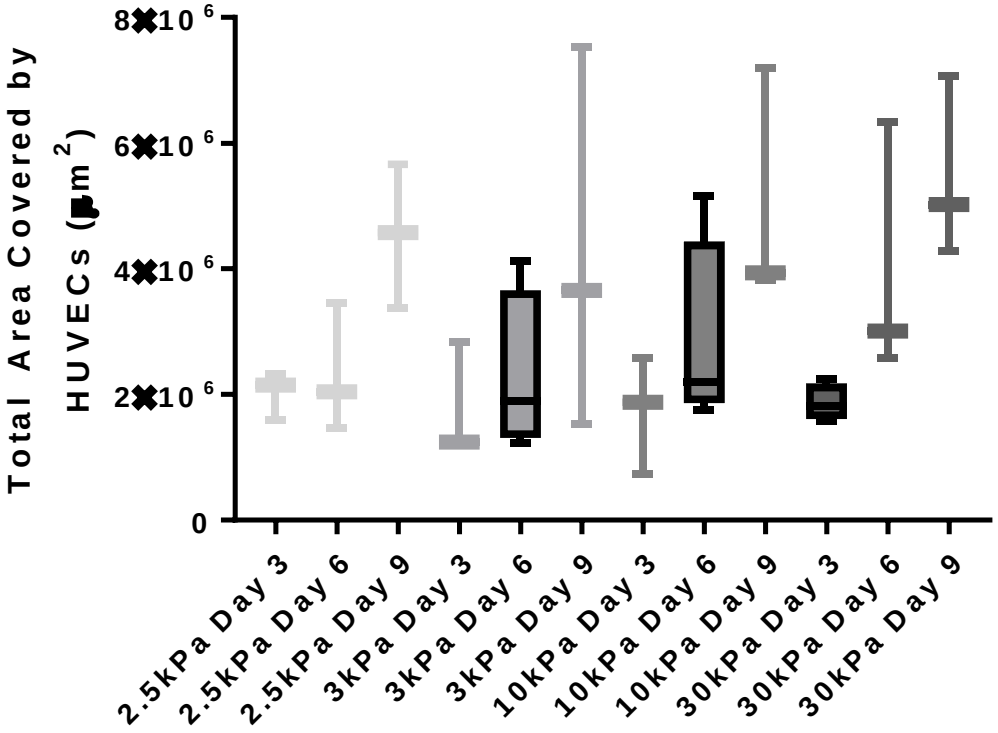

Figure 6. Comparison of the total area occupied by HUVECs after 3, 6 and 9 days of incubation on varying PAC gel stiffness; with enriched MCBD131 media at 37°C with 5% CO_2 (n=3-4). Cells imaged using Panoptiq digital imaging (ViewsIQ, Richmond, BC) and measured using Image J (NIH, MD, USA). Statistical analysis was done using a non-parametric Mann-Whitney U test comparing stiffness at a given time point to 2.5kPa (Control) of the same time point ($p<0.05$).

with Tukey's Post Hoc analysis for between-group comparisons. Although the total area occupied increased with time, there was no difference between groups. The fold increase in the area occupied by cells at each stiffness was calculated between days 3-6 and 6-9. Although the softer matrices (2.5kPa and 3kPa) were found to have a higher fold increase in the total area occupied, the fold increase of the stiffer matrix (30kPa) was found to decline with the progression of time, and there was no change in fold increase for the 10kPa matrix (Table 5).

3.3. Characterization of HUVECs Grown on Stiffened PAC Matrices – Release of Cytokines

To further examine the impact of culturing cells on a stiffened matrix, ELISA assays were performed to measure IL-6, MCP-1, and sICAM-1 production.

3.3.1. IL-6

Measured cytokine levels were standardized using the mean cell count for each relative stiffness to express the amounts released as relative ng/mL/cell. The cytokine levels were then summated to allow for regression analysis using a one-way ANOVA. It was found that the relative levels of IL-6 production did not differ significantly amongst stiffness conditions; however, when levels of IL-6 were compared between 3kPa and 30kPa it was found that a trend towards significance was observed, where cultures grown on 30kPa gels produced slightly higher levels of IL-6. When cytokine levels were compared over time, an increase in IL-6

Table 5. Fold change in total area occupied by HUVECs between day 3-6 and day 6-9. Cells imaged using Panoptiq digital imaging (ViewsIQ, Richmond, BC) and counted using Image J (NIH, MD, USA). (n= 3-4)

Stiffness Group	**Fold Change**	
(kPa)	Day 3-6	Day 6-9
2.5	1.149	1.953
3	1.294	1.851
10	1.638	1.761
30	2.130	1.374

production at all stiffness levels was observed. Comparing IL-6 concentration between day 3 and day 6, all groups were found to significantly increase their levels of IL-6 production. When comparing day 6 and day 9, significant differences were found across all conditions with the exception of 30kPa, where the level of IL-6 did not significantly increase (Figure 7).

3.3.2. MCP-1

Measured cytokine levels were standardized using the mean cell count for each relative stiffness to express the amounts released as relative ng/mL/cell. The cytokine levels were then summated to allow for regression analysis using a one-way ANOVA. It was found that the relative levels of MCP-1 did not differ significantly between stiffness conditions at each time point; however, the levels changed between time points for most of the stiffness conditions. Comparing MCP-1 concentration between day 3 and day 6, and day 6 and 9, there was a significant increase in MCP-1 concentration over time with the exception of the 30kPa treatment group where the level MCP-1 production did not differ significantly from day 3 to 6, or 6 to 9 (Figure 8).

3.3.3. sICAM-1

Measured cytokine levels were standardized using the mean cell count for each relative stiffness to express the amounts released as relative ng/mL/cell. The cytokine levels were then summated to allow for regression analysis using a one-

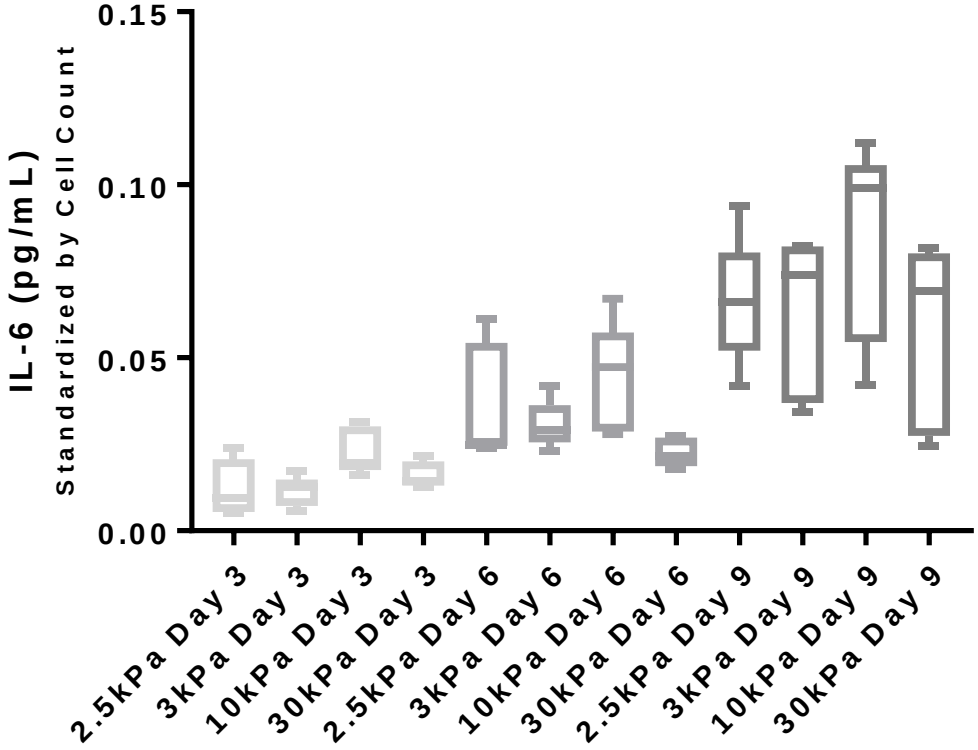

Figure 7. IL-6 production by HUVEC culture grown on stiffened extracellular matrices for 3, 6 and 9 days (n=5). Data represents standardized IL-6 production by average cell count for related treatment groups. Statistical analysis was done using a one way ANOVA comparing stiffness at a given time point to 2.5kPa (Control) of the same time point ($p<0.05$).

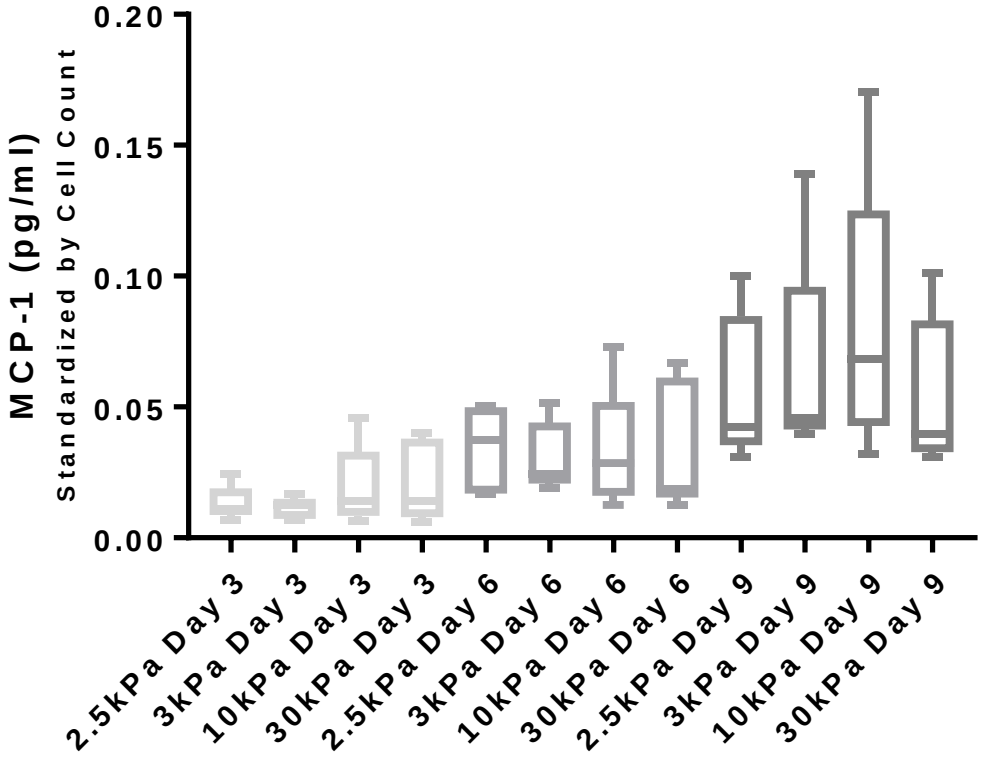

Figure 8. MCP-1 production by HUVEC culture grown on stiffened extracellular matrices for 3, 6 and 9 days (n=5). Data represents standardized MCP-1 production by average cell count for related treatment groups. . Statistical analysis was done using a one way ANOVA comparing stiffness at a given time point to 2.5kPa (Control) of the same time point ($p<0.05$).

way ANOVA. It was found that the relative levels of sICAM-1 did not differ significantly between stiffness conditions at each time point. Additionally, the levels only differed between time points for one of the stiffness conditions. Comparing sICAM-1 concentration between day 3 and day 6, and day 6 and 9, a significant increase was found only in the 3kPa condition (Figure 9), with other stiffness groups not showing significant increases over time.

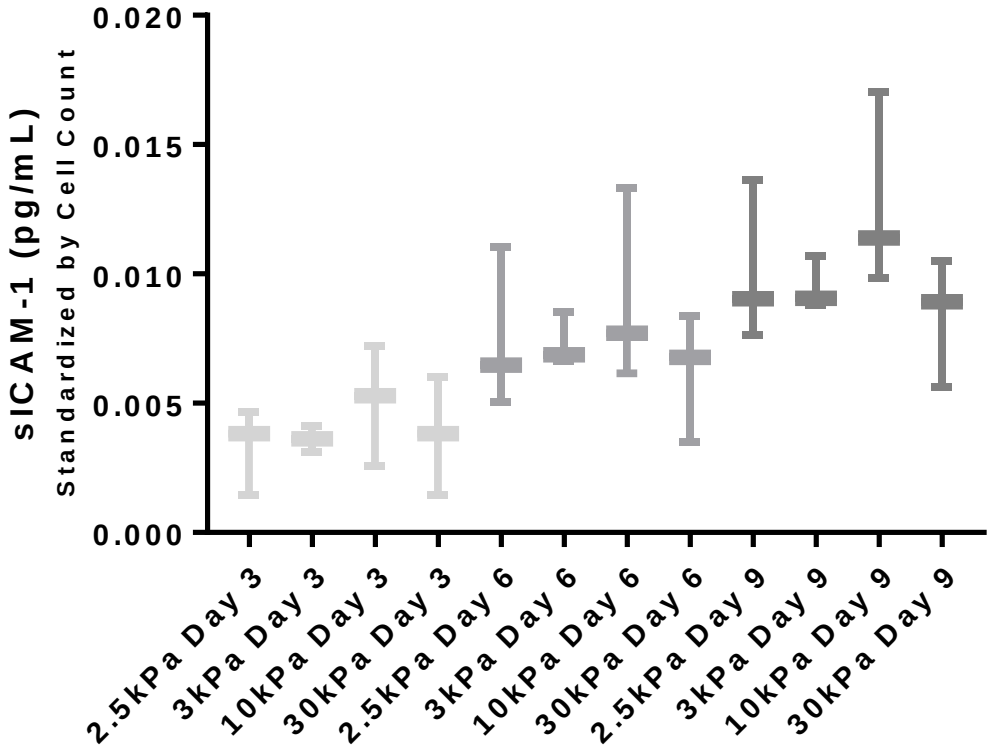

Figure 9. Soluble ICAM-1 production by HUVEC culture grown on stiffened extracellular matrices for 3, 6 and 9 days (n=3). Data represents standardized sICAM-1 production by average cell count for related treatment groups. Statistical analysis was done using a one way ANOVA comparing stiffness at a given time point to 2.5kPa (Control) of the same time point ($p<0.05$).

4. DISCUSSION

4.1. Cell Culture

A mixed culture of HUVECs was purchased from the supplier (ThermoFisher, MA, USA) which represented pooled umbilical vein samples from multiple donors, although single donor cell lines are available. Genotyping of HUVEC samples by short nucleotide polymorphism (SNP) sequencing has allowed researchers to look for polymorphic differences in endothelial cell responses. For example, the NOS3 gene which codes for eNOS has single nucleotide differences in exon 7 which changes glutamic acid to aspartic acid (Hingorani *et al.,* 1995). The effect of this SNP on NO production has been evaluated and has produced controversial results where some have reported lower NO liberation in genotypes carrying the SNP (Plantefeve *et al.,* 1999), and others have reported no difference in between isoforms (Isabel *et al.,* 2010). Due to the uncertainty surrounding atypical results from a single donor, a culture representing a mixed population was chosen. However, it was not determined if the phenotypes in the pooled sample include high (Glu/Glu), low (Asp/Asp) or moderate (Glu/Asp) NO producers and if the response of the mixed culture was effectively a combination of all various responses. Certainly, the response within and between all HUVEC cultures in terms of NO production, growth characteristics and viability was highly variable, even when culture conditions, media, and plating protocols were kept identical. Variation was also observed between cell sample sources; for

example, samples delivered from AllCells (California, U.S.A.) had markedly different culture adherence and proliferation characteristics (cell doubling time) than HUVECs obtained from ThermoFisher, prompting our repeated purchase of only batch number 1391153 for all subsequent experiments in order to maintain as much consistency as possible.

4.2. Nitric Oxide Liberation by Bioactive Peptides

Bioactive peptides derived from the fermentation of α-casein have shown to have a range of action on the endothelium through antihypertensive actions, immunomodulatory effects, and NO liberation. Two tripeptides, VPP and IPP, have been shown to exhibit significant antihypertensive properties (Aihara *et al.,* 2005) as well as upregulate the production of NO in culture (Hirota *et al.,* 2011). Beyond these two well-known peptides, a short list of nine other peptides was compiled (Table 1); these peptides have exhibited anti-hypertensive properties (Fitzgerald *et al.,* 2000) including ACE inhibition (Adams, 2015); however, NO liberating capacities of these peptides are yet to be fully understood. NO is liberated through the action of eNOS through converting the amino acid L -arginine to L –citrulline (Cockcroft, 2005). NO then diffuses into the smooth muscle layer within the vasculature and promotes vasorelaxation. As such, it is important to evaluate the nitric oxide liberating capacities of these bioactive peptides in order to obtain a thorough understanding of their bioactivity in relation to healthy endothelial functioning as well as CVD reduction or prevention.

The current study demonstrates that while the bioactive peptides have no statistically significant influence on liberating NO from the HUVEC culture, there was a wide range of responses by individual cultures (Figure 3). It was also found that while some peptides had very little effect, others accounted for up to 10.5% of the NO liberated from culture. The remaining NO could be attributed to the conversion of L –arginine present within the basal media. Since the basal media was estimated to contain 360μM of L –arginine, attempts were made to counter this by including a separate NO liberation assay performed on cells starved of L –arginine for 1 hour with Dulbecco's Modified Eagle Medium (DMEM), high glucose, no glutamine, no lysine, no arginine (ThermoFisher, MA, USA). The media was supplemented to match specifications of the MCDB131 basal media, however, serum was omitted due to the increased glucose levels within the DMEM media. The cells were unable to survive the one-hour incubation in the absence of L–arginine, and serum.

Looking more closely at the levels of NO liberated (Figure 3), VPP, IPP, and KVLPVP are seen to liberate slightly more NO from the culture when compared to the other peptides. In our studies, VPP and IPP demonstrated similar NO liberating capabilities when compared to the findings of Hirota *et al.,* (2011) where these peptides liberated ~50% more NO than basal media control treatment. This disparity could be account for by differences in cell culturing methods; since Hirota *et al.,* (2011) used single donor HUVECs it is unclear whether their results

are based on low, high or moderate NO producers related to SNPs that may be present. Hirota *et al.,* (2011) also allowed cultures to reach confluency prior to treating with peptides whereas in the present study cultures were allowed to proliferate for up to 24 hours. These three peptides, interestingly, all contain a C-terminal proline. The structure of proline is unique in that its side chains are cyclized onto the backbone nitrogen atom; when there are multiple prolines in the peptide structure a PPII helix is formed (Kay *et al.,* 2000). This structure allows for the residues to be on the same face and interact with proteins. This structure has previously been shown to interact with the SH3 domains of the PI3K regulatory subunit. This is interesting to note because eNOs activity and NO production in endothelial cells has been shown to be due to the activation of PI3K signaling through the insulin dependent pathway (Montagnani *et al.,* 2002). Therefore, it could be hypothesized that peptides demonstrating a PPII helix could interact with PI3K initiating the pathway leading to increased levels of NO. Longer culture periods in the presence of these peptides would be needed in order to observe activation of this signaling pathway resulting in increased eNOs activity.

A separate mechanism for NO liberation could be employed by peptide 9 (LYQEPVLGPVR), in that this peptide could act as a nitric oxide donor due to its C-terminal arginine. This arginine would donate its guanidinium ring to be citrullinated by eNOS and liberate NO. This use of additional arginine has been shown to contribute to the synthesis of NO. In a study by Balijepalli *et al.,* (2015)

epithelial cells were cultured with arginine-rich low molecular weight peptides derived from protamine. It was found that the peptides were able to generate a 0.2 fold increase in nitric oxide production over control culture, demonstrating the ability of culture to take up additional arginine and employ it in the generation of NO. In our study, excess arginine in the culture media may have obscured individual NO generating capacities of the peptides and higher levels of arginine-rich peptides were not explored.

4.3. Characterization of HUVECs Grown on Stiffened PAC Matrices – Growth Metrics

Under traditional culture conditions, HUVECs have been demonstrated to have a population doubling time of 48 hours (Terramani *et al.,* 2000). However, an investigation into how HUVECs behave when grown on substrates of varying stiffness are just coming to the forefront of endothelial research (Wang *et al.,* 2000, Huynh *et al.,* 2011, Yeh *et al.,* 2012, and Kohn *et al.,* 2015). Therefore, it is important to characterize how HUVECs grow and respond over time when grown on these extracellular matrices.

The current study indicates that cell growth was impacted by the stiffness of the ECM, with the highest stiffness (30kPa) treatment group on day 6 displaying significantly more cells than the lower stiffness groups. In this instance, it was found that all other treatment groups were statistically lower in cell count when compared to this treatment group (Figure 4). The results found in the current

study support the findings of Yeh *et al.*, (2012) where endothelial cells grown on stiffer matrices demonstrated increased levels of proliferation while endothelial cells grown on softer matrices exhibited lower proliferation rates. This difference in proliferation rate could be accounted for through mechanical forces sensed by integrins within the cell membrane. Integrins have been demonstrated to form unstable bonds with extracellular matrices that normally promote cellular attachment. Some of these bonds are strong and long lasting while other are easily broken by low mechanical forces (Danen *et al.,* 2002). These force-sensitive integrins were investigated by Yeh *et al.*, (2012) for their role in activation of the RhoA pathway in endothelial cells grown on increasing PAC stiffness. They proposed that increased cell proliferation was due to activation of the RhoA pathway as a result of integrin force sensing detected in cells grown on higher stiffness. In a study by Huang *et al.,* (1998), it was reported that p27 – a cyclin-dependent kinase (CDK) inhibitor – was upregulated in cells grown on lower stress matrices. This increase in p27 was correlated to cell arrest in G1 phase, thereby halting mitosis. p27 is phosphorylated and degraded through cyclin E/CDK2 which is a downstream signaling molecule of RhoA (Hu *et al.,* 1999). Therefore, it is suggested that the increased activation of RhoA in cells grown on stiffer matrices allows for the activation of E/CDK2 which actively degrades p27 and allows cells to progress through the G1/S gateway.

In order to look at cell growth rates in our experiments, fold change between time-points was compared (Table 3). Interestingly it was found that on softer matrices (2.5kPa and 3kPa) fold change was found to increase as time progressed, perhaps indicating normal HUVEC population doubling and maintained viability. In contrast, there is a decrease in fold change in cultures grown on stiffer matrices. This could indicate cell culture decline and slower population doubling over extended growth on stiffer matrices (day 6 – 9). It is proposed that the increase in cell number stimulated by the higher stiffness may cause a faster population doubling, limiting HUVEC viability and/or induce culture senescence on days 6-9. This increase in proliferation is likely due to the external mechanical forces exerted on the culture by the stiffness of the gels as reported by Yeh *et al.* (2012).

Mean cell area was also found to differ between treatment groups across the days (Table 5), however, the results are varied in terms of response to stiffness. In most cases, cellular areas from the 2.5kPa control group were found to be larger than the cellular areas of the other treatment groups (3kPa, 10kPa, and 30kPa) indicating smaller cell areas with increasing stiffness. Overall it was found that cells grown on stiffer matrices exhibited higher cell count with generally smaller cells areas. These two characteristics may be due to the activation of the RhoA pathway and the resulting actin redistribution that leads to differences in the location of actin stress fibers in cells grown on matrices of varying stiffness. Peripheral actin stress fiber distribution is observed in cells grown on softer

matrices, while actin stress fibers become distributed more centrally in cells grown on stiffer matrices due to RhoA activation (Yeh *et al.,* 2012). The authors of the study discuss peripheral distribution of actin on softer matrices as conferring isotonic tension in cells, where the cells become distended but tension remains the same, while cells were grown on stiffer matrices with higher central actin distribution experience isometric tension, where tension across the cell changes but the size of the cell remains the same. Huang *et al*., (1998) suggest that it is the increase in this isometric tension that increases the proliferative abilities of cells.

Cells grown on stiffer matrices have also been reported to have fewer junctional complexes and are less able to withstand force (Krishnan *et al.,* 2011). The decrease in cell – cell connections may be another stimulus for cell proliferation on higher stiffness matrices. Under normal conditions, the process of contact inhibition halts cell growth, once cells come into contact with each other (Kim *et al.,* 2011). Without contact inhibition on the stiffer matrices, proliferation would be greater. Therefore, the slower growth and larger cell areas of the cells grown on softer matrices may more closely resemble cell behavior *in vivo*. Specifically for endothelial cells, these cell-cell connections are crucial to their barrier function (Huynh *et al.,* 2011) without which immune cells can begin to infiltrate underneath the endothelial cell layer. With higher cell number and smaller cell areas, cells in this study grown on the higher stiffness matrices may be

replicating the high cell turnover and increased apoptotic events reported by Wang *et al.,* (2000) in their NIH/3T3 cell model of cells grown on stiffer ECM.

An assay to visualize apoptotic cells in culture on each stiffness would be interesting to add to this study. Beyond this, adding staining procedures to visualize gap junction and E-cadherins to further understand the cell contact and proliferative patterns in HUVECS would be of interest. By furthering this study in these directions, additional measures such as the tendency to cluster and monolayer formation could be mapped allowing for further investigations into HUVEC behavior on stiffened matrices.

4.4. Characterization of HUVECs Grown on Stiffened PAC Matrices – Release of Cytokines

In the vasculature, the endothelial layer functions to sense mechanical changes such as increased blood flow, and cyclical tension. This cyclical tension is characterized by the pulsatile movements of the vasculature in tandem with systolic heartbeat (Lehoux, and Tegui, 2003). When changes occur, the endothelial layer converts the mechanical stimulus to a chemical signal cascade that orchestrates a response (Jufri *et al.,* 2015). When these mechanical stimuli are prolonged and amplified, dysfunction within the endothelial layer begins to occur with this signaling cascade chronically activated. Typically, investigations of atherosclerotic pathways *in vitro* bypass the initiating mechanical stimulus that led to endothelial dysfunction and opt for an inflammatory activation of endothelial

cells through the use of TNF-α or LPS (Franchi *et al*., 2008). When cells are activated with TNF-α, NF-κB translocates to the nucleus of the cell; this then promotes the expression of adhesion molecules – E-selectin, VCAM-1, ICAM-1 – as well as cytokines – IL-6 and IL-8 (Modur *et al*., 1996). However, the concentrations of TNF-α used in these studies may not always mimic *in vivo* environments or the progressive nature of the dysfunction. In order to obtain a more biologically relevant model of the process of endothelial dysfunction in order to study inhibition or amelioration of the inflammatory response pathway, the cultures should be exposed to the initiating mechanical stimulus, such as, exposing endothelial cells to shear stress or culturing on stiffened extracellular matrices. These models would allow for the culture to experience a mechanical source of stress rather than chemically induced activation.

Interleukin-6 (IL-6) is produced to signal the immune system to release monocytes, and guide them towards areas of distress. IL-6 also decreases lipoprotein lipase (LPL) activity and monomeric LPL levels in the plasma. This causes macrophages to increase uptake of LDL, thus perpetuating the formation of foam cells and increasing the load of the atherosclerotic plaque (Kaplanski *et al.,* 2003). In a stretch model, Kobayashi *et al.,* (2003), demonstrated that HUVECs exposed to progressive stretch will increasingly release IL-6 over time until a plateau is achieved; in fact, HUVECs stretched by 150% released a maximum amount of IL-6 after 24 hours. In the present study, although it was demonstrated

that HUVECs increasingly produced IL-6 over the 9 day incubation time, there was no observed difference in IL-6 production between the control and treatment groups. This lack of increase could account for IL-6 production reaching its maximal expression levels. Since spent media was taken on the third, sixth and ninth days, the IL-6 could have reached a plateau. According to Kobayashi *et al.,* (2003) after 24 hours there was no change in the amount of IL-6 expressed in confluent HUVECs stretched by 125% and 150%. However, since there was no statistical difference in IL-6 levels amongst stiffness treatments, it can also be postulated that none of the experimental cells were exhibiting immune related activity. This lack of inflammatory response can be viewed as a positive outcome for the characterization of cells grown on stiffness matrices, as they would not be classified as undergoing inflammatory distress signaling. In this way, the model may be used to further study endothelial permeability and leukocyte transmigration, as investigated by Huynh *et al.* (2011), or furthered by studies concerning oxLDL accumulation, insulin signaling, and eNOS activity.

Intercellular adhesion molecule- 1 (ICAM-1) is expressed on endothelial cell surfaces to allow for leukocyte adhesion. Soluble ICAM-1 (sICAM-1) is the cleaved derivative of this adhesion molecule and has been implicated as a measure of bound ICAM-1 (Witkowska and Borawska, 2004). Once leukocytes bind to the endothelium they transmigrate to the smooth muscle layer; this transmigration is assisted through the production of monocyte chemoattractant protein- 1 (MCP-1).

MCP-1 is produced byendothelial cells as well as smooth muscle cells; the difference in the level of release creates a chemoattractant gradient which allows for bound leukocytes to transmigrate the endothelial layer and begin clearing foreign bodies; typically oxLDLs (Hansson and Libby, 2006).

Activation of MCP-1 and sICAM-1 is typically through NF-κB signaling, where NF-κB is upregulated by TNF-α. In a study by Wagner *et al.,* (2009), the upregulation of MCP-1 and sICAM-1 in endothelial cells can occur independently of TNF-α due to the presence of H_2O_2 as an activator of NF-κB signaling. Cyclic stretch increases the activity of NADPH oxidase (NOX2) which increases the formation of O_2^- which is readily converted to H_2O_2, this then accumulates in the vasculature (Wagner *et al.,* 2009). The accumulation of H_2O_2 then promotes the activation of NF-κB which subsequently activates expression of MCP-1 and sICAM-1. In the present study, MCP-1 and sICAM-1 production were found to steadily increase over the course of time. However, the differences found between stiffness groups were found to not be significant (Figure 7 and 8). This lack of significance could be attributed to media changes, where levels of H_2O_2 were not allowed to accumulate to a level where NF-κB activation would be exaggerated; however, levels of NF-κB activation were not measured in this study.

MCP-1 levels and endothelial cell-cell junctions were investigated by Stamatovic *et al.,* (2003) who showed increasing MCP-1 levels led to reduced gap junctional coupling. However, MCP-1 was directly delivered to the cells in this model for up

to 2 hours. The action of MCP-1 on modulating the cell-cell junctions was found to be caused by downstream effects of the RhoA pathway, where ROCK stimulated actin-myosin interaction for prolonged periods of time causing increased tension across the cell. The increasing levels of MCP-1 seen over the 9 days of culture may have influenced the cell – cell junctional behavior of the HUVECs and contributed to the decline in proliferation rate seen on the stiffer matrices.

Overall, this model indicates that there was no significant amount of inflammatory signaling induced by the increase in matrix stiffness, perhaps indicating that the endothelium does not respond to ECM stiffening with inflammatory cytokine release. This is an unexpected finding due to the reported decline in cell-cell junctional connections (Huynh *et al.,* 2011), as well as the reported NF-κB activation that occurs in cultures stretched on PAC matrices (Kobayashi *et al.,* 2003). It does not appear from our data that the high stiffness gels used in this experiment were sufficient to cause endothelial cell distress as determined by measuring the production of cytokines IL-6, MCP-1, and sICAM-1, although detection of NF-κB activation levels at each stiffness was not measured as an indicator of inflammatory signaling.

Tumor necrosis factor alpha (TNF-α) and monocyte colony stimulating factor (M-CSF) were also measured in this study, however, levels of these cytokines were undetectable.

4.5.Conclusions and Future Directions

In future investigations into bioactive peptide induced signaling by endothelial cells, longer term exposure of cell cultures to proline and arginine-rich peptides could be used to investigated PI3K signaling, eNOS expression levels, and NO liberation. Unfortunately, it is doubtful that the one-hour exposure employed in this study would reveal these longer term impacts of PI3 kinase signaling on endothelial cell function.

Additionally, the use of proline-rich peptides in combination with arginine-rich peptides could be used to explore the potential for a combination of mechanisms that generate endothelial cell responses. In this way, the peptides might employ multiple cardioprotective mechanisms in a synergistic fashion, and these investigations would more closely simulate the presence of multiple bioactive peptides in milk ferment products. Previous studies have shown that consumption of fermented dairy products is able to regulate many mediators of cardiovascular disease. More specifically, studies have shown that ingestion of fermented dairy products can lead to a reduction of intimal thickening (Ivey *et al.,* 2011), can lower hypertension (Aihara *et al.,* 2005), while also acting to reducing inflammatory activities of monocytes (Aihara *et al.,* 2009).

The use of softer matrix substrates to culture cells would appear from this study to encourage and regulate normal HUVEC cell growth. Due to the limits of primary cell culture of HUVECs, the maintained cell growth over 9 days on

softer matrices may be advantageous; it may be that growing on these soft matrices would reduce population doubling time and extend the culture viability of HUVECs. Additionally, these matrices do not induce an overt inflammatory response in the cells, leaving other factors to be investigated as instigators of this type of response.

More experiments are needed to determine if a stiffened ECM contributes to endothelial dysfunction beyond a decrease in cell-cell junctional complexes and higher cell turnover as has been reported. The loss of junctional complexes on stiffer ECM disrupts the barrier functionality, leading to infiltration of blood components, but it may be only the latter that leads to an inflammatory signaling response. Detection of NF-κB signaling levels in cells cultured on high stiffness gels would add to our knowledge of how arterial stiffness and endothelial dysfunction are connected.

5. WORKS CITED

Adams, C. 2015. Analysis of peptide production by Lactobacillus species and evaluation of their antihypertensive and immunomodulatory activities. University of Ontario Institute of Technology, Oshawa, ON, Canada.

Aihara, K., Kajimoto, O., Hirata, H., Takahashi, R., Nakamura, Y. 2005. Effect of powdered fermented milk with Lactobacillus helveticus on subjects with high-normal blood pressure or hypertension. Journal of the American College of Nutrition. 24(4): 257-265

Aihara, K., Ishii, H., Yoshida, M. 2009. Casein-derived tripeptide, Val-Pro-Pro (VPP), modulates monocyte adhesion to vascular endothelium. Journal of Atherosclerosis and Thrombosis. 16: 594-603

Aihara, K., Osaka, M., Yoshida, M. 2014. Oral administration of the milk casein-derived tripeptide Val-Pro-Pro attenuates high-fat diet induced adipose tissue inflammation in mice. British Journal of Nutrition. 112: 513-319

Angeline T, Isabel W, Tsongalis GJ (2010) Endothelial nitric oxide gene polymorphisms, nitric oxide production and coronary artery disease risk in a South Indian population. Experimental and Molecular Pathology. 89(3): 205–208.

Baeyens, N., Shwartz, M. 2015. Biomechanics of vascular mechanosensation and remodeling. Perspective on Cell Biology and Human Health. 27: 7-11

Balijepalli, A., Comstock, A., Wang, X., Jensen, G., Hershenson, M., Zacharek, M., Sajjan, U., Meyerhoff, M. 2015. Enhancement of inducible nitric oxide synthase activity by low molecular weight peptides derived from protamine: A potential therapy for chronic rhinosinusitis. Molecular Pharmaceutics. 12: 2396-2405

Bazzoni, G., Dejana, E. 2004. Endothelial cell-to-cell junctions: Molecular organization and role in vascular homeostasis. Physiological Reviews. 84(3): 869-901

Biswas, P., Delfanti, F., Bernasconi, S., Mengozzi, M., Cota, M., Polentarutti, N., Mantovani, A., Lazzarin, A., Sozzani, S., Poli, G. 1998. Interleukin-6 induces monocyte chemotactic protein-1 in peripheral blood mononuclear cells and in the U937 cell line. Blood. 1: 258-265

Blair, A., Shaul, P., Yuhanna, I., Conrad, P., Smart, E. 1999. Oxidized low density lipoprotein displaces endothelial nitric-oxide synthase (eNOS) from plasmalemmal caveolae and impairs eNOS activation. Journal of Biological Chemistry. 472: 32512-32519

Bobryshev, Y. 2006. Monocyte recruitment and foam cell formation in atherosclerosis. Micron. 37(3): 208-222

Bourtrou, T., Gaudichon, C., Dupont, D., Jardin, J., Airinei, G., Marsset-Baglieri, A., Benamouzig, R., Tomé, D., Leonil, J. 2013 Sequential release of milk proteinderived bioactive peptides in the jejunum in healthy humans. American Journal of Clinical Nutrition. 97: 1314-1323

Cecelja, M., Chowienczyk, P. 2012. Role of arterial stiffness in cardiovascular disease. Journal of the Royal Society of Medicine Cardiovascular Disease. 1(11): 1-10

Chae, C., Lee, R., Rifai, N., Ridker, P. 2001. Blood pressure and inflammation in apparently healthy men. Hypertension. 38: 399-403

Cockcroft, J. 2005. Exploring vascular benefits of endothelium-derived nitric oxide. American Journal of Hypertension. 18: 177s-183s

Coolican, H. 2009. In Research methods and statistics in psychology. United Kingdom. Routledge.

Cybulsky, M., Marsden, P. 2014. Effect of disturbed blood flow on endothelial cell gene expression: A role for changes in RNA processing. Atherosclerosis, Thrombosis and Vascular Biology. 34: 1806-1808

Danen, E., Sonneveld, P., Brakebusch, C., Fässler, R., Sonnenberg, A. 2002. The fibronectin-binding integrins α5ß1 and αvß3 differentially modulate RhoA-GTP loading, organization of cell matrix adhesions, and fibronectin fibrillogenesis. Journal of Cell Biology. 159: 1071-1086

Davies, P., Remuzzi, A., Gordon, E., Dewey, F., Gimbrone, M. 1986. Turbulent fluid shear stress induces vascular endothelial cell turnover in vitro. Proceedings of the National Academy of Sciences of the United States of America. 83: 2114-2117

Davignon, J., Ganz, P. 2004. Role of endothelial dysfunction in atherosclerosis. Circulation. 109(Suppl 1): III-27 - III-32

Deshmane, S., Kremlev, D., Amini, S., Sawaya, B. 2009. Monocyte chemoattractant protein 1 (MCP-1): An overview. Journal of Interferon Cytokine Research. 29(6): 313-326

Díez, J. 2007. Arterial stiffness and extracellular matrix. In Atherosclerosis, large arteries and cardiovascular risk. Edited by Safar, M., Frohlick, E, 76-95 . Elora, ON: Karger Publishers, 2007

Fischer, R., Myers, K., Gardel, M., Waterman, C. 2012. Stiffness-controlled three-dimensional extracellular matrices for high-resolution imaging of cell behaviour. Nature Protocols. 7(11): 2056-2066

Fitzgerald, R., Meisel, H. 2000. Milk protein-derived peptide inhibitors of angiotensin-I-converting enzyme. British Journal of Nutrition. 84 (Supplemental 1):S33-S37

Flögel, U., Decking, U., Gödecke, A., Schrader, J. 1999. Contribution of NO to ischemia-reperfusion injury in the saline-perfused heart: a study in endothelial NO synthase knockout mice. *Journal of Molecular and Cellular Cardiology. 31(4):* 827-836

Föstermann, U., Sessa, W. 2012. Nitric oxide synthases: regulation and function. European Heart Journal. 33: 829-837

Franchi, J., Marteau, C., Crola Da Silva, C., Mitterrand, M., André, P., Kieda, C. 2008. Cell model of inflammation. Bioscience Reports. 28: 23-32

Galie, P., van Oosten, A., Chen, C., Janmey, P. 2015. Application of multiple levels of fluid shear stress to endothelial cells plated on polyacrylamide gels. Lab Chip. 15(4): 1205-1212

Gho, Y., Kleinman, H., Sosne, G. 1999. Angiogenic activity of human soluble intercellular adhesion molecule-1. Cancer Research. 59(20): 5128-5132

Gho, Y., Kim, P., Li, H., Elkin, M., Kleinman, H. 2001. Stimulation of tumar growth by human solucle intercellular adhesion molecule-1. Cancer Research. 61(10): 4253-4257

Gourine, A., Gonon, A., Pernow, J. 2001. Involvement of nitric oxide in cardioprotective effect of endothelin receptor antagonist during ischemia-reperfusion. *American Journal of Physiology- Hear and Circulatory Physiology. 280(3):* H1105-H1112

Govers, R., Rabelink, T. 2001. Cellular regulation of endothelial nitric oxide synthase. American Journal of Physiology Renal Physiology.280: F193-F206

Green, L., Wagner, D., Glogowski, J., Skipper, P., Wishnok, J., Tannenbaum, S. 1982. Analysis of nitrate, nitrite and [15N] nitrate in biological fluids. Analytical Biochemistry. 126: 131-138

Gunda, N., Singh, M., Norman, L., Kaur, K., Mitra, S. 2014. Optimization and characterization of biomolecule immobilization on silicon substrates using (3-aminopropyl) triethoxysilane (APTES) and glutaraldehyde linker. Applied Surface Science. 305: 522-530

Hansson, G., Libby, P. 2006. The immune response in atherosclerosis: a double-edged sword. Nature. 6: 508-519

Heusch, G., Posst, H., Michel, M., Kelm, M., Schulz, R. 2000. Endogenous nitric oxide and myocardial adaptation to ischemia. *Circulation Research. 87:* 146-152

Hingorani, A., Jia, H., Stevens, P., Monteith, M., Brown, M. (1995). A common variant in exon 7 of the endothelial constitutive nitric oxide synthase gene: Identification of a single strand conformational polymorphism analysis. Clinical Science. 88(Pt s32): 21P-21p

Hirota, T., Nonaka, A., Matsushita, A., Uchida, N., Ohki, K., Asakura, M., Kitakaze, M. 2011. Milk casein-derived tripeptides, VPP and IPP induced NO production in cultured endothelial cells and endothelium-dependent relaxation of isolated aortic ring. Heart Vessels. 26: 549-556

Hsieh, H., Liu, C., Huang, B., Tseng, A., Wang, D. 2014. Shear-induced endothelial mechanotransduction: the interplay between reactive oxygen species (ROS) and nitric oxide (NO) and the pathophysiological implications. Journal of Biomedical Science. 21(3): 1-15

Hu, W., Bellone, C., Baldassare, J. 1999. RhoA stimulates p27Kip degradation through its regulation of cyclin E/CDK2 activity. Journal of Biological Chemistry. 274(6): 3396-3401

Huang, S., Chen, C., Ingber, D. 1998. Control of cyclin D1, p27Kip1, and cell cycle progression in human capillary endothelial cells by cell shape and cytoskeletal tension. Molecular Biology of the Cell. 9: 3179-3193

Huynh, J., Nishimura, N., Rana, K., Peloquin, H., Califano, J., Montague, C., King, M., Schaffer, C., Reihnart-King, C. 2011. Age-related intimal stiffening enhances endothelial permeability and leukocyte transmigration. Science Translational Medicine. 3(112): 112-122

Hwang, S., Ballantyne, C., Sharrett, R., Smith, L., Davis, C., Gotto, A., Boerwinkle, E. (1997). Circulating adhesion molecules VCAM-1, ICAM-1 and E-selectin in carotid atherosclerosis and incident coronary heart disease cases. Circulation. 96: 4219-4225

Ignarro, L., Buga, G., Wood, K., Byrns, R., Chaudhuri, G. 1987. Endothelium derived relaxing factor produced and released from artery and vein is nitric oxide. Proceedings of the National Academy of Sciences of the United States of America. 84: 9265-9269

Intengan, H., Schiffrin, E. 2000. Structure and mechanical properties of resistance arteries in hypertension: Role of adhesion molecules and extracellular matrix determinants. Hypertension. 36: 312-318

Jauhiainen, T., Rönnback, M., Vapaatalo, H., Wuolle, K., Kautiainen, H., Korpela, R. 2007. Lactobacillus helveticus fermented milk reduces arterial stiffness in hypertensive subjects. International Dairy Journal. 17: 1209-1211

Jongstra-Bilen, J., Hairdari, M., Zhu, S., Chen, M., Guha, D., Cybulsky, M. 2006. Low-grade chronic inflammation in regions of the normal mouse arterial intima predisposed to atherosclerosis. Journal of Experimental Medicine. 203(9): 2073-2983

Jufri, N., Mohamedali, A., Avolio, A., Baker, M. 2014. Mechanical stretch: physiological and pathological implications for human vascular endothelial cells. Vascular Cell. 7(8): 1-12

Kaplanski, G., Marin, V., Montero-Julian, F., Mantovani, A., Farnarier, C. 2003. IL-6: a regulator of the transition from neutrophil to monocyte recruitment during inflammation. Trends in Immunology. 24(1): 25-29

Kay, B., Williamson, M., Sudol, M. 2000. The importance of being proline: the interaction of proline-rich motifs in signaling proteins with their cognate domains. Journal of the Federation of American Societies for Experimental Biology. 14: 231-241

Kim, N., Koh, E., Chen, X., Gumbiner, B. 2011. E-cadherin mediates contact inhibition of proliferation through Hippo signaling-pathway components. Proceedings of the National Academy of Sciences. 108(29): 11930-11935

King, G., Park, K., Li, Q. 2016. Selective insulin resistance and the development of cardiovascular disease in diabetes: The 2015 Edwin Bierman award lecture. Diabetes. 65: 1462-1471

Kobayashi, S., Nagino, M., Komatsu, S., Naruse, K., Nimura, Y., Nakanishi, M., Sokabe, M. 2003. Stretch-induced IL-6 secretion from endothelial cells requires NF-□B activation. Biochemical and Biophysical Research Communications. 308: 306-312

Kohn, J., Zhou, D., Bordeleau, F., Zhou, A., Mason, B., Mitchell, M., King, M., Reinhart-King, C. 2015. Cooperative effects of matrix stiffness and fluid shear stress son endothelial cell behaviour. Biophysical Journal. 108:471-478

Krishnan, R., Klumpers, D., Park, C., Rajendran, K., Trepat, X., van Bezu, J., van Hinsbergh, V., Carman, C., Brain, J., Fredberg, J., Butler, J., van Nieu Amerongen, N. 2011. Substrate stiffening promotes endothelial monolayer disruption through enhanced physical forces. American Journal of Cell Physiology. 300: C146-C154

Kuboki, K., Jiang, X., Takahara, N., Ha, S., Igarashi, M., Yamauchi, T., Feener, E., Herbert, T., Rhodes, C., King, G. 2000. Regulation of endothelial constitutive nitric oxide synthase gene expression in endothelial cells and in vivo: A specific vascular action of insulin. Circulation. 101: 676-681

Lehoux, S., Tedgui, A. 2003. Cellular mechanics and gene expression in blood vessels. Journal of Biomechanics. 36(5): 631-643

Levitan, I., Shenty, T. 2011. Impact of oxLDL on cholesterol-rich membrane rafts. Journal of Lipids. 2011: 1-11

Libby, P. 2002. Inflammation in atherosclerosis. Nature. 420: 868-874

Libby, P. 2006. Inflammation and cardiovascular disease mechanisms. American Journal of Clinical Nutrition. 83(Supple): 456S-460S

Libby, P., Ridker, P., Hansson, G. 2011. Progress and challenges in translating the biology of atherosclerosis. Nature. 473: 317-325

Libermann, T., Baltimore, D. 1990. Activation of interleukin-6 gene expression through the NF-kB transcription factor. Molecular and Cellular Biology. 10(5): 2327-2334

Lo, C., Wang, H., Dembo, M., Wang, Y. 2000. Cell movement is guided by the rigidity of the substrate. Biophysical Journal. 79: 144-152

MacMillan, J. 2009. Using silanes as adhesion promoters. Computational Chemistry. 28(11): 1-87

Maeno, M., Yamamoto, N., Takano, T. 1996. Identification of an anti-hypertensive peptide from casein hydrolysate produced by a proteinase from Lactobacillus helveticus CP790. Journal of Dairy Science. 79: 1316-1321

Marcone, S., Haughton, K., Simpson, P., Belton, O., Fitzgerald, D., 2015. Milk-derived bioactive peptides inhibit human endothelial monocyte interactions via PPARg dependent regulation of NF-□B. Journal of Inflammation. 12:1-13

Mesinga, T., Speijers, G., Meulenbelt, J. 2003. Health implications of exposure to environmental nitrogenous compounds. *Toxicology Research. 22(1):* 41-51

Meyer, D., Dustin, M., Carron, C. 1995. Characterization of intercellular adhesion molecule-1 ectodomain (sICAM-1) as an inhibitor of lymphocyte function-associated molecule-1 interaction with ICAM-1. Journal of Immunology. 155(7): 3578-3584

Modur, V., Zimmerman, G., Prescott, S., McIntyre, T. 1996. Endothelial cell inflammatory responses to tumor necrosis factor α. Journal of Biological Chemistry. 271(22): 13094-13102

Mohanty, D., Mohapatra, S., Misra, S., Sanhu P. 2015. Milk derived bioactive peptides and their impact on human health- A review. Saudi Journal of Biological Sciences. 23(5): 577-583

Montagnani, M., Golovchenko, I., Kim, I., Koh, G., Goalstone, M., Mundhekar, A., Johansen, M., Kucik, D., Quon, M., Draznin, B. 2002. Inhibition of phosphatidylinositol 3-kinase enhances mitogenic actions of insulin in endothelial cells. Journal of Biological Chemistry. 277(3): 1794-1799

Morel, D., Hessler, J., Chisolm, G. 1983. Low density lipoprotein cytotoxicity induced by free radical peroxidation of lipid. Journal of Lipid Research. 24: 1070-1076

Mori, E., Haramaki, N., Ikeda, H., Imaizumi, T. 1998. Intra-coronary administration of L-arginine aggravates myocardial stunning through production of peroxynitrite in dogs. *Cardiovascular Reasearch. 40:* 113-123

Muñoz, K., Krebs-Smith, S., Ballard-Barbash, R., Cleveland, L. 1997. Food intakes of US children and adolescents compared with recommendations. Pediatrics. 100(3): 323-329

Nagai, M., Kamide, K., Rakugi, H., Takiuchi, S., Imai, M., Kida, I., Matsukawa, N., Higaki, J., Ogihara, T. 2003. Role of endothelin-1 induced by insulin in the

regulation of vascular cell growth. American Journal of Hematology. 16: 223-228

Nakamura, Y., Yamamoto, N., Sakai, K., Okubo, A., Yamazaki, S., Takano T. 1995. Purification and characterization of Angiotensin I- Converting Enzyme Inhibitors from Sour Milk. Journal of Dairy Science. 78(4): 777-783

National Heart, Lung and Blood Institute. 2013. What is Atherosclerosis? Last Modified. 2016. https://www.nhlbi.nih.gov/health/health-topics/topics/atherosclerosis

Okayasu, T., Tomizawa, A., Suzuki, K., Manaka, K., Hattori, Y. 2008. PPARα activators upregulate eNOS activity and inhibit cytokine-induced NF-κB activation through AMP-activated protein kinase activation. *Life Sciences. 82(15-16): 884-891*

O'Rourke, M., Staessen, J., Vlachopoulos, C., Duprez D., Plante, G. 2002. Clinical applications of arterial stiffness; definitions and reference values. American Journal of Hypertension. 15(5):426-444

Papapetropoulos, A., Fulton, D., Lin, M., Fontant, J., McCabe, T., Soellner, S., García-Cardeña, G., Zhou, Z., Gratton, J., Sessa, W. 2004. Vanadate is a potent activator of endothelial nitric-oxide synthase: evidence for the role of the serine/threonine kinase Akt and the 90-kDa heat shock protein. *Molecular Pharmacology. 65(2):* 407-415

Philip I, Plantefeve G, Vuillaumier-Barrot S, Vicaut E, LeMarie C, et al. (1999) G894T polymorphism in the endothelial nitric oxide synthase gene is associated with an enhanced vascular responsiveness to phenylephrine. Circulation. 99(24): 3096–3098.

Public Health Agency of Canada. 2016. Cardiovascular Disease. http://www.phac-aspc.gc.ca/cd-mc/cvd-mcv/index-eng.php

Qin, L., Xu, J., Han, S., Zhang, Z., Zhao, Y., Szeta I. 2015. Dairy Consumption and rich of cardiovascular disease: an updated meta-analysis of prospective cohort studies. Asia Pacific Journal of Clinical Nutrition. 24(1):90-100

Rai, H., Parveen, F., Kumar, S., Kapoor, A., Sinha, N. 2014. Association of endothelial nitric oxide synthase gene polymorphisms with coronary artery disease: An updated meta-analysis and systematic review. Public Library of Science. 9(11): 1-19

Rask-Marsden, C., King, G. 2007. Mechanisms of disease: endothelial dysfunction in insulin resistance and diabetes. Nature. 3(1): 46-56

Ren, X., Ren, K., Wei, Q., Chen, L., Liu, N. 2017. Advanced glycation end-products decreases expression of endothelial nitric oxide synthase through oxidative stress in human coronary artery endothelial cells. Cardiovascular Diabetology. 16(52): 1-12

Ridker, P., Hennekens, C., Roitman-Johnson, B., Stampfer, M., Allen, J. 1998. Plasma concentration of soluble intercellular adhesion molecule 1 and risks of future myocardial infarction in apparently healthy men. The Lancet. 351(9096): 88-92

Romano, M., Sironi, M., Toniatti, C., Polentarutti, N., Fuscella, P., Ghezzi, P., Faggioni, R., Luini, W., van Hinsbergh, V., Sozzani, S., Bussolino, F., Poli, V., Ciliberto, G., Mantovani, A. 1997. Role of IL-6 and its soluble receptor in induction of chemokines and leukocyte recruitment. Immunity. 6: 315-325

Rubin, E., Damjanov, I. 1989. Pathology Reviews 1989. New Jersey. Humana Press. p178

Rychter, M., Gaucher, C., Boudier, A., Leroy, P., Lulek, J. 2016. S-Nitrosothiols-NO donors regulating cardiovascular cell proliferation: Insight into intracellular pathway alterations. International Journal of Biochemistry and Cell Biology.78: 156-161

Shaul, P. 2003. Endothelial nitric oxide synthase, caveolae and the development of atherosclerosis. Journal of Physiology. 541(1): 21-33

Sitterley, G. 2008. Collagen attachment protocols, solubility and stability. BioFiles. 3(8): 5

Soedamah-Muthu, S., Ding, E., Al-Delaimy, W., Hu, F., Engberink, M., Willett, W., Geleijnse, J. 2011. Milk and dairy consumption and incidence of cardiovascular disease and all-cause mortality: dose-response meta-analysis of prospective cohort studies. American Journal of Clinical Nutrition. 93: 158-171

Sonestedt, E., Wirfält, E., Wallström, P., Gullberg, B., Orho-Melander, M., Hedblad, B. 2011. Dairy products and its association with incidence of cardiovascular disease: the Malmö diet and cancer cohort. European Journal of Epidemiology. 26: 609-618

Stamatovic, S., Keep, R., Kunkel, S., Andjelkovic, A. 2003. Potential role of MCP-1 in endothelial cell tight junction 'opening': signaling via Rho and Rho Kinase. Journal of Cell Science. 116(22): 4615-4628

Steinbrecher, U., Parthasarathy, S., Leake, D., Witztum, J., Steinberg, D. 1983. Modification of low density lipoprotein by endothelial cells involves lipid peroxidation and degradation of low density lipoprotein phospholipids. Proceedings of the National Academy of Sciences of the United States of America. 81(12): 3883-3887

Stonebridge, P., Brophy, C. 1991. Spiral laminar flow in arteries? Lancet. 338(8779): 1360-1365

Sütas, Y., Hurme, M., Isolauri, E. 1996. Down regulation of anti-CD3 antibody induced IL-4 production by bovine caseins hydrolysed with Lactobacillus GG-derived enzymes. Scandinavian Journal of Immunology. I43: 687-689

Tarride, J., Lim, M., DesMeules, M., Luo, W., Burke, N., O'Reilly, D., Bowen, J., Goeree, R. 2009. A review of the cost of cardiovascular disease. Canadian Journal of Cardiology. 25(6): e195-e202

Tellez, A., Corredig, M., Brovko, K., Griffiths, M. 2010. Characterization of immune-active peptides obtained from milk fermented by Lactobacillus helveticus. Journal of Dairy Research. 77(2): 129-136

Terramani, T., Eton, D., Bui, P., Wang, Y., Weaver, F., Yu, H. 2000. Human macrovascular endothelial cells: Optimization of culture conditions. In Vitro Cellular and Developmental Biology - Animal. 36: 125-132

Tricot, O., Mallat, Z., Heymes, C., Belmin, J., Leseche, G., Tedguie, A. 2000. Relation between endothelial cell apoptosis and blood flow direction in human atherosclerotic plaques. Circulation. 101: 2450-2453

Tsutamoto, T., Wada, A., Maeda, K., Mabuchi, N., Hayashi, M., Tsutsui, T., Ohnishi, M., Sawaki, M., Fujii, M., Matsumoto, T., Kinoshita, M. 2000. Angiotensin II type 1 receptor antagonist decreases plasma levels of tumor necrosis factor alpha, interleukin-6 and soluble adhesion molecules in patients with chronic heart failure. Journal of the American College of Cardiology. 35(3): 714-721

Turner, A., Hooper, N. 2002. The angiotensin-converting enzyme gene family: genomics and pharmacology. Trends in Pharmacological Sciences 23(4):177-183

Verzijl, N., DeGroot, J., Thorpe, S., Band, R., Shaw, J., Lyons, T., Bijlsma, J., Lafeber, F., Baynes, J., TeKoppele, J. 2000. Effect of collagen turnover on the accumulation of advanced glycation end products. Journal of Biological Chemistry. 275(50): 39027- 39031

Wagner, A., Kautz, O., Fricke, K., Zerr-Fouineau, M., Demicheva, E., Güldenzoph, B., Bermejo, J., Korff, T., Hecker, M. 2009. Upregulation of glutathione peroxidase offsets stretch-induced proatherogenic gene expression in human endothelial cells. Atherosclerosis Thrombosis and Vascular Biology. 29: 1894-1901

Wang, D., Yang, X., Liu, Y., Carretero, O., LaPointe, M. 1999. Reduction of myocardial infarct size of inhibition of inducible nitric oxide synthase. *American Journal of Hypertension. 12(2):* 174-182

Wang, H., Dembo, M., Wang, Y. 2000. Substrate flexibility regulates growth and apoptosis of normal but not transformed cells. American Journal of Physiology: Cell Physiology. 279: C1345-1350

Wang, P., Xian, M., Tang, X., Wu, X., When, Z., Cai, T., Janczuk, A. 2002. Nitric oxide donors: chemical activities and biological applications. *Chemical Reviews. 102(4)*: 1091-1134

Warren, M. 2017. Embolism from aortic plaque: Thromboembolism. https://www.uptodate.com/contents/embolism-from-aortic-plaque-thromboembolism?source=see_link#H1

Witkowska, A., Borawska, M. 2004. Soluble intercellular adhesion molecule-1 (sICAM-1): An overview. European Cytokine Network. 15(2): 91-98

World Health Organization. 2017. Cardiovascular diseases. http://www.who.int/mediacentre/factsheets/fs317/en/

Yamamoto, N. 1997. Antihypertensive peptides derived from food protein. Biopolymers. 43: 129-134

Yamamoto, N., Maeno, M., Takno, T. 1999. Purification and characterization of an antihypertensive peptide from a yogurt-like product fermented by Lactobacillus helveticus CPN4. Journal of Dairy Science. 82: 1388-1393

Yeh, Y., Hur, S., Chang, J., Wang, K., Chiu, J., Li, Y., Chien, S. 2012. Matrix stiffness regulates endothelial cell proliferation through Septin 9. Public Library of Science. 7(10): 1-13

Yeung, T., Georges, P., Flanagan, L., Marg, B., Ortiz, M., Funaki, M., Zahir, N., Ming, W., Weaver, V., Janmey, P. 2005. Effects of substrate stiffness of cell morphology, cytoskeletal structure and adhesion. Cell Motility and the Cytoskeleton. 60: 24-34

Zhao, T., Xi, L., Chelliah, J., Levasseur, J., Kukreja, R. 2000. Inducible nitric oxide synthase mediated delated myocardial protection induced by activation of adenosine A_1 receptors. *Circulation. 102:* 902-907

Zieman, S., Melenovsky, V., Kass, D. 2005. Mechanisms, pathophysiology and therapy of arterial stiffness. Arteriosclerosis Thrombosis Vascular Biology. 25: 932-943

I. APPENDIX A

Copyright agreement allowing use of previously published figures.

NATURE PUBLISHING GROUP LICENSE
TERMS AND CONDITIONS

Jun 20, 2017

This Agreement between Farrah A Edun ("You") and Nature Publishing Group ("Nature Publishing Group") consists of your license details and the terms and conditions provided by Nature Publishing Group and Copyright Clearance Center.

License Number	4122110679045
License date	Jun 04, 2017
Licensed Content Publisher	Nature Publishing Group
Licensed Content Publication	Nature
Licensed Content Title	Progress and challenges in translating the biology of atherosclerosis
Licensed Content Author	Peter Libby, Paul M Ridker, Göran K. Hansson
Licensed Content Date	May 18, 2011
Licensed Content Volume	473
Licensed Content Issue	7347
Type of Use	reuse in a dissertation / thesis
Requestor type	academic/educational
Format	print and electronic
Portion	figures/tables/illustrations
Number of figures/tables/illustrations	1
High-res required	no
Figures	Figure 1
Author of this NPG article	no
Your reference number	
Title of your thesis / dissertation	Endothelial Cell Response to Bioactive Peptides and Stiffened Extracellular Matrices: An Investigation into Atherogenic Pathways
Expected completion date	Aug 2017
Estimated size (number of pages)	100

Requestor Location	Farrah A Edun 2000 Simcoe Street Oshawa, ON L1H7K4 Canada Attn: Farrah A Edun
Billing Type	Invoice
Billing Address	Farrah A Edun 2000 Simcoe Street Oshawa, ON L1H7K4 Canada Attn: Farrah A Edun
Total	0.00 USD

Terms and Conditions

Terms and Conditions for Permissions

Nature Publishing Group hereby grants you a non-exclusive license to reproduce this material for this purpose, and for no other use,subject to the conditions below:

1. NPG warrants that it has, to the best of its knowledge, the rights to license reuse of this material. However, you should ensure that the material you are requesting is original to Nature Publishing Group and does not carry the copyright of another entity (as credited in the published version). If the credit line on any part of the material you have requested indicates that it was reprinted or adapted by NPG with permission from another source, then you should also seek permission from that source to reuse the material.

2. Permission granted free of charge for material in print is also usually granted for any electronic version of that work, provided that the material is incidental to the work as a whole and that the electronic version is essentially equivalent to, or substitutes for, the print version.Where print permission has been granted for a fee, separate permission must be obtained for any additional, electronic re-use (unless, as in the case of a full paper, this has already been accounted for during your initial request in the calculation of a print run).NB: In all cases, web-based use of full-text articles must be authorized separately through the 'Use on a Web Site' option when requesting permission.

3. Permission granted for a first edition does not apply to second and subsequent editions and for editions in other languages (except for signatories to the STM Permissions Guidelines, or where the first edition permission was granted for free).

4. Nature Publishing Group's permission must be acknowledged next to the figure, table or abstract in print. In electronic form, this acknowledgement must be visible at the same time as the figure/table/abstract, and must be hyperlinked to the journal's homepage.

5. The credit line should read:
   Reprinted by permission from Macmillan Publishers Ltd: [JOURNAL NAME] (reference citation), copyright (year of publication)
   For AOP papers, the credit line should read:
   Reprinted by permission from Macmillan Publishers Ltd: [JOURNAL NAME], advance

online publication, day month year (doi: 10.1038/sj.[JOURNAL ACRONYM].XXXXX)

Note: For republication from the *British Journal of Cancer,* the following credit lines apply.
Reprinted by permission from Macmillan Publishers Ltd on behalf of Cancer Research UK: [JOURNAL NAME] (reference citation), copyright (year of publication)For AOP papers, the credit line should read:
Reprinted by permission from Macmillan Publishers Ltd on behalf of Cancer Research UK: [JOURNAL NAME], advance online publication, day month year (doi: 10.1038/sj.[JOURNAL ACRONYM].XXXXX)

6. Adaptations of single figures do not require NPG approval. However, the adaptation should be credited as follows:

   Adapted by permission from Macmillan Publishers Ltd: [JOURNAL NAME] (reference citation), copyright (year of publication)

   Note: For adaptation from the *British Journal of Cancer,* the following credit line applies.
   Adapted by permission from Macmillan Publishers Ltd on behalf of Cancer Research UK: [JOURNAL NAME] (reference citation), copyright (year of publication)

7. Translations of 401 words up to a whole article require NPG approval. Please visit http://www.macmillanmedicalcommunications.com for more information.Translations of up to a 400 words do not require NPG approval. The translation should be credited as follows:

   Translated by permission from Macmillan Publishers Ltd: [JOURNAL NAME] (reference citation), copyright (year of publication).

   Note: For translation from the *British Journal of Cancer,* the following credit line applies.
   Translated by permission from Macmillan Publishers Ltd on behalf of Cancer Research UK: [JOURNAL NAME] (reference citation), copyright (year of publication)

We are certain that all parties will benefit from this agreement and wish you the best in the use of this material. Thank you.
Special Terms:
v1.1

Questions? customercare@copyright.com or +1-855-239-3415 (toll free in the US) or +1-978-646-2777.

II. APPENDIX B

Structure and properties of bioactive peptides

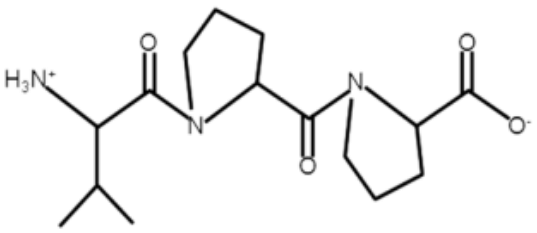

P1 –VPP
Molar mass = 311.39 g/mol
Net charge at pH 7 = 0

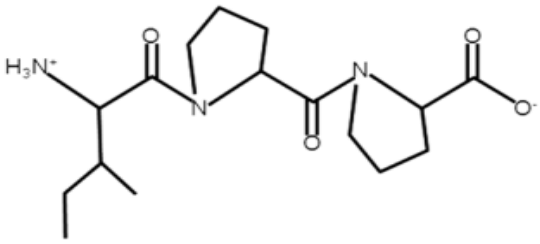

P2 – IPP
Molar mass = 325.4 g/mol
Net charge at pH 7 = 0

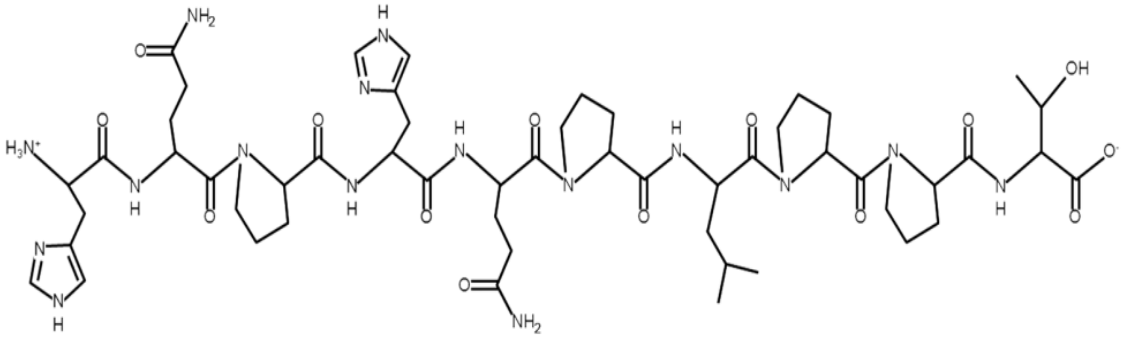

P3 – HQPHQPLPPT
Molar mass = 1151.27 g/mol
Net charge at pH 7 = 0.2

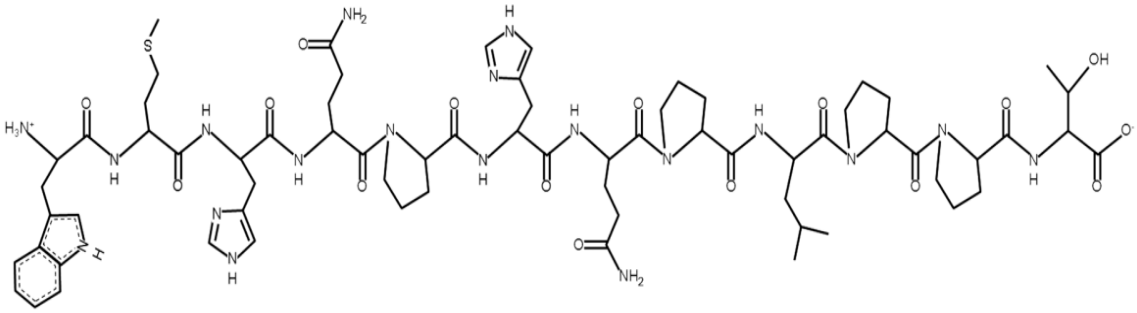

P4 – WMHQPHQPLPPT
Molar mass = 1468.68 g/mol
Net charge at pH 7 = 0.2

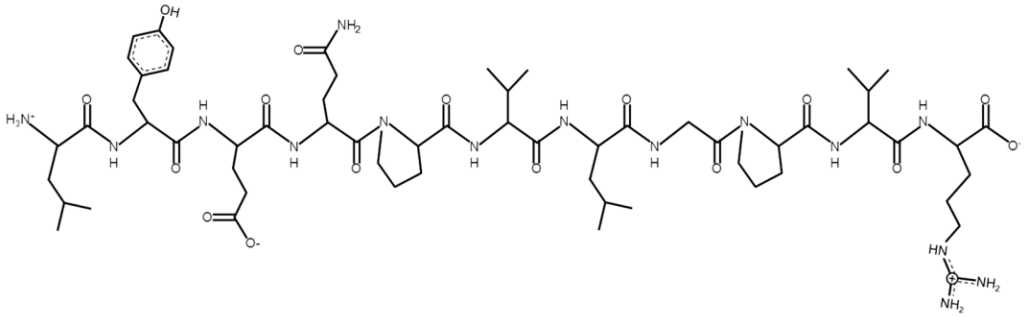

P5 – LYEQPVLGPVR
Molar mass = 269.71 g/mol
Net charge at pH 7 = 0

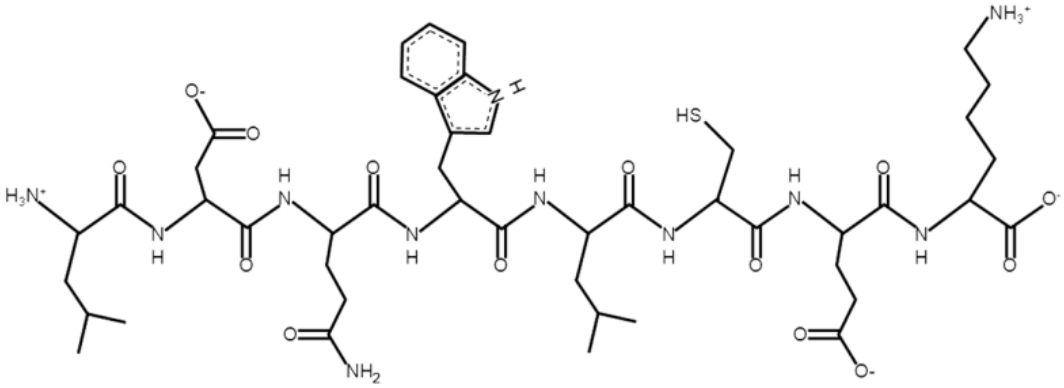

P6 – LDQWLCEK
Molar mass = 1034.19 g/mol
Net charge at pH 7 = 3.93

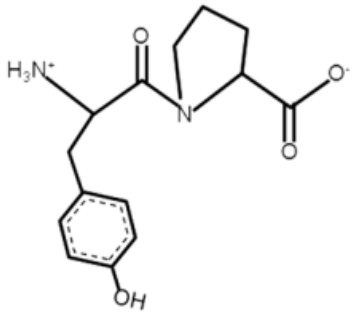

P7 – YP
Molar mass = 278.3 g/mol
Net charge at pH 7 = 0

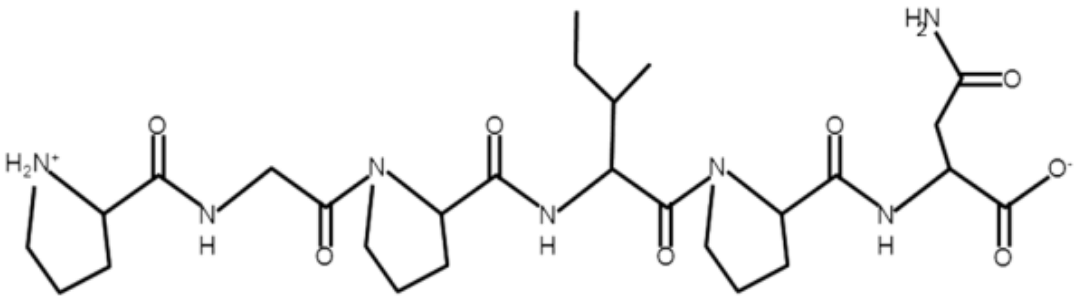

P8 – PGPIPN
Molar mass = 593.67 g/mol
Net charge at pH 7 = 0

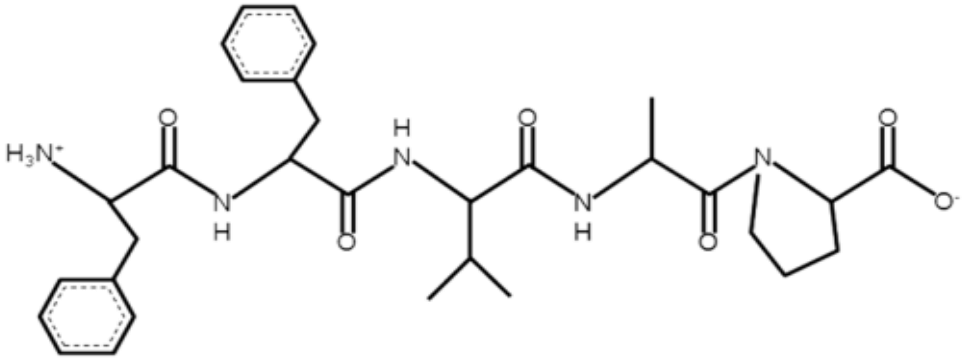

P9 – FFVAP
Molar mass = 579.69 g/mol
Net charge at pH 7 = 0

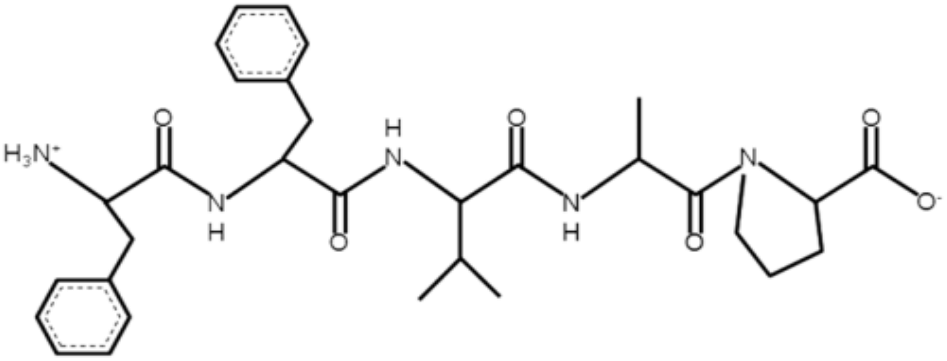

P10 – KVLPVP
Molar mass = 651.84
Net charge at pH 7 = 1

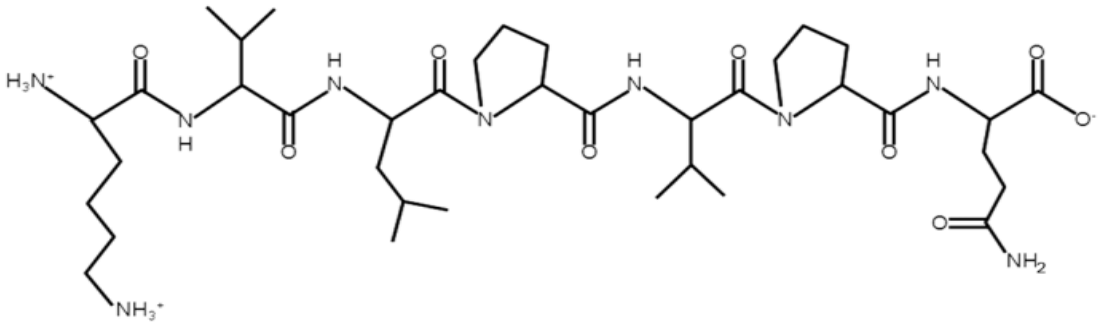

P11 – KVLPVPQ
Molar mass = 779.97 g/mol
Net charge at pH 7 = 1

III. APPENDIX C

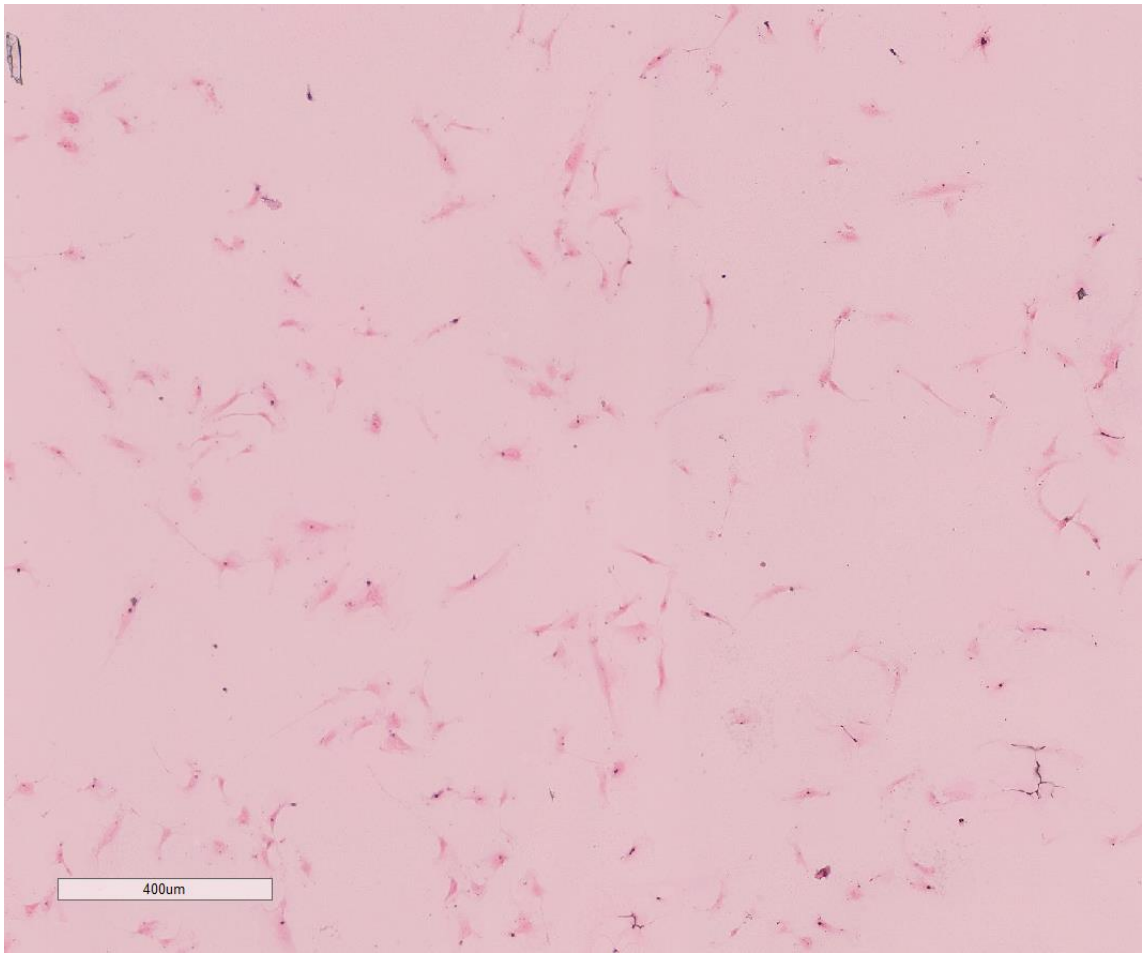

Supplementary Figure 1.

HUVEC culture grown on collagen coated cover slips 3 days after initial seeding (passage=2,3). Fixed with 2% paraformaldehyde and stained with safranin. Images obtained using digital microscopy 10x (Panoptiq). Images were then loaded into Image J for cell count and area measurements. The image above was loaded into ImageScope (Leica Biosystems) and a sample of the image was captured at 5x magnification (total magnification 500x).

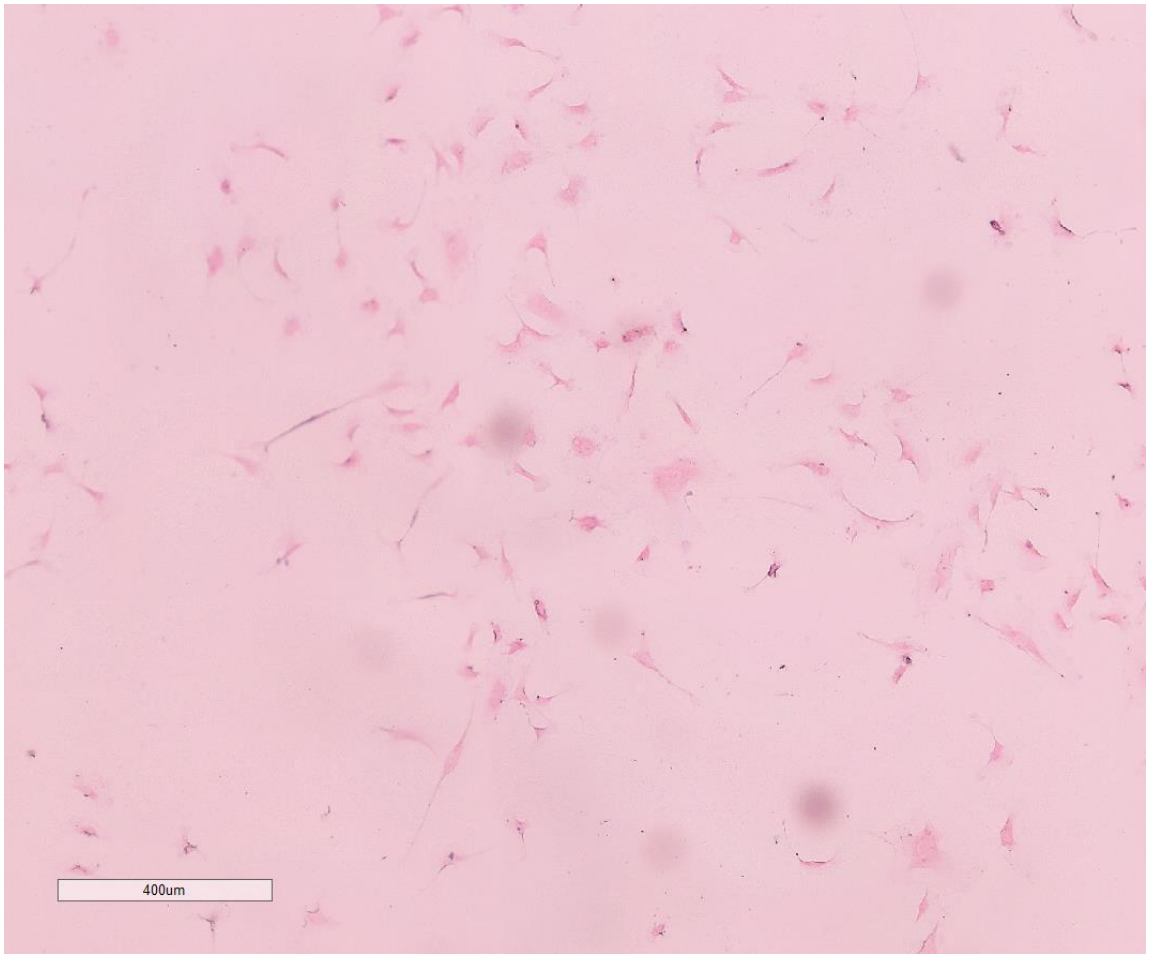

Supplementary Figure 2.

HUVEC culture grown on collagen coated cover slips 6 days after initial seeding (passage=2,3). Fixed with 2% paraformaldehyde and stained with safranin. Images obtained using digital microscopy 10x (Panoptiq). Images were then loaded into Image J for cell count and area measurements. The image above was loaded into ImageScope (Leica Biosystems) and a sample of the image was captured at 5x magnification (total magnification 500x).

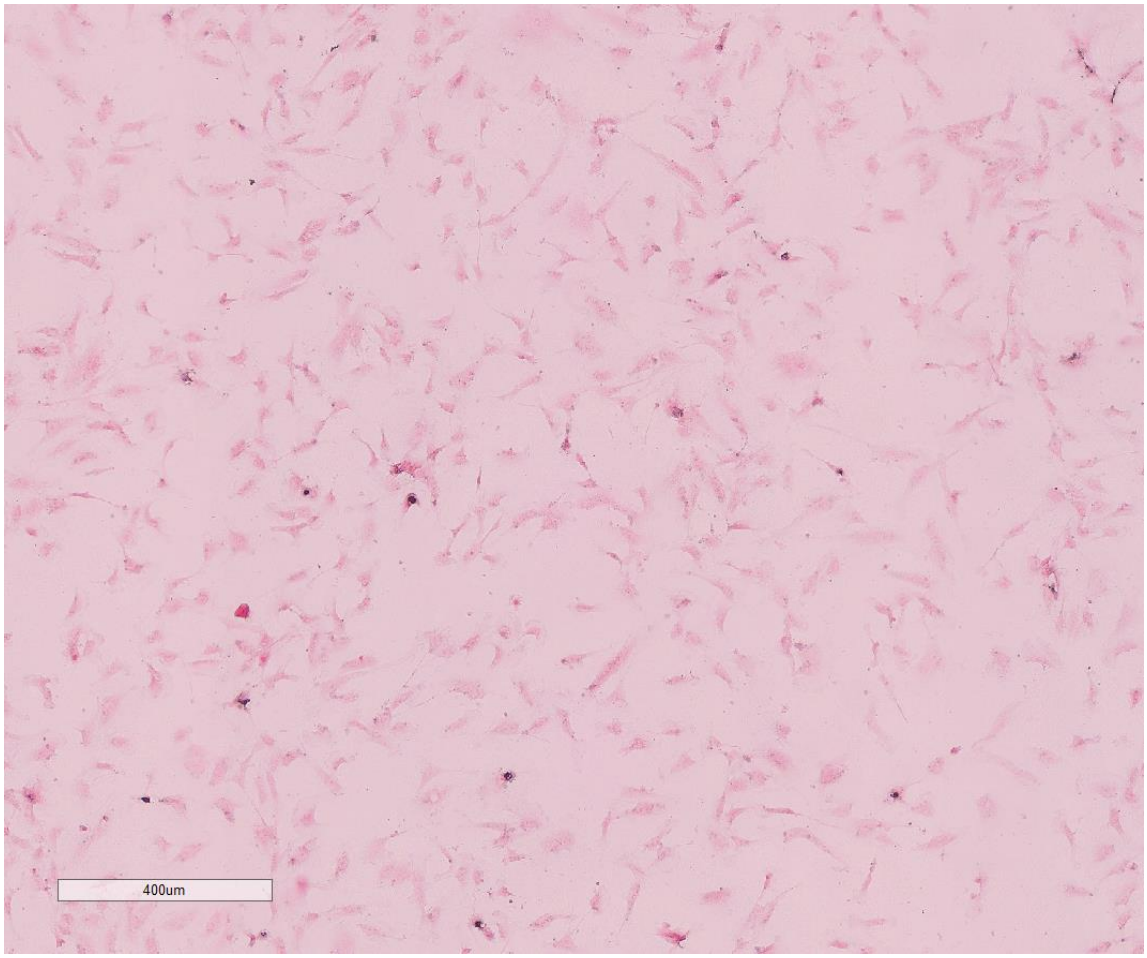

Supplementary Figure 3.

HUVEC culture grown on collagen coated cover slips 9 days after initial seeding (passage=2,3). Fixed with 2% paraformaldehyde and stained with safranin. Images obtained using digital microscopy 10x (Panoptiq). Images were then loaded into Image J for cell count and area measurements. The image above was loaded into ImageScope (Leica Biosystems) and a sample of the image was captured at 5x magnification (total magnification 500x).

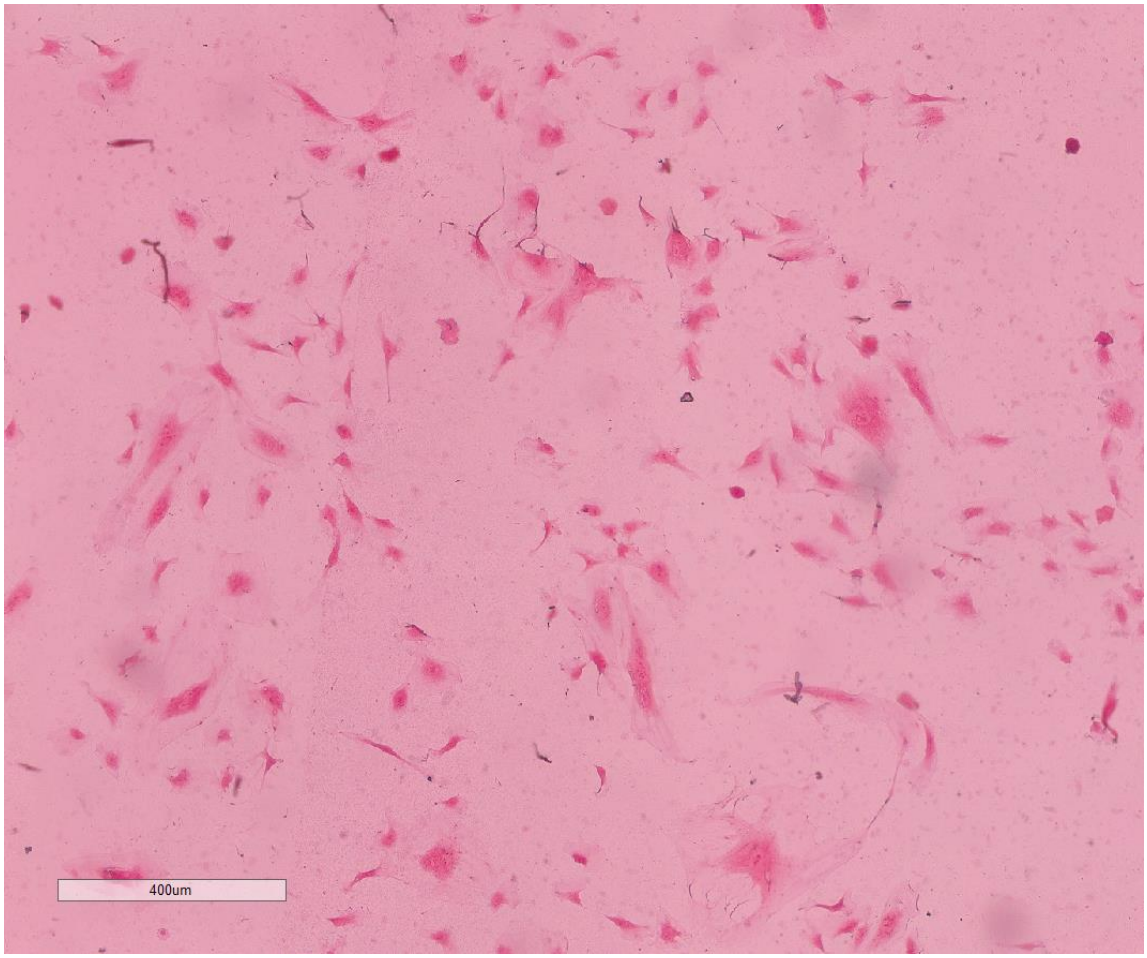

Supplementary Figure 4.

HUVEC culture grown on 2.5kPa polyacrylamide gel overlaid on cover slips, 3 days after initial seeding (passage=2,3). Fixed with 2% paraformaldehyde and stained with safranin. Images obtained using digital microscopy 10x (Panoptiq). Images were then loaded into Image J for cell count and area measurements. The image above was loaded into ImageScope (Leica Biosystems) and a sample of the image was captured at 5x magnification (total magnification 500x).

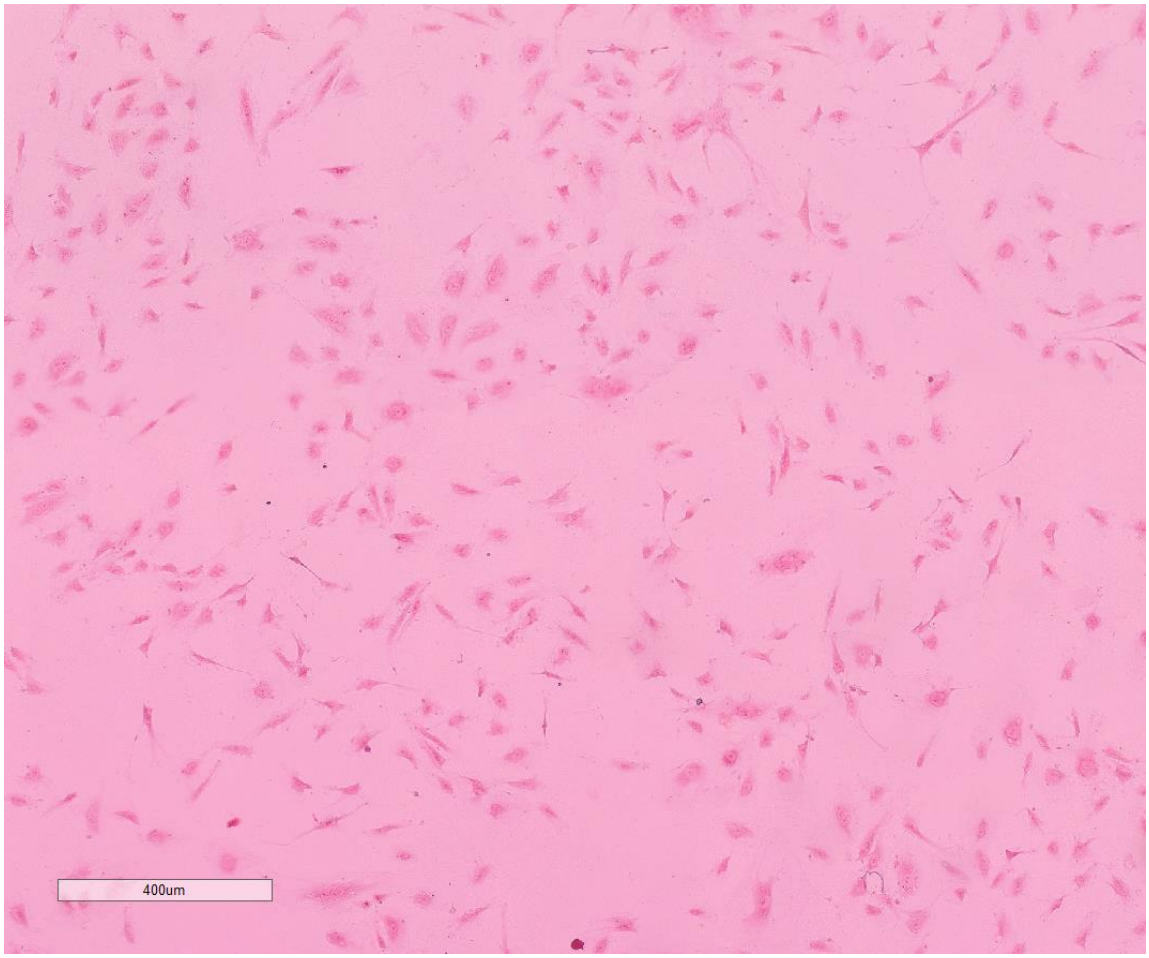

Supplementary Figure 5.

HUVEC culture grown on 2.5kPa polyacrylamide gel overlaid on cover slips, 6 days after initial seeding (passage=2,3). Fixed with 2% paraformaldehyde and stained with safranin. Images obtained using digital microscopy 10x (Panoptiq). Images were then loaded into Image J for cell count and area measurements. The image above was loaded into ImageScope (Leica Biosystems) and a sample of the image was captured at 5x magnification (total magnification 500x).

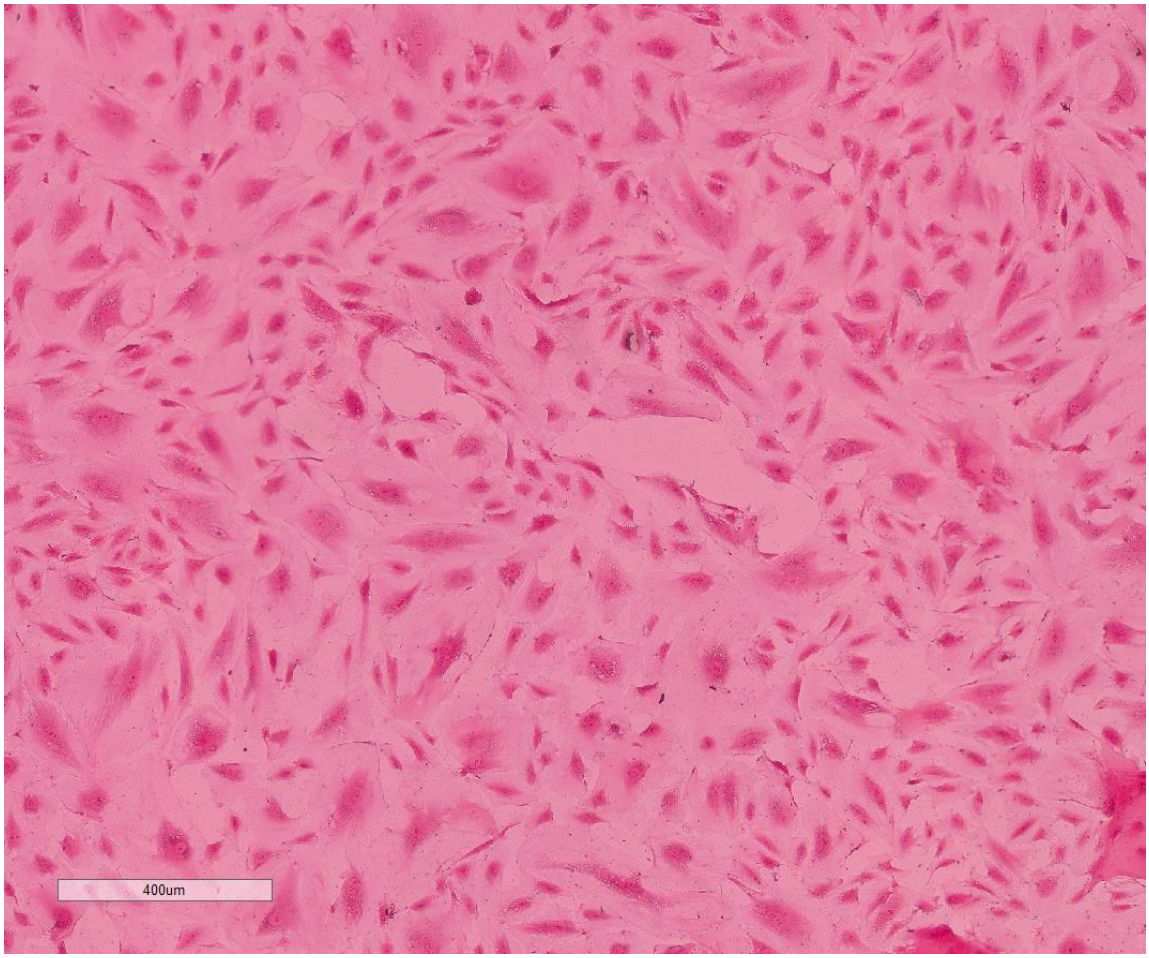

Supplementary Figure 6.

HUVEC culture grown on 2.5kPa polyacrylamide gel overlaid on cover slips, 9 days after initial seeding (passage=2,3). Fixed with 2% paraformaldehyde and stained with safranin. Images obtained using digital microscopy 10x (Panoptiq). Images were then loaded into Image J for cell count and area measurements. The image above was loaded into ImageScope (Leica Biosystems) and a sample of the image was captured at 5x magnification (total magnification 500x).

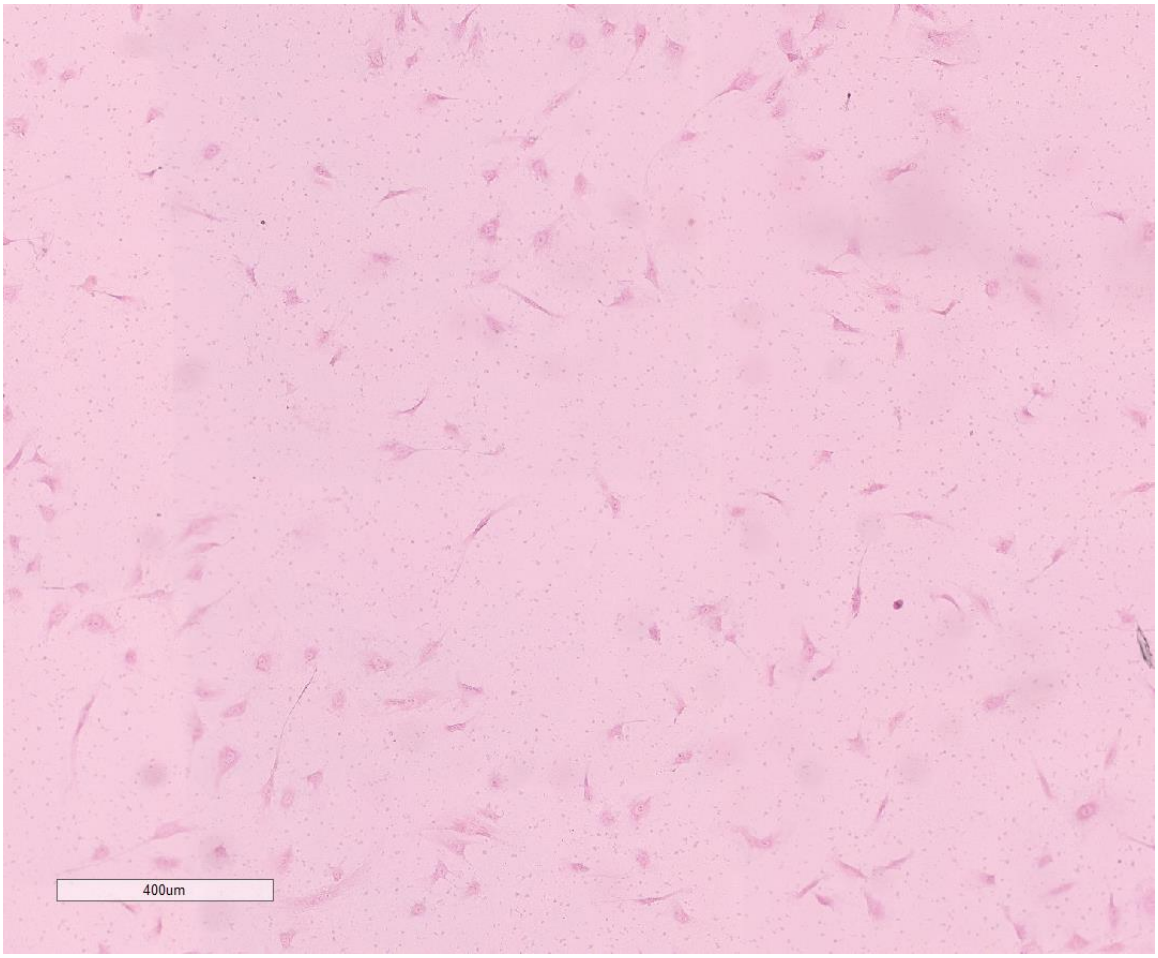

Supplementary Figure 7.

HUVEC culture grown on 3kPa polyacrylamide gel overlaid on cover slips, 3 days after initial seeding (passage=2,3). Fixed with 2% paraformaldehyde and stained with safranin. Images obtained using digital microscopy 10x (Panoptiq). Images were then loaded into Image J for cell count and area measurements. The image above was loaded into ImageScope (Leica Biosystems) and a sample of the image was captured at 5x magnification (total magnification 500x).

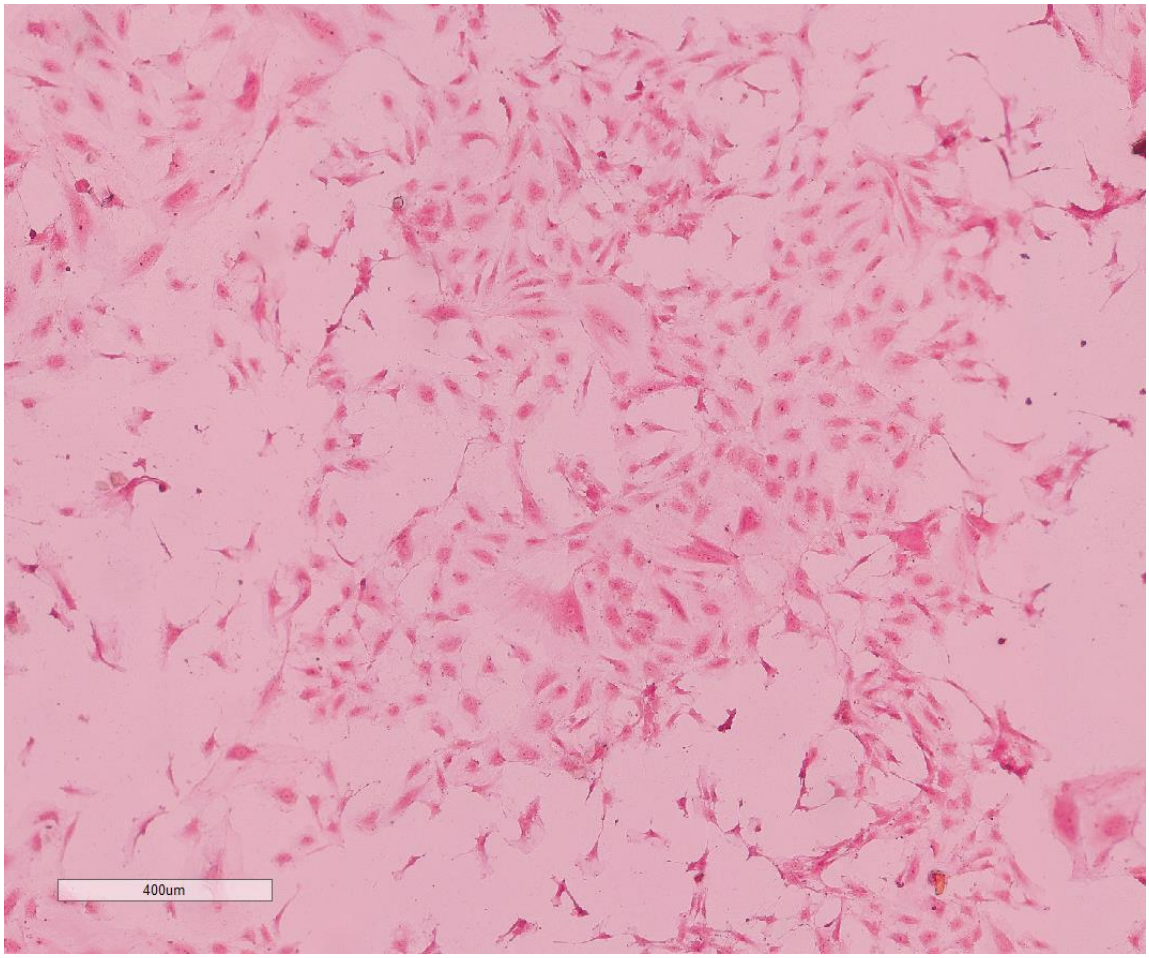

Supplementary Figure 8.

HUVEC culture grown on 3kPa polyacrylamide gel overlaid on cover slips, 6 days after initial seeding (passage=2,3). Fixed with 2% paraformaldehyde and stained with safranin. Images obtained using digital microscopy 10x (Panoptiq). Images were then loaded into Image J for cell count and area measurements. The image above was loaded into ImageScope (Leica Biosystems) and a sample of the image was captured at 5x magnification (total magnification 500x).

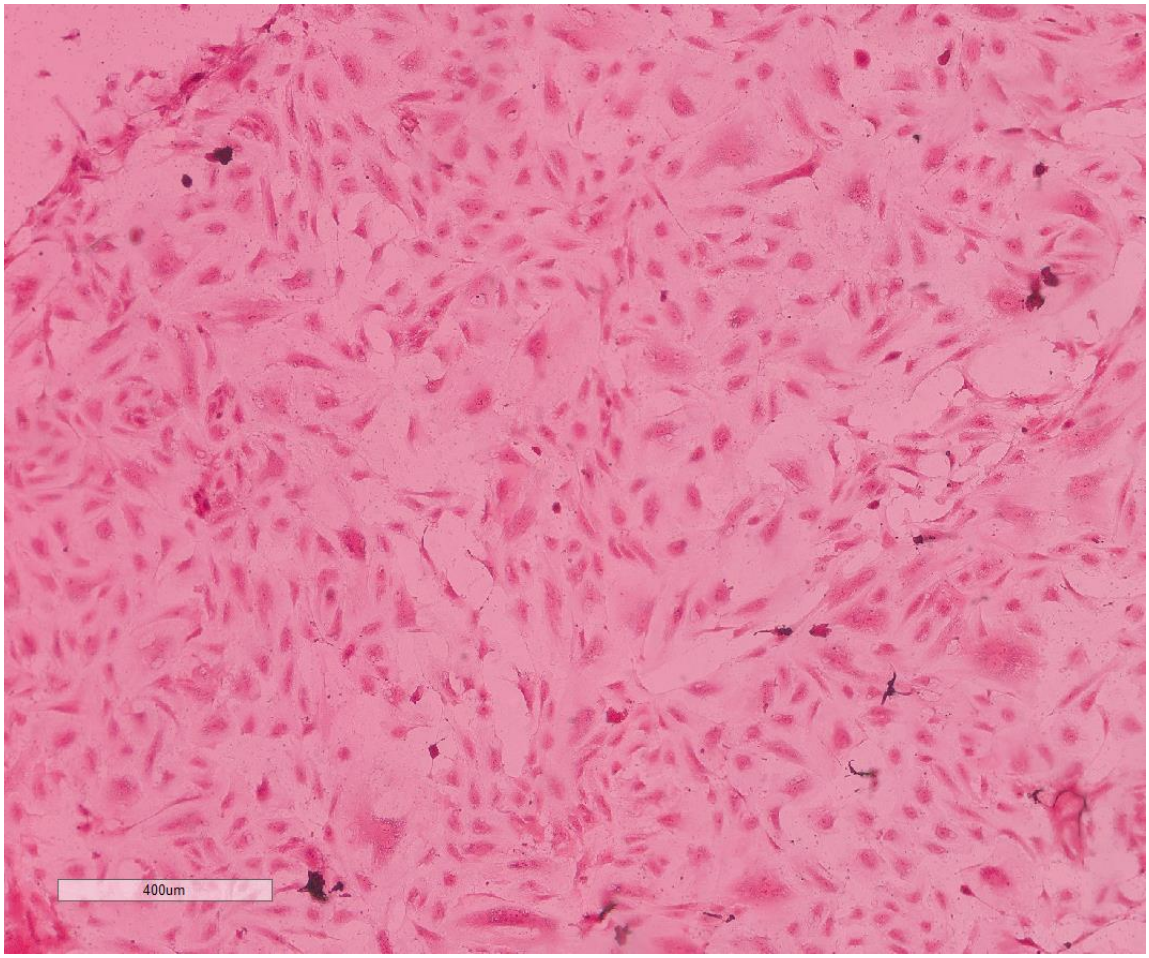

Supplementary Figure 9.

HUVEC culture grown on 3kPa polyacrylamide gel overlaid on cover slips, 9 days after initial seeding (passage=2,3). Fixed with 2% paraformaldehyde and stained with safranin. Images obtained using digital microscopy 10x (Panoptiq). Images were then loaded into Image J for cell count and area measurements. The image above was loaded into ImageScope (Leica Biosystems) and a sample of the image was captured at 5x magnification (total magnification 500x).

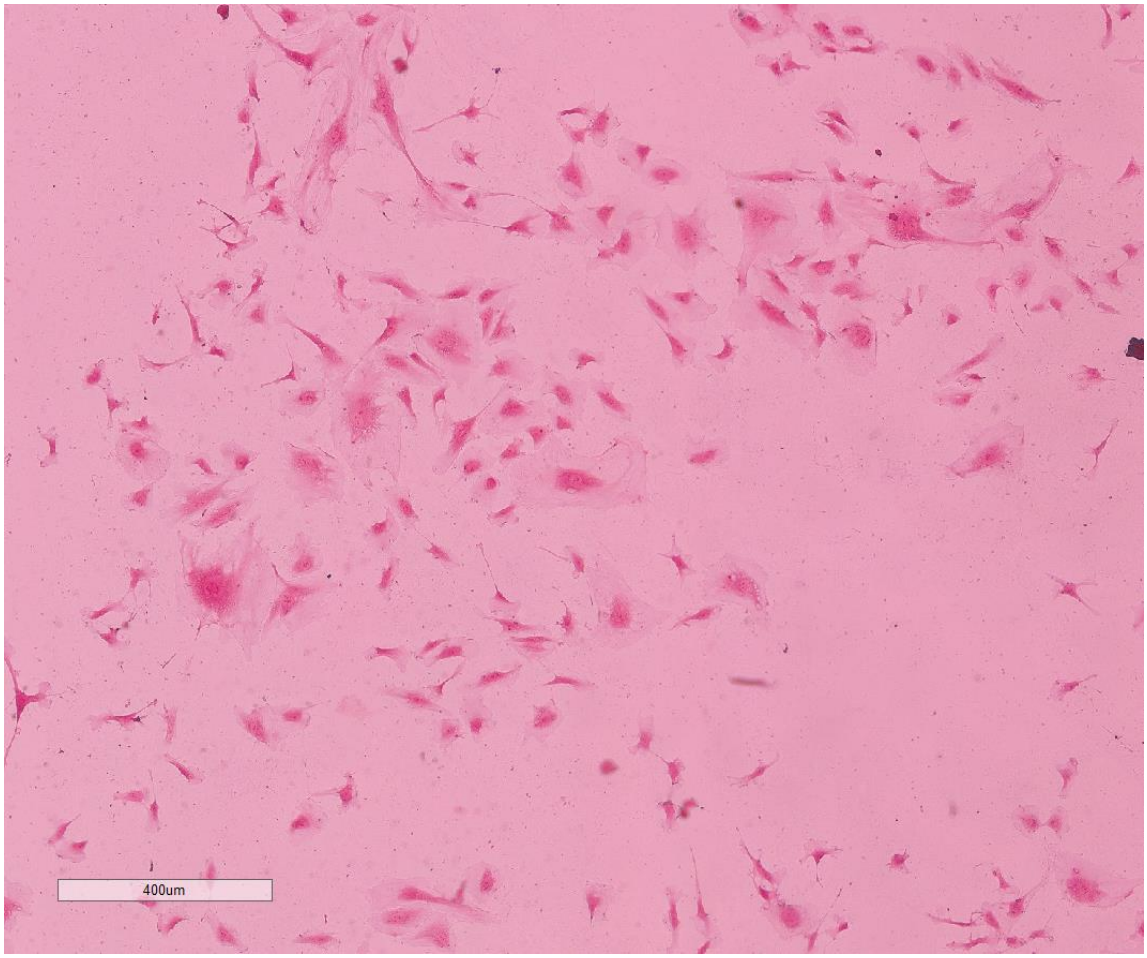

Supplementary Figure 10.

HUVEC culture grown on 10kPa polyacrylamide gel overlaid on cover slips, 3 days after initial seeding (passage=2,3). Fixed with 2% paraformaldehyde and stained with safranin. Images obtained using digital microscopy 10x (Panoptiq). Images were then loaded into Image J for cell count and area measurements. The image above was loaded into ImageScope (Leica Biosystems) and a sample of the image was captured at 5x magnification (total magnification 500x).

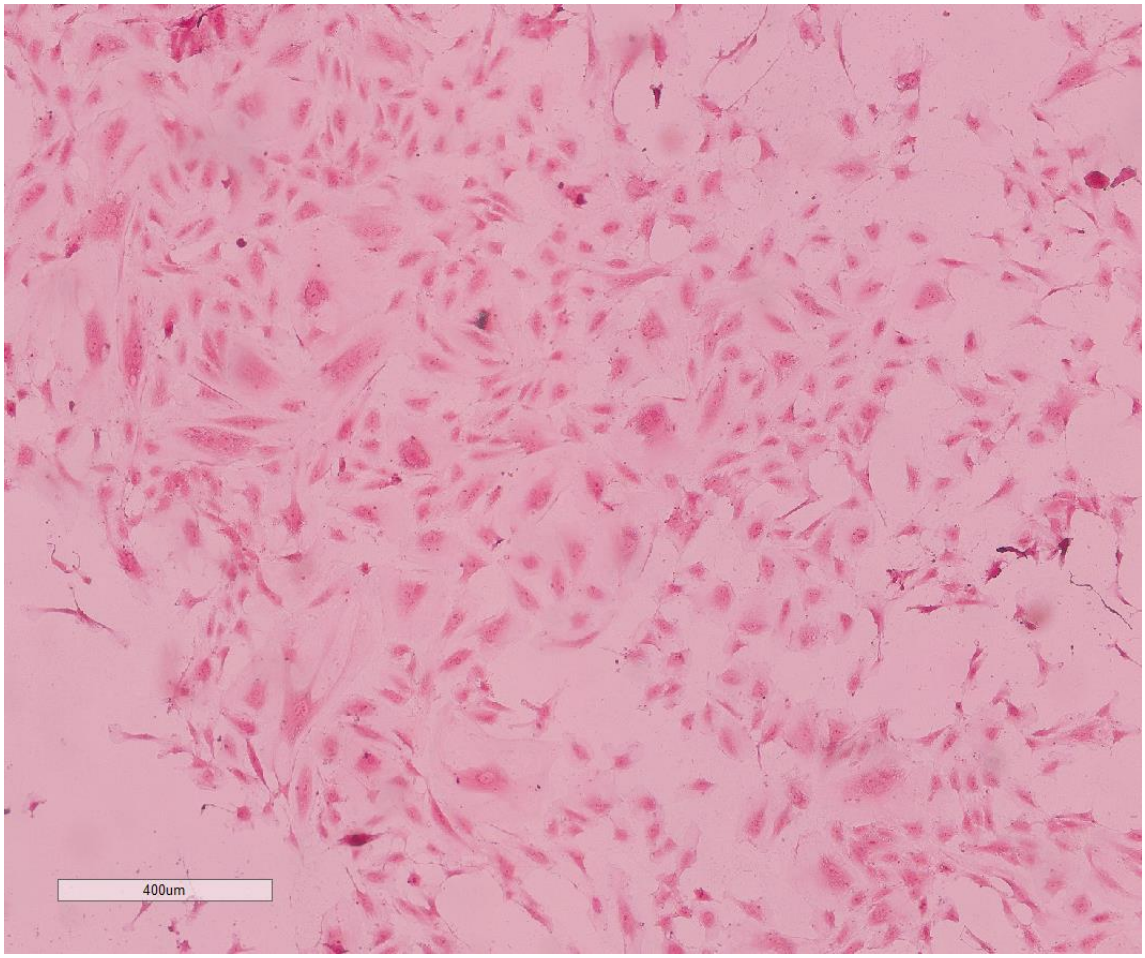

Supplementary Figure 11.

HUVEC culture grown on 10kPa polyacrylamide gel overlaid on cover slips, 6 days after initial seeding (passage=2,3). Fixed with 2% paraformaldehyde and stained with safranin. Images obtained using digital microscopy 10x (Panoptiq). Images were then loaded into Image J for cell count and area measurements. The image above was loaded into ImageScope (Leica Biosystems) and a sample of the image was captured at 5x magnification (total magnification 500x).

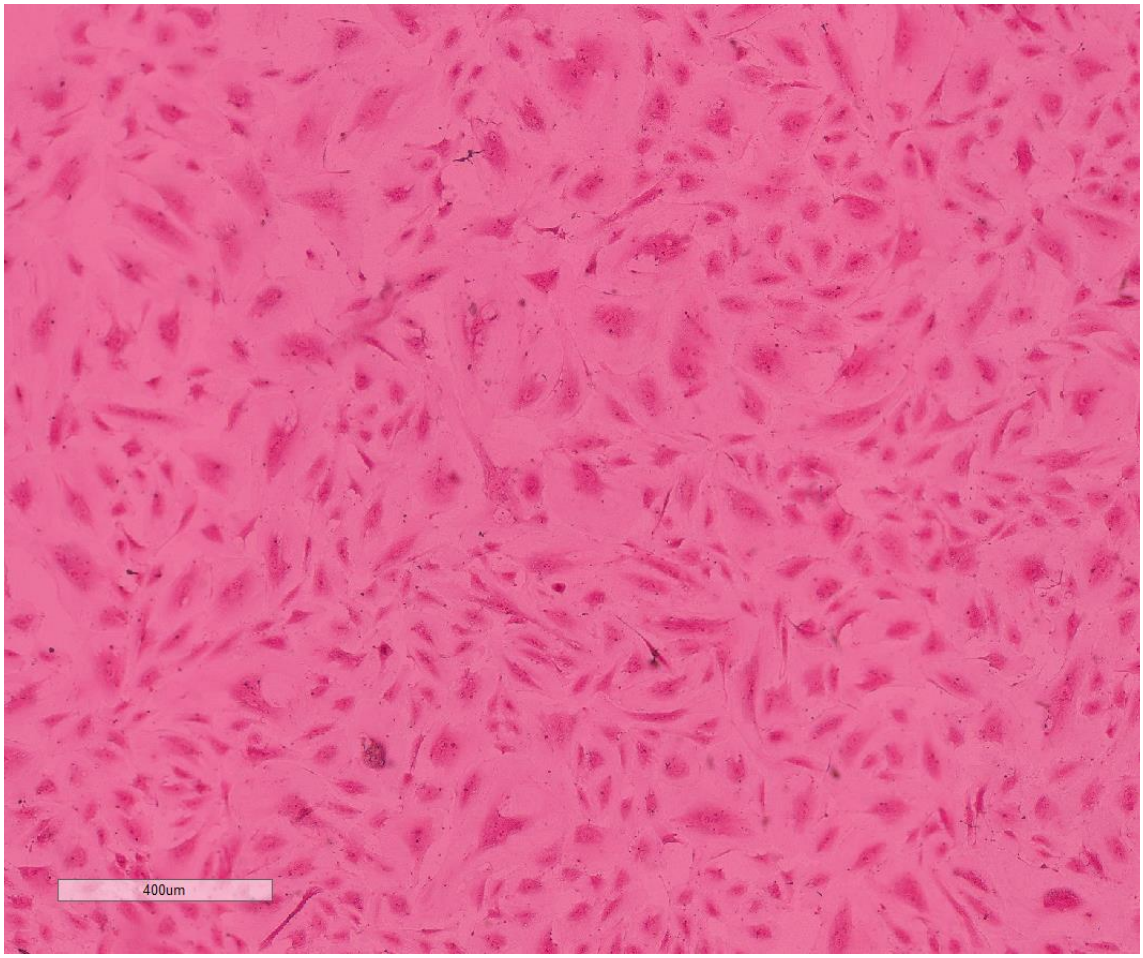

Supplementary Figure 12.

HUVEC culture grown on 10kPa polyacrylamide gel overlaid on cover slips, 9 days after initial seeding (passage=2,3). Fixed with 2% paraformaldehyde and stained with safranin. Images obtained using digital microscopy 10x (Panoptiq). Images were then loaded into Image J for cell count and area measurements. The image above was loaded into ImageScope (Leica Biosystems) and a sample of the image was captured at 5x magnification (total magnification 500x).

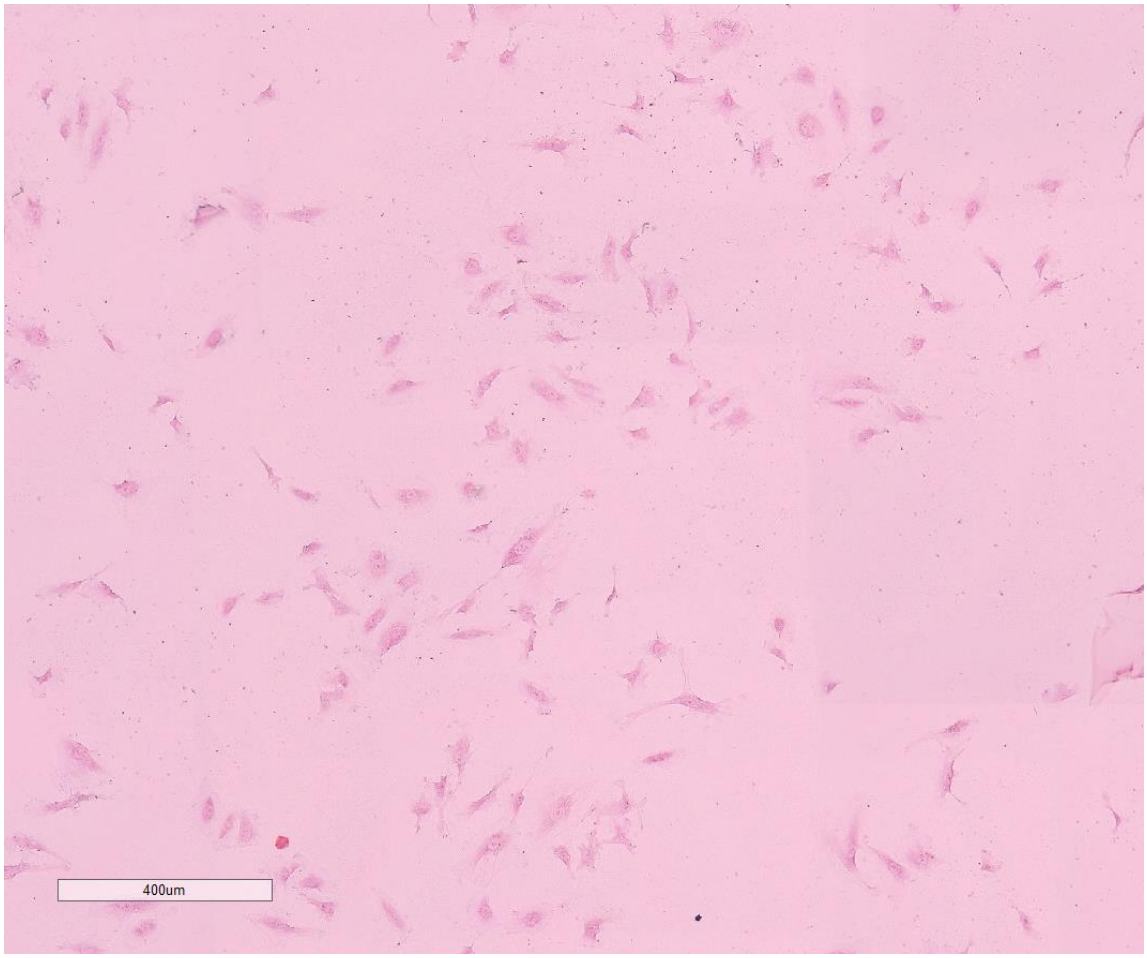

Supplementary Figure 13.

HUVEC culture grown on 30kPa polyacrylamide gel overlaid on cover slips, 3 days after initial seeding (passage=2,3). Fixed with 2% paraformaldehyde and stained with safranin. Images obtained using digital microscopy 10x (Panoptiq). Images were then loaded into Image J for cell count and area measurements. The image above was loaded into ImageScope (Leica Biosystems) and a sample of the image was captured at 5x magnification (total magnification 500x).

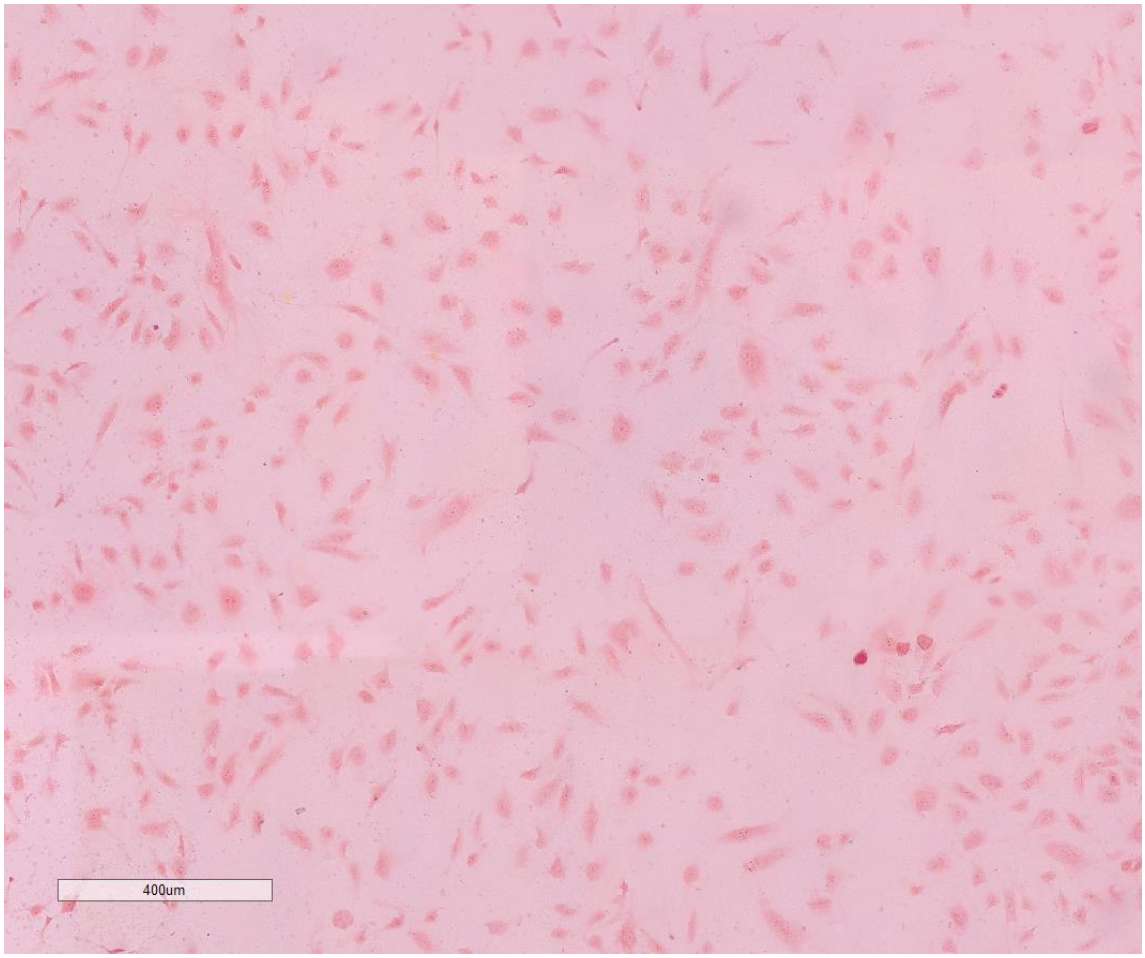

Supplementary Figure 14.

HUVEC culture grown on 30kPa polyacrylamide gel overlaid on cover slips, 6 days after initial seeding (passage=2,3). Fixed with 2% paraformaldehyde and stained with safranin. Images obtained using digital microscopy 10x (Panoptiq). Images were then loaded into Image J for cell count and area measurements. The image above was loaded into ImageScope (Leica Biosystems) and a sample of the image was captured at 5x magnification (total magnification 500x).

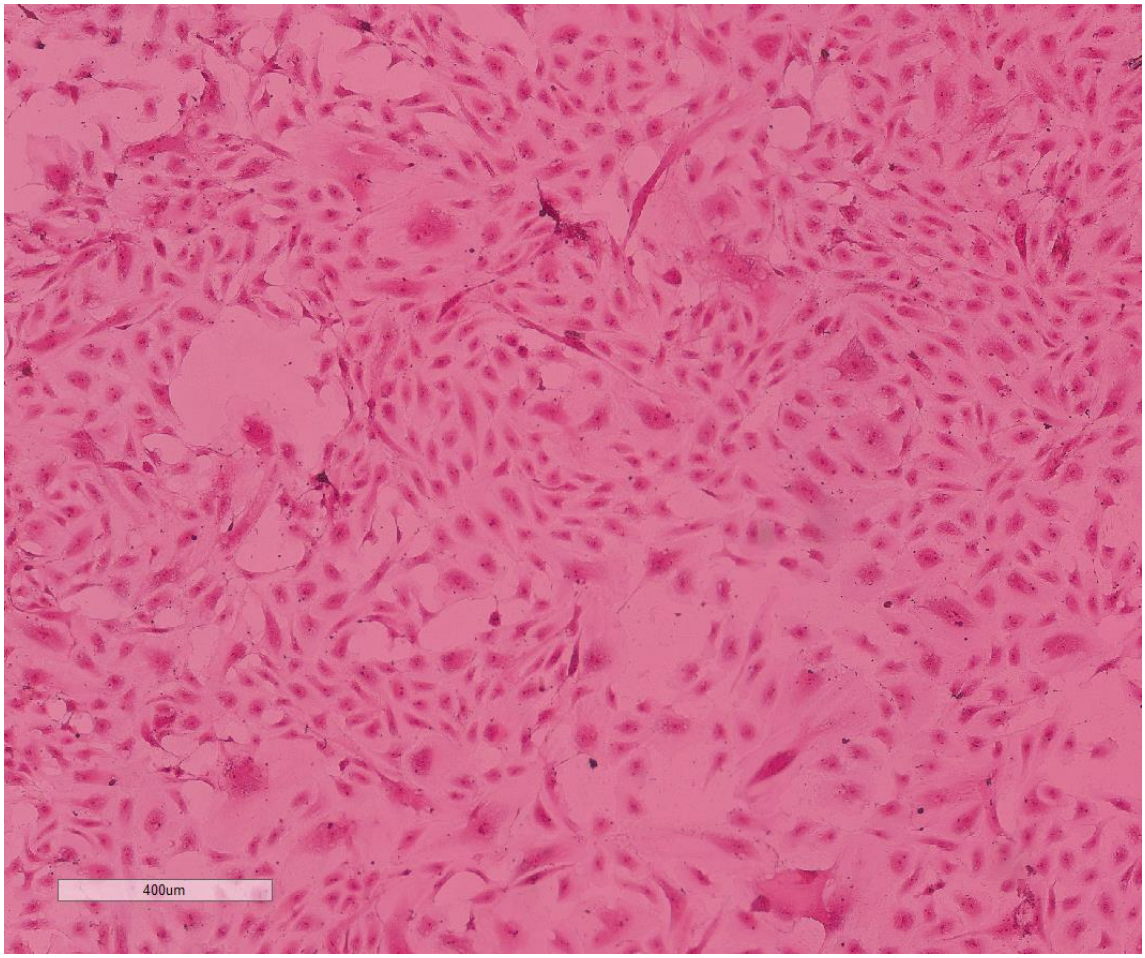

Supplementary Figure 15.

HUVEC culture grown on 30kPa polyacrylamide gel overlaid on cover slips, 9 days after initial seeding (passage=2,3). Fixed with 2% paraformaldehyde and stained with safranin. Images obtained using digital microscopy 10x (Panoptiq). Images were then loaded into Image J for cell count and area measurements. The image above was loaded into ImageScope (Leica Biosystems) and a sample of the image was captured at 5x magnification (total magnification 500x).